

Theme 1: Thin-walled components: new developments in theory and practice

Objektyp: **Group**

Zeitschrift: **IABSE reports = Rapports AIPC = IVBH Berichte**

Band (Jahr): **49 (1986)**

PDF erstellt am: **23.07.2024**

Nutzungsbedingungen

Die ETH-Bibliothek ist Anbieterin der digitalisierten Zeitschriften. Sie besitzt keine Urheberrechte an den Inhalten der Zeitschriften. Die Rechte liegen in der Regel bei den Herausgebern.

Die auf der Plattform e-periodica veröffentlichten Dokumente stehen für nicht-kommerzielle Zwecke in Lehre und Forschung sowie für die private Nutzung frei zur Verfügung. Einzelne Dateien oder Ausdrucke aus diesem Angebot können zusammen mit diesen Nutzungsbedingungen und den korrekten Herkunftsbezeichnungen weitergegeben werden.

Das Veröffentlichen von Bildern in Print- und Online-Publikationen ist nur mit vorheriger Genehmigung der Rechteinhaber erlaubt. Die systematische Speicherung von Teilen des elektronischen Angebots auf anderen Servern bedarf ebenfalls des schriftlichen Einverständnisses der Rechteinhaber.

Haftungsausschluss

Alle Angaben erfolgen ohne Gewähr für Vollständigkeit oder Richtigkeit. Es wird keine Haftung übernommen für Schäden durch die Verwendung von Informationen aus diesem Online-Angebot oder durch das Fehlen von Informationen. Dies gilt auch für Inhalte Dritter, die über dieses Angebot zugänglich sind.



THEME 1

Thin-Walled Components New Developments in Theory and Practice

Chairmen:

R. Baehre, FRG, and S. Hjelte, Sweden

Leere Seite
Blank page
Page vide

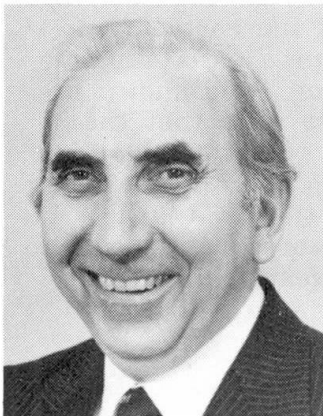
Cold-Formed Steel Structures and New British Code of Practice

Structures en acier formés à froid et nouveau règlement britannique

Kaltprofilkonstruktionen und neue englische «Code of Practice»

Eric R. BRYAN

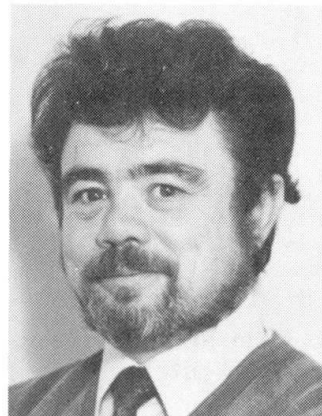
Professor
Univ. of Salford
Salford, UK



Professor Bryan is Chairman of the British Standards Committee for the new code. He is the author and co-author of three books and many publications on stressed skin design, sheeting and cold formed steel structures, and acts as a consultant in these fields.

James RHODES

Reader
Univ. of Strathclyde
Strathclyde, UK



Dr. Rhodes is consultant drafter for the new code. He is editor of the international journal «Thin-Walled Structures» and has organised several major conferences on the subject. He is technical adviser to the Cold Rolled Sections Association and has published widely.

SUMMARY

Existing uses and new developments in cold-formed steel structures are reviewed. The part played by new codes of practice in stimulating and encouraging these developments is emphasized. In particular, some aspects of buckling effects in the new BS 5950 Part 5 are outlined and compared with the AISI Specification and with experiment.

RÉSUMÉ

Les utilisations actuelles et les nouveaux développements en matière de structures en acier formé à froid sont passés en revue. Le rôle joué par les nouveaux règlements stimulant et encourageant ces développements est mis en valeur. En particulier, des aspects d'effets du flambement et du voilement dans le nouveau règlement anglais «BS 5950 Part 5» sont esquissés et comparés avec les spécifications de l'AISI et avec l'expérimentation.

ZUSAMMENFASSUNG

Bereits existierende Anwendungsmethoden und Neuentwicklungen von Kaltprofilstahlkonstruktionen werden nochmals überprüft. Die neuen Normen geben Anregung und Ermunterung zu solch neuen Entwicklungen. Insbesondere werden einige Aspekte der Instabilitätserscheinungen (Knicken, Kippen, Beulen) im neuen BS 5950, Teil 5, aufgezeigt und mit den AISI-Vorschriften und mit Versuchen verglichen.



1. INTRODUCTION

1.1 Production of steel strip

Since 1975, one of the few areas of steel production which has seen an increase in Britain is the rolling of coated steel strip, as used in sheeting and galvanised cold formed members. In fact, over half the British steel output is now in the form of sheet steel in one form or another. This is a remarkable figure, and one which has crept up upon us. Although, in the structural field, we have given a lot of attention to the design of hot rolled sections and tubes, we have not given enough attention to the design of strip steel. We should remedy this situation and give strip products the design that their importance and tonnage warrants.

	%	
Main frames	27)
Gable framing	3) hot rolled steel 31%
Tubular bracing	1)
Purlins and sheeting rails	6)
Roof sheeting	23) cold formed steel 42%
Side sheeting	13)
Gutters and downpipes	3	
Insulation to roof and walls	24	
	100	

Fig.1. Costs of a 30 m span x 90 m long x 6 m high pitched roof building.

Of all structural steelwork produced in Britain, about 70% goes into industrial buildings, and a breakdown of the costs of a typical building - as supplied by a fabricator - is shown in Fig. 1. It is seen that the value of cold rolled steel in purlins, sheeting rails and sheeting is more than that of the hot rolled steel, though it is safe to assume that nearly all of the design effort went into the frames.

1.2 Cold formed sections

Cold formed steel sections are usually formed by a series of rolls which bends them, stage by stage, into the desired shape. Once the rolls have been set up, it is almost as easy to form an intricate shape as a simple one, so that the optimum shape for a structural member may be rolled very economically.

Cold formed steel members have several additional advantages over conventional steel sections: they are usually formed from galvanised strip so that they do not need painting; they are automatically cut to length and punched for holes; they often 'nest' so that they may be easily transported; and they are light and easy to erect. Moreover, the process of cold forming enhances the yield strength, so that by using extra bends in a section, not only is the stability of the various flat elements improved, but a higher design stress may also be used.

2. PRESENT USE OF COLD ROLLED SECTIONS

2.1 Purlins and sheeting rails

By far the largest structural use of cold rolled sections in Britain has been in purlins and sheeting rails. The Zed profile was one of the major shapes used but this has now largely been superseded by the Zeta profile (Fig. 2) to meet the requirements of smaller roof pitches and to use the benefits of extra bends. Because the section is reversible, offcuts can be used as sleeves. In the design process, the actual moment-rotation characteristics of the sleeves were taken into account so that the bending moment diagram approached the optimum condition shown in Fig.3a rather than the continuous or simply supported conditions shown in Figs. 3b and 3c.

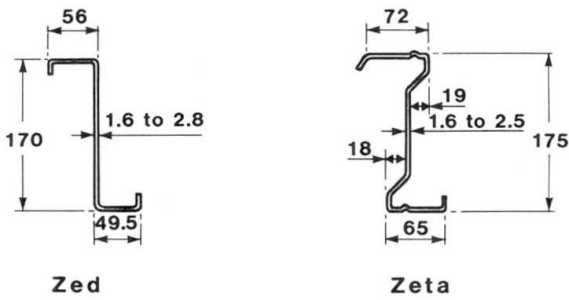


Fig. 2. Zed and Zeta sections

In the design of sheeting rails, the same principles as for purlins apply but because of door and window openings there is less opportunity to have multi-span members. Also, provision must be made for carrying the vertical weight of the side cladding (Fig. 4).

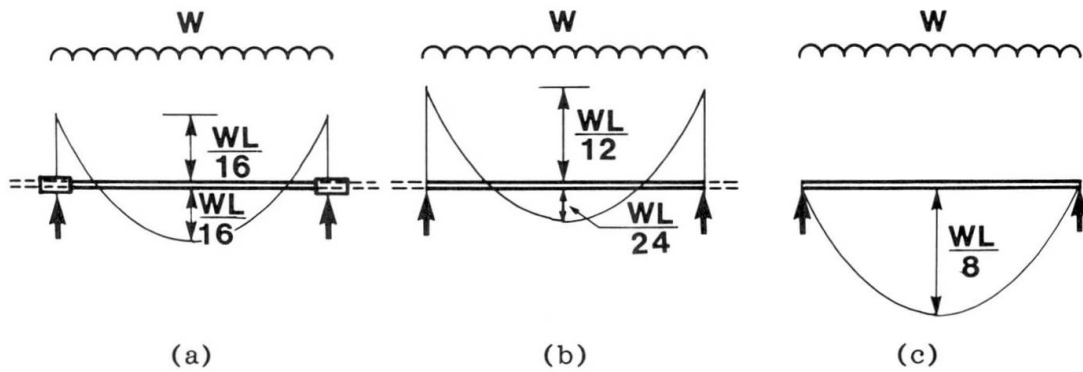


Fig. 3. Bending moment diagrams for purlins

Because of the substantial experience gained with cold rolled zed purlins and sheeting rails, simplified rules for their design and use have been drawn up, and these have been incorporated into the new British Code of Practice.

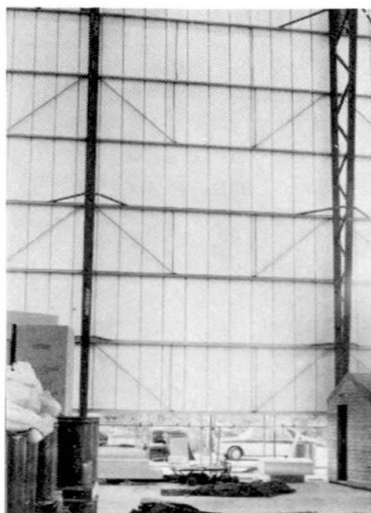


Fig. 4. Bracing to sheeting rails

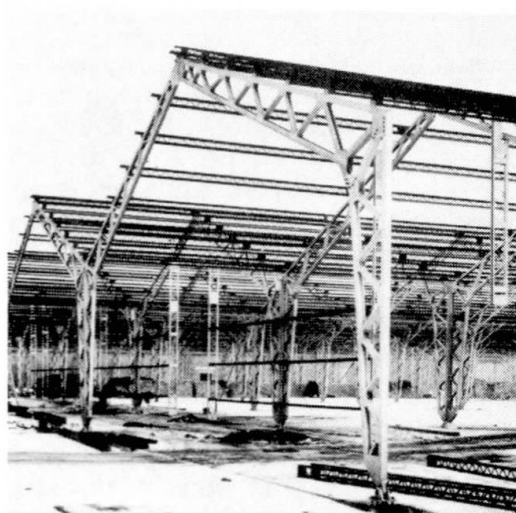


Fig. 5. Latticed portal frames - c.1950



2.2 Other structural uses

Shortly after the war, due to shortage of hot rolled sections, latticed building frames were fabricated in Britain from cold rolled sections (Fig. 5). Although they were economical in terms of material they were expensive at that time in terms of fabrication and jointing, and so the method was not further exploited. Perhaps they were ahead of their time. However, lattice joists are still used.

In France, welded cold formed sections have been used in columns and in various novel forms of beams. These components have been used instead of hot rolled members in conventional school and office construction.

In the United States, cold formed steel has been used for many years as wall studs in domestic and office buildings, but the principle has not been widely used in Europe.

3. CODES OF PRACTICE

3.1 Limitation of existing codes

The uses of cold rolled sections just described have largely occurred without a great deal of dependence on codes of practice. For example, purlin and sheeting rail design in Britain, although soundly based theoretically, has been verified and refined by full scale testing. One of the reasons for this is that the present code of practice for cold formed steel sections - Addendum No. 1 to BS 449 : Part 2 : 1969 - is inadequate to deal with the problems involved because knowledge at the time it was written was limited. For instance, the only laterally unrestrained beam with which it deals is an I section, composed of two channel sections, connected back to back. Any other beam has to be dealt with on an experimental basis.

3.2 Development of new codes

In recent years, several new codes have either been published or are being written. The AISI Specification [1] was revised in 1980 and a further revision is under way. In Sweden, a comprehensive new Code [2] which deals with sheeting as well as sections was published in 1982. European Recommendations [3] have been drafted by the European Convention for Constructional Steelwork, first in Committee TC8 and subsequently in Committee TC7. The draft for comment has recently been circulated to the various National Associations.

Against this background, Britain, amongst other countries, has been preparing a new code of practice on the design of cold formed sections. It is part 5 of a comprehensive new code, BS 5950, on the "Structural use of steelwork in building" [4]. Like all parts of the code, it is written in limit state terms and deals with material and section properties, connections, simplified rules and testing, as well as the fundamental aspects of local buckling, stiffeners, beams and columns which are treated in the latter part of this paper.

A good design code must not just follow in the wake of existing practice: it must be adequate to allow for new developments. It must also be soundly based, both theoretically and experimentally, so that it has authority in the profession, and it must be practical. It is expected that the new code will satisfy these requirements and will act as a stimulus to develop more complex and efficient sections which may be used as main members in structures and not merely as secondary members. It should also signal the acceptance by the structural steelwork industry of cold rolled sections as an equal alternative to hot rolled sections.

4. SOME NEW DEVELOPMENTS IN PRACTICE

4.1 Swagebeam section

Recently a channel section has been introduced in Britain which has grooves or "swages" rolled into the web (Fig. 6a). These swages increase the stress at which web buckling occurs, so that they also permit a higher stress in the flanges. The b/t ratio for the flanges is sufficiently low for the flanges to be fully effective (or nearly so) and the double lip improves the section properties.

A major advantage of the swages is that they can lock on to similar swages on the jointing components (Fig. 6b) to give a stronger and more rigid joint. This takes advantage of a feature of cold formed sections which is not available for conventional sections. It is a challenge to designers to find other ways of maximising such opportunities.

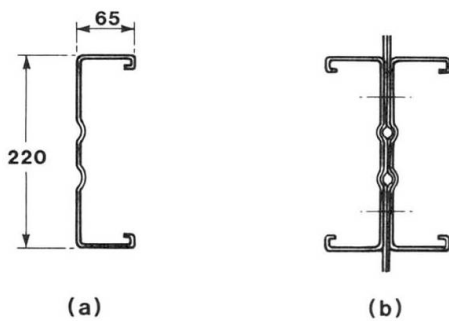


Fig. 6. Swagebeam section and joint

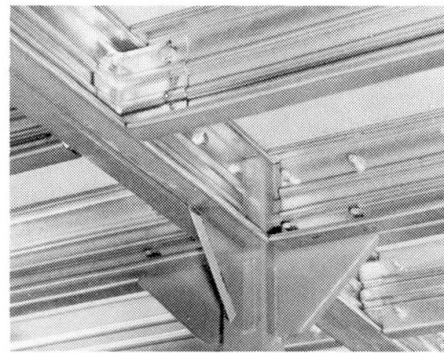


Fig. 7. Joints in storage platform

4.2 Swagebeam structures

Swagebeams have been used, both singly and in pairs, as the members for storage platforms. The rigidity at the joints (Fig. 7) has ensured a stable structure.

Another use has been in the development of a new pitched roof portal frame building system with spans between 9 and 15 metres, and with the swaged gusset plates formed from 2 - 3 mm plates with lips. The crucial factors in the design were the behaviour of the joints and the individual behaviour of the two swagebeam sections in the rafters, since they were connected together only at the purlin positions. The first point was resolved by bending tests on the apex and eaves joints which showed that the joints could be regarded as fully rigid and that they were stronger than the members which they connected. The second point - lateral buckling of the individual members between purlin points - was resolved by calculation to BS 5950 Part 5 and by bending tests.

After the design of the frames had been checked theoretically and experimentally, a pair of 12m span frames were test loaded to collapse at Salford (Fig. 8). The actual behaviour confirmed the design method and showed that the frames were adequately strong.

A further recent use of the swagebeam section has been in the fabrication and testing of a 21.6m span latticed portal frame (Fig. 9). This design, using 1.5mm thick members, did not use the interlocking properties of the section, but it did show the importance of frame geometry and joint detailing. By re-arranging the internal bracing and re-designing the joints, the strength was nearly tripled.

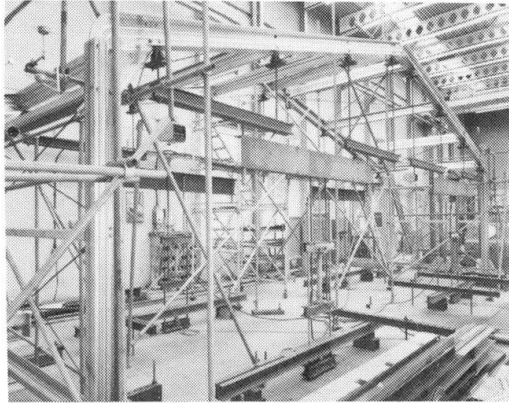


Fig. 8. Test on Swagebeam portal frames

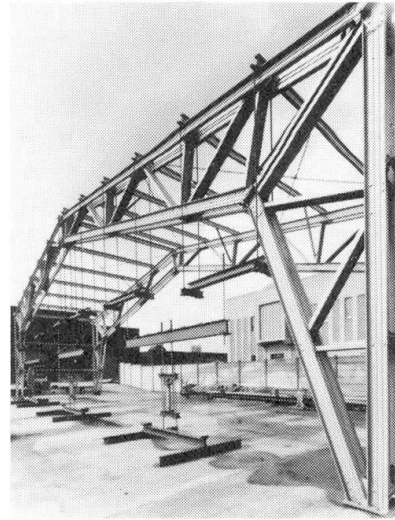


Fig. 9. Latted test frame - 1985

5. SOME DESIGN DEVELOPMENTS AND COMPARISONS

5.1 Plastic design in cold formed sections

In the new British code, as in the AISI Specification, some utilization of plastic bending capacity is allowed in cold formed sections, but full plastic design including moment redistribution is not allowed except for compact sections. This is because the plastic rotation capacity of many sections is insufficient.

However, in many structures, as in continuous purlins, the maximum moments occur in the joints. If the joints are bolted, as is usually the case in cold formed members, there is a "plastic plateau" in the moment-rotation relationship which allows redistribution of moment. This aspect of design has not yet been investigated although considerable test data on joints have been accumulated by TNO in Holland [5] and by Corcoran [6] and Geha [7] at Salford.

5.2 Comparison of BS 5950 Part 5 and AISI Specification

In the process of writing and monitoring the new British code, comparisons were made with the 1980 AISI Specification. Allowance was made for the fact that the British code was in limit state terms while the American specification was in terms of permissible stress.

The comparisons of effective width of elements, moments of resistance of beams and ultimate axial compressive load for various sections are given in Fig.10. It is seen that the results of the two codes are very similar.

6. FEATURES OF THE NEW CODE

Some of the requirements of a new code have already been listed; in particular, Part 5 was required to give safe yet economical design rules while stimulating the growth of the product and encouraging new development. It also had to be compatible with BS 5950 Part 1, design in hot rolled steel.

In writing the code, the results of research carried out in other countries was used where appropriate, and the provisions of other codes - particularly the AISI Specification and the European Recommendations - were taken into account.

Nevertheless, the approach to some of the buckling effects in cold formed sections is different from that used elsewhere and so the rest of the paper is devoted to dealing with these aspects in greater depth.

Case	Section	Yield stress Y_s N/mm ²	Required condition	BS 5950	AISI	
Effective widths	Stiffened element $b = 130$ mm $t = 2$ mm	(1) 280 (2) 350	Effective widths mm (1) (2) Element (A) Element (B)	82.9	85.1	
		280		51.1	47.7	
				59.0	44.0	
Beams		345	Moment of resistance kNm	6.125	5.876	
		250		15.39	16.31	
Columns		280	Effective length 3.0 m	Ultimate compressive load kN	18.97	19.15
		228	Effective length 2.75 m		29.69	28.17

Fig. 10. Comparison of BS 5950 Part 5 and AISI Specification
(by R. Plater)

7. TREATMENT OF LOCAL BUCKLING

In the new code [4], local buckling of both stiffened and unstiffened elements is treated using the effective width approach. The code stipulates that the effective portions of each element be positioned at the supported edges. In this way effective section properties for beams and columns may be derived, which result in changes in the neutral axis position and other data.

7.1 Stiffened elements

The effective width of a stiffened element under uniform compression is taken as:

$$\frac{b_{\text{eff}}}{b} = [1 + 14 (\sqrt{f_c/p_{\text{cr}}} - 0.35)^4]^{-1/5} \quad (1)$$

where f_c is the applied stress and p_{cr} is the critical buckling stress given by $p_{\text{cr}} = 185000 K (t/b)^2$ N/mm², K being the buckling coefficient.

The effective widths so given are slightly lower than those of the AISI Specification [1] if the minimum value of K is used.

7.2 Unstiffened elements

Theory shows, and experiments verify, that unstiffened elements under uniform compression have a greater effective width ratio at a given f_c/p_{cr} ratio than stiffened elements, although their much lower p_{cr} and the strong tendency to behave asymmetrically necessitate the use of care in dealing with these elements. In the new code, unstiffened effective widths are obtained on the basis of equation (1) and thereafter increased using the expression:

$$b_{\text{eu}} = 0.89 b_{\text{eff}} + 0.11b \quad (2)$$



The increased effective widths have been shown in reference [8] to be in good agreement with experimental results.

7.3 K factors

For stiffened elements, K may be taken as 4 and for unstiffened elements K may be taken as 0.425. The new code permits the use of higher K values if these can be justified, and gives details of higher values for a range of different sections and loading conditions.

Figure 11 illustrates the effective widths of various stiffened and unstiffened plate elements of sections. For unstiffened elements, increases in effective width of the order of 60% are obtained if the supported edges are highly restrained in comparison to the simply supported-free condition. In the case of stiffened elements the AISI effective width variation is shown for comparison purposes.

8. STIFFENERS

In the new code, the coverage of stiffeners is increased from that of its predecessor [9] to come more into line with the AISI Specification and the new European Recommendations [3].

8.1 Edge stiffeners

The minimum required second moment of area for an edge stiffener is given as:

$$I_{\min} = \frac{b^3 t}{375} \quad (3)$$

where I_{\min} is determined with respect to the plate middle surface and b is the full plate width.

For b/t less than 60, a simple 90° lip of full width equal to b/5 satisfies this requirement, but for b/t greater than 60 a compound lip is required. Edge stiffened elements of b/t ratio greater than 90 are not allowed.

8.2 Intermediate stiffeners

The required rigidity for adequate intermediate stiffeners is obtained from:

$$I_{\min} = 0.2 \left(\frac{w}{t}\right)^2 \frac{Y_s}{280} \quad (4)$$

where w is the flat width of the sub-element between stiffeners, and Y_s is the material yield stress.

This equation is an approximation to the linear equations covering three different ranges as specified in the European Recommendations, and based on the work of Desmond, Pekoz and Winter [10]. It should be mentioned that in the new code, I_{\min} is determined with respect to the plate middle surface, rather than with respect to the stiffener neutral axis as in other codes.

9. TREATMENT OF BEAMS

9.1 Laterally stable beams

The moment capacity of laterally stable beams is determined on the basis of a limiting stress, obtained by considering the web, which is then used to evaluate the effective width of the compression elements. Failure is assumed to occur when the limiting stress, p_c , is reached in compression. If the section geometry is such that tension yield occurs before p_c is attained, then this can be

taken into account using an elasto-plastic stress distribution, and yield in tension is allowed to occur in any section.

The limiting stress, p_c , is given by

$$p_c = (1.13 - 0.0019 \frac{D}{t} \sqrt{\frac{Y_s}{280}}) Y_s < Y_s \quad (5)$$

where D is the web depth. For intermediately stiffened webs, modified values of p_c can be used.

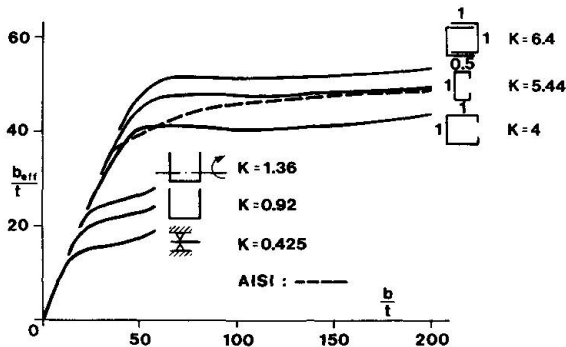


Fig. 11. Effective widths

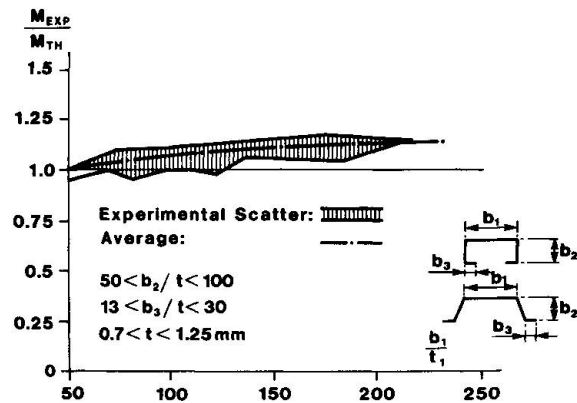


Fig. 12. Comparison of calculated and experimental failure moments

Figure 12 shows a comparison of the moment capacities obtained on the above basis for channel and trapezoidal section beams with the results of a series of 48 tests on these beams detailed in reference [11]. The comparisons indicate that the approach is accurate, although the results become slightly conservative at b/t ratios around 200.

In cases where the lips of these beams are small, tension yield occurs long before failure, and the benefits of permitting tension yield become apparent. This is illustrated in Fig. 13 which compares the new code predictions for such sections with predictions based on tensile yield indicating failure. Test results show reasonable accuracy for the new code predictions, whereas those of the AISI Specification (and of the new code if tensile yield were taken as the failure criterion) are very conservative under these conditions. In plotting the AISI ultimate moments the design moments obtained using this specification were divided by 0.6 to remove the safety factor.

9.2 Post yield capacity of compact sections

The new code recognises the fact that if a section is sufficiently compact, post compression yield may be tolerated, and perhaps even plastic limit analysis, involving redistribution of moments, may be used. To take this into account, then subject to a number of conditions regarding section geometry, web dimensions, loading and material ductility, similar to those of the AISI Specification, sections with compression element b/t ratios less than certain limits are designated 'plastic cross sections'. The required limits are $25\sqrt{280/Y_s}$ for stiffened elements and $8\sqrt{280/Y_s}$ for unstiffened elements.

For plastic cross sections, full plasticity may be assumed and limit analysis involving moment redistribution may be used. For non plastic cross sections, design is based on elastic considerations. However, for compression element width to thickness ratios less than 1.6 times the plastic cross section limits, some limited increase in moment capacity due to post compression yield plasticity may be utilised.

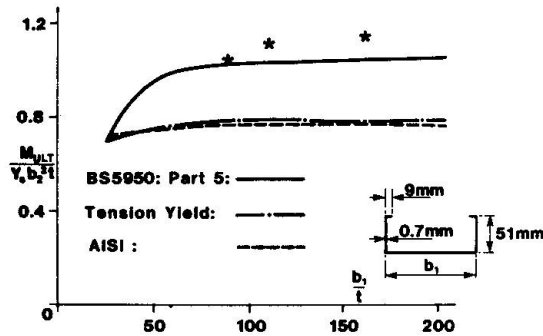


Fig. 13. Failure moments for channels with small lips

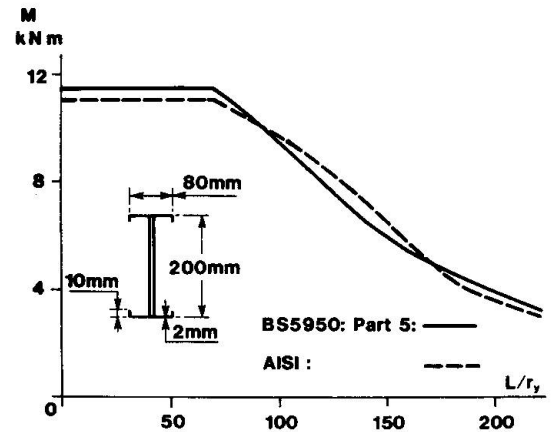


Fig. 14. Lateral buckling capacity of I section beam

9.3 Lateral buckling

In the new code, I, C, Z and T beams, which cover the bulk of lateral-buckling-prone beams used in practice, are considered. Determination of the lateral buckling capacity of these beams is made on the basis of a Perry-Robertson formula which uses the fully plastic moment M_p , and the elastic critical moment M_E . In determination of M_E , effective lengths are used. The effective length depends on the support conditions and varies from $0.7L$ to $1.1L$, where L is the span between supports. For most circumstances a value of $0.9L$ is applicable if the support restrains twisting but permits rotation about major and minor axes.

The moment capacity of the section is taken as the lower of its lateral buckling capacity, determined as above, and its capacity evaluated as for a laterally stable beam.

Figure 14 shows a comparison of the working moments for an I section under pure bending with those of the AISI Specification. The working moments used in connection with the new code were the ultimate moments divided by 1.6, which is the maximum load factor used in this code. As can be seen, the working moments given by both codes are similar.

10. TREATMENT OF COLUMNS

10.1 Singly symmetric columns - beam-columns

In the new code all single symmetric columns are treated as beam-columns to take account of the well known 'wandering centroid' phenomenon due to local buckling. For a column under centroidal loading the effective area, and the Q factor is determined using the effective widths of individual elements. The effective neutral axis position is also determined and the magnitude and direction of the neutral axis movement, e_s , is calculated.

The ultimate load, P_c , neglecting neutral axis movement is evaluated on the basis of a Perry-Robertson curve which uses the squash load for the effective section and the Euler load for the full section. The effects of neutral axis movement are then taken into account using the expression

$$P_{ULT} = \frac{P_c}{\left(1 + \frac{P_c}{M_y} e_s\right)} \quad (6)$$

where M_y is the moment capacity of the section, considering bending in the direction dictated by e_s .

Figure 15 shows the design loads evaluated for plain channel columns, as a ratio of the fully effective squash load, using a load factor of 1.6. The AISI design loads are shown for comparison, indicating significant differences in some cases. Comparisons of failure predictions using the above method for plain and lipped channels are shown to agree well with experimental results in reference [8].

10.2 Torsional-flexural buckling

The old U.K. specification [9] uses effective length multiplication factors, α , to deal with torsional-flexural buckling. These α factors allow the designer to treat torsional-flexural buckling using the tables and formulae set up for flexural buckling, but considering different effective column lengths. This method of approach is continued in the new code, because of its simplicity, although the more general treatment is also detailed.

Reference [9] differs from other specifications with regard to torsional-flexural buckling inasmuch as this code assumed warping restraint at the supports, whereas the AISI and other specifications assumed zero warping restraint. To obtain a balance between the over-optimistic approach of reference [9] and the over-pessimistic views of other codes, the new code assumes partial warping restraint.

Figure 16 shows the variation of α factors given in the new code for a typical cross section. Multiplying the effective column length by the relevant α factor permits evaluation of the torsional-flexural buckling capacity using the Perry-Robertson curve for flexural buckling.

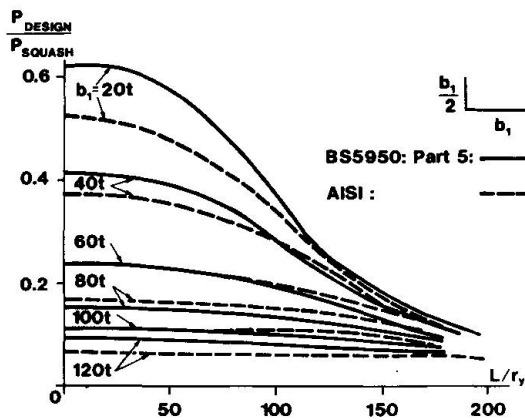


Fig. 15. Failure loads for plain channel columns

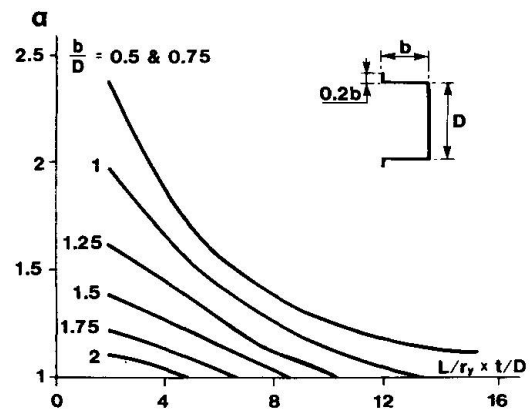


Fig. 16. α factors

11. CONCLUSIONS

This paper shows the importance of cold formed members in steel design. It reviews the existing structural uses and notes the new developments which are occurring in theory and practice. In particular it observes that new codes of practice should stimulate the product and encourage these developments.

In particular, some of the more prominent aspects of the treatment of buckling effects in the new British code BS 5950 Part 5 are outlined and comparisons with the AISI Specification and with experiment have been used to illustrate the predictions of the approaches used.



REFERENCES

1. "Specification for the design of cold-formed steel structural members". American Iron and Steel Institute, September, 1980.
2. "Swedish code for light-gauge metal structures". Swedish Institute of Steel Construction, March, 1982.
3. "European Recommendations for the design of light gauge steel members" Draft for comment, ECCS, September, 1985.
4. BS 5950 Part 5. Draft British Standard. "Code of practice for the design of cold formed sections" BSI, September, 1984.
5. "European Recommendations for the design and testing of connections in steel sheeting and sections". ECCS, May, 1983.
6. D. CORCORAN. Unpublished test results on bolted joints. University of Salford.
7. G. GEHA "The ultimate strength and slip of bolted connections in light gauge steel members" CUST, Université de Clermont II, June, 1984.
8. J. RHODES and A. C. WALKER "Current problems in the design of cold formed steel sections". Aspects of the analysis of plate structures edited by D. J. Dawe, R. W. Horsington, A. G. Kamtekar, G.H. Little, Oxford University Press, 1985.
9. Addendum No. 1 to BS 449 (1969) "Specification for the use of cold formed steel sections in building". BSI, April, 1975.
10. T. P. DESMOND, T. PEKOZ and G. WINTER "Intermediate stiffeners for thin-walled members". Proceedings 5th International Specialty Conference on Cold Formed Steel Structures, St. Louis, 1980.
11. J. RHODES "The non-linear behaviour of thin-walled beams subject to pure moment loading". PhD thesis, University of Strathclyde, 1969.

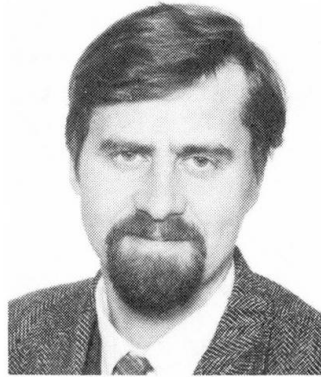
Elastically Braced Light Gauge Beams with Open Sections

Poutres à parois minces et section ouverte tenues latéralement de façon élastique

Berechnung von dünnwandigen Pfetten mit offenen Querschnitten

Lars HESELIUS

Civil Engineer
Techn. Res. Centre of Finland
Espoo, Finland



Lars Heselius, born 1947, received his civil engineering degree at Helsinki University of Technology. For fourteen years he has been working at Technical Research Centre of Finland in the Laboratory of Structural Engineering in the division of metal structures.

SUMMARY

Light gauge steel purlins have been studied both theoretically and experimentally. The classical equations for bending-torsion problems have been solved numerically with the finite-difference method regarding the bracing structure as elastic springs acting against torsion and sidesway and taking the nonlinear effects into account. Simple design formulae have been derived taking account of local and global buckling of the purlin. Structures that can be analyzed are both purlins under gravity load or wind suction and purlins in compression with one or both flanges braced. Both elastic and inelastic design are considered.

RÉSUMÉ

Des pannes à parois minces en acier ont été étudiées aussi bien en théorie qu'expérimentalement. Les équations classiques propres aux problèmes de déversement ont été résolues numériquement par la méthode des différences finies. La structure destinée à stabiliser la poutre contre la torsion et le déversement a été représentée par des ressorts élastiques. Le comportement non-linéaire a été pris en compte. Des formules simples de dimensionnement tenant compte du voilement local et de la stabilité globale de la poutre sont proposées. Les structures que l'on peut analyser sont aussi bien les pannes soumises aux charges de gravité, à l'aspiration du vent que les pannes soumises à la compression, avec une aile ou les deux tenues latéralement. L'analyse peut être élastique ou non-élastique.

ZUSAMMENFASSUNG

Dünnwandige Pfetten sind theoretisch und experimentell untersucht worden. Die klassischen Beziehungen für Biegung und Torsion wurden numerisch mit der Differenzenmethode gelöst. Der Effekt der stützenden Konstruktion wurde als elastische Federkonstanten angenommen. Nicht-lineare Effekte sind beachtet. Einfache Berechnungsregeln, die örtlichem Beulen und der Gesamtstabilität Rechnung tragen, werden vorgestellt. Die untersuchten Konstruktionen sind sowohl Pfetten unter Eigengewicht oder Windsog als auch Pfetten unter Druck mit einem oder beiden Flanschen gestützt. Elastische sowie nicht elastische Bemessung werden betrachtet.



1. INTRODUCTION

A thin walled beam with an open cross section shown in fig. 1 has the shear centre often out of the loading plane. Thus it is subjected to torsion and in the case of nonsymmetry which is affected by local buckling also to bi-axial bending. Owing to the weak torsional stiffness the warping stresses due to torsion can be of the same order as those due to bending if the beam is free to rotate. The Z- and C-purlins in the roof or wall structures are often fixed to the sheeting with mechanical fasteners which give an elastic restraint to the purlins against rotation and sideways. This causes a complex problem for exact solutions. The solution is in this work obtained in accordance with classical theory of elasticity [1], [2].

The analytical solutions have formed the base for the derivation of design formulae. Despite of the fact that similar studies have earlier been made in the 70'ies, there has been a lack of models suitable for engineering calculations taking into account the partial restraint of sideways and rotation. In the beginning of 1980s some models [3, 4, 5] have been presented taking into account the torsional effect of the bracing structure mostly applied to structures subjected to wind uplift. In this work a model is presented where also the partial restraint of the sideways of the flange in compression in the case of soft material between the purlin and the sheeting structures subjected to gravity load, wind uplift and structures in compression are included. The calculation model is also extended to give a tool to take into account the inelastic reserve of the bending capacity in continuous purlin systems.

2. ANALYTICAL SOLUTION

For an unsupported beam-element we have the formulas

$$EI_y \cdot u^{IV} = q_x \quad (1a)$$

$$EI_x \cdot v^{IV} = q_y \quad (1b)$$

$$EI_\omega \cdot \theta^{IV} - GI_d \cdot \theta'' = m \quad (1c)$$

where I_x, I_y are the moments of inertia for the effective area (mm^4)
 I_ω is the warping constant for the effective area (mm^4)
 I_d is the torsion constant for the gross area (mm^4)
 q_x, q_y are the components of the applied load q (N/mm)
 $m = q \cdot e$ is the torque (Nmm/mm)
 E is the modulus of elasticity. (N/mm^2)

The elastic support is according to Vlasov [1] regarded as external forces acting in the shear centre:

$$\begin{aligned} \bar{q}_x &= -k_x \cdot u_H \\ \bar{q}_y &= -k_y \cdot v_H \\ \bar{m} &= -k_\theta \cdot \theta_H + (h_x - a_x) \cdot \bar{q}_y - (h_y - a_y) \bar{q}_x \end{aligned} \quad (2)$$

where k_x, k_y are the stiffnesses of the foundation against sideways (N/mm/mm)
 k_θ is the stiffness of the foundation against rotation (Nmm/mm/rad)
 u_H, v_H, θ_H are the deformations in the supporting point (mm).

In the analysis the forces causing instability have been expressed in the terms derived by Roik et. al. [2]:

$$\begin{aligned}
 \tilde{q}_x &= [N(u' + a_y \cdot \theta)']' - (M_x \theta)'' \\
 \tilde{q}_y &= [N(v' - a_x \cdot \theta)']' - (M_y \theta)'' \\
 \tilde{m} &= a_y (N \cdot u')' - a_x (N \cdot v')' - M_x \cdot u'' - M_y \cdot v'' \\
 &\quad + [(r^2 N + 2 \beta_y M_x - 2 \beta_x M_y) \theta']' \\
 &\quad - [q_x (e_x - a_x) + q_y (e_y - a_y)] \theta
 \end{aligned} \tag{3}$$

where $r^2 = \frac{I_x + I_y}{A} + a_x^2 + a_y^2$

$$\beta_x = \frac{U_y}{2 I_y} - a_x \quad ; \quad U_y = \int_A x^3 dA + \int_A y^2 x dA$$

$$\beta_y = \frac{U_x}{2 I_x} - a_y \quad ; \quad U_x = \int_A y^3 dA + \int_A x^2 y dA$$

N is the normal force (N).

By substituting the formulas (2) and (3) to the right side of the equation (1) we get three differential equations that are coupled and suitable for nonlinear analysis with step by step solution. They are solved with the difference-method. Calculations have been made for a number of one-bay and two-bay structures with a computer program specially made for these studies.

3. A PROPOSAL FOR DESIGN FORMULAE

3.1 General

The design formulae are derived based on computer calculations of the combined expressions (1), (2) and (3) for Z- and C-profiles and are based on the assumptions that the transversal load is acting in the direction of the web and that the lateral support is acting perpendicular to the web.

The derivation of the formulae is done outgoing from the idea also used in other similar calculation models [3, 4, 5] to solve the problem by calculating the critical buckling force for a column formed by the compressed flange and a part of the web (fig. 2). The column is on an elastic foundation. The stiffness coefficients of the foundation k_x and k_θ are determined experimentally.



3.2 Purlin under bending

3.2.1 Purlin with both flanges free

$$\sigma_{e11} = \frac{\pi^2 E}{\lambda^2} \cdot k \quad (\text{N/mm}^2) \quad (4)$$

where $k = \frac{e_x}{\| e_x + \frac{m}{3} \|} < 1$

$$\lambda = 1/\sqrt{\frac{I_1}{A_1}}$$

A_1 is the area of the column (mm^2)

I_1 is the moment of inertia about the axis $y - y$ for the section of the column (mm^4)

l is the length of the span (mm)

e_x is the distance between the web and the loading point (mm)

m is the distance between the web and the shear centre (mm)

3.2.2 Purlin with one flange braced

For laterally supported beams the critical buckling stress is determined as:

$$\sigma_{e12} = \frac{2}{A_1} \sqrt{\frac{E I_1}{\delta}} \cdot k > \sigma_{e11} \quad (5)$$

where δ is the lateral deformation due to the unit force in the supporting point H.

The lateral deformation δ depends on the two coefficients of the stiffness k_θ and k_x as follows:

pressure load:

$$\delta = \frac{30 \cdot e_y^2}{10 \cdot e_y^2 \cdot k_x + 3 \cdot k_\theta} \quad (\text{mm/N/mm}) \quad (6)$$

uplift load:

$$\delta = \frac{e^2}{4 \cdot k_\theta} \quad \text{for } k > 0,01 \quad (\text{N/mm}^2) \quad (7)$$

Expression (6) is derived on the assumption that two springs work parallel-coupled together and in the case of uplift load that no sideways occurs in the tension flange (7). The numbers 4, 10 etc are determined as results from analysis.

3.2.3 Both flanges braced

In the case of both flanges being braced the rotation stiffness of the bracing structure to the tension flange is added to that of the flange in compression reduced with the factor $(e_y^c/e_y^t)^2$.

Having calculated the critical stress σ_{e1} (σ_{e11} or σ_{e12}), the design strength f_{cd} is obtained from the ECCS curve c for flexural buckling with $\lambda = \sqrt{f_y/\sigma_{e1}}$. The reduction of the bending capacity due to lateral buckling is then $r = f_{cd}/f_y$.

The bending capacity M_D is calculated from:

$$M_D = \eta \cdot f_{cd} \cdot W_e \quad (8)$$

where $\eta = 0,9$ for structures braced along one flange and 1.0 with both flanges braced taking into account the effect of shear deformation of the profile [3]. W_e is determined taking into account the local buckling in accordance with fig. 3.

3.3 The inelastic reserve M_{p1}

The inelastic reserve of the bending capacity of the profile is calculated for an edge strain that is three times the yielding strain, that is putting $f'_y = 3 \cdot f_y$ in the formulae in the fig. 3 to calculate the effective area A_e in the inelastic stage. This method is based on the notation (Rockey et. al.) that the formulae for the effective area gives a good agreement using the edge strain in the post-yielding stage for plates in compression. Though this gives an overestimating of the inelastic reserve for both trapezoidal sheets and sections (see fig. 4), it has been assumed in accordance with [6] that the strain in the first plastic hinge at the support in a 2-bay beam is $\epsilon_m = 3 \cdot \epsilon_y$ when the bending capacity is reached in the field. For purlins the inelastic reserve is reduced in the same manner as in the elastic stage with the coefficient $r = f_{cd}/f_y$. For a 2-span beam the ultimate load is thus:

$$q_u = \frac{M_D}{l_2} [(4 + 2 \cdot j \cdot m) + 4 \sqrt{1 + j \cdot m}] \quad (9)$$

where M_D is the moment capacity in the field reduced with the factor r
 j is the inelastic reserve at the support calculated for $\epsilon_m = 3 \cdot \epsilon_y$; $j = M_{p1}/M_D$
 m is the relation between the moment capacity at the support and in the field
 l is the span.

3.4 Purlin in compression

For the case of structure in compression the critical stress is in a similar way calculated for the flange with the weaker restraint by putting (10) into (5)



$$\delta = \frac{1}{k_x} + \frac{e_y^2}{k_\theta} \cdot 10 \quad (10)$$

The capacity for the compression force is

$$N_d = f_{cd} \cdot A_e \quad (11)$$

with f_{cd} obtained from the ECCS curve c and A_e is the effective area of the whole section.

4. TEST RESULTS FOR PURLINS SUBJECTED TO BENDING, COMPARISON WITH CALCULATED VALUES

In table 1 results are given for tests on one-bay purlins (Z and C profiles) under pressure load and uplift load.

Table 1. Results from a test series at the Technical University of Helsinki in 1982 - 83.

Test nr	Profile h/t	Yield strength f_y N/mm ²	Steel thickness t_{Fe} mm	Span l (mm)	Load direction	Fasteners (screws)	Bracing structure	Material between purlin and bracing	k_θ N	k_x N/mm ²	Bending capacity (kNm)			
											Plane bending without lateral buckling	Difference method	Calculation model	Test results
1	Z 200/2.5	341	2.37	7200	pressure	∅ 6.3 cc 750 mm	Trap.sheet 45/0.7	min.wool 50 mm	400	0.01	17.8	8.2	11.1	10.6 ¹⁾
2	Z 300/3	333	2.98	7200	pressure	∅ 6.3 cc 300	Trap.sheet 45/0.7	min.wool 50 mm	400	0.025	52.0	20.7	30.6	31.2
3	Z 200/2	416	1.86	7200	uplift	∅ 5.5 cc 300	Trap.sheet 45/0.7	no	2290	0.71	-16.4	-14.0	-10.1	-11.0
4	Z 300/2.5	353	2.39	7200	uplift	∅ 6.3 cc 150	Trap.sheet 45/0.7	min.wool 50 mm	400	0.05	-39.1	-19.8	-14.8	-19.6
5	C 100/1.2	387	1.08	7200	pressure	2 ∅ 5.5 cc 1200	20/0.8	no	290	0.77	2.44	2.49	1.66	2.81
6	C 200/2.5	353	2.39	7200	pressure	2 ∅ 5.5 cc 1200	20/0.8	no	290	0.77	18.8	12.6	11.7	15.0
7	C 100/1.2	387	1.08	7200	uplift	2 ∅ 5.5 cc 1200	20/0.8	no	900	0.77	- 2.44	- 2.44	- 1.54	- 2.39
8	C 200/2	433	1.91	7200	uplift	2 ∅ 5.5 cc 1200	20/0.8	no	900	0.77	-17.6	-11.8	- 7.67	- 7.41

In table 2 results are given for tests on two-bay purlins. The reduction factor is determined for the section at the middle of the span.

Table 2. Results from tests on 2-bay beams. Span is 4200 + 4200 mm. Purlin Z 200/1.5. In tests nr 9 to 15 the profile was overlapped 1400 mm at the midspan. In the test nr 16 the purlin was continuous without overlapping.

test	yield strength (N/mm ²)	plate thickness (mm) ²	load direction	stiffness coefficients		ultimate load q kN/m		
				k_x (N/mm ²)	k_θ (Nmm/mm)	test result	diff.method	calculation model
9	412	1.46	pressure	1.25	1050	5.78	6.46	4.87
10	416	1.63	pressure	1.25	1050	6.89	7.36	5.72
11	420	1.62	uplift	1.25	1050	5.91	5.36 ¹⁾	5.49 ¹⁾
12	412	1.64	pressure	0.17	1220	5.95	6.42	5.99
13	400	1.63	uplift	0.17	1220	5.32	5.92 ¹⁾	5.38 ¹⁾
14	410	1.64	pressure	0.22	1450	5.37 ²⁾	6.43	5.71
15	422	1.62	uplift	0.22	1450	6.43	5.83 ¹⁾	5.55
16 ³⁾	278	1.43	pressure	0.44	1530	4.48 ²⁾	- (yield at 2.97)	2.93 (yield at 2.50)
						4.28 (yield at 3.43)		

¹⁾ the deflection of the web is included in the rotation θ

²⁾ slipping occurred in the seams of the bracing structure leading to failure

³⁾ continuous beam without overlapping

5. CONCLUSIONAL REMARKS

A calculating model for a wide range of use has been presented. Tests that have been performed show a satisfactory agreement between tests results and calculated values. The results show also the need of taking into account the side slip of the flange in compression even when it is braced especially if there is material between the purlin and the bracing stucture.

6. REFERENCES

- [1] Wlassow, W.S., Dünnewandige elastische Stäbe. Verlag für Bauwesen. Berlin 1965.
- [2] Roik, Carl & Lindner, Biegetorsionsprobleme gerader dünnwandiger Stäbe. Berlin W. Ernst & Sohn 1972.
- [3] Tunnpåsnorm 79. StBK-N5. Statens Stålbyggnadskommitté. Uppsala 1980. (Swedish Code for Thin-Walled Structures).
- [4] Peköz, T., Soroushian, P., Behaviour of C- and Z-purlins under wind uplift. Sixth Specialty Conference on Cold-Formed Structures. University of Missouri-Rolla.
- [5] Sokol, L., Proposal for design of purlins with one flange braces. 8.2.2.3 in European Recommendations for the Design of Light Gauge Steel Members. Draft 1985.
- [6] Schardt, R., Besonderheiten des Trageverhaltens dünnwandiger Querschnitte, Berechnungsgrundlagen.
- [7] Heselius, L., Continuous Purlins of Steel. Technical Research Centre of Finland. Research notes. 1986. (In finnish).

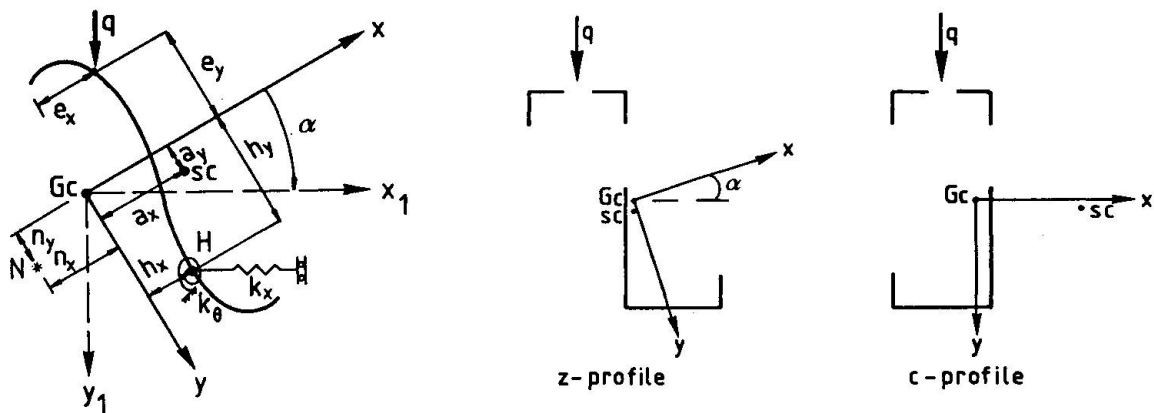


Fig. 1 Thin-walled open cross sections. G_c = gravity centre. S_c = shear centre. x, y are main axes. y_1 is load direction.

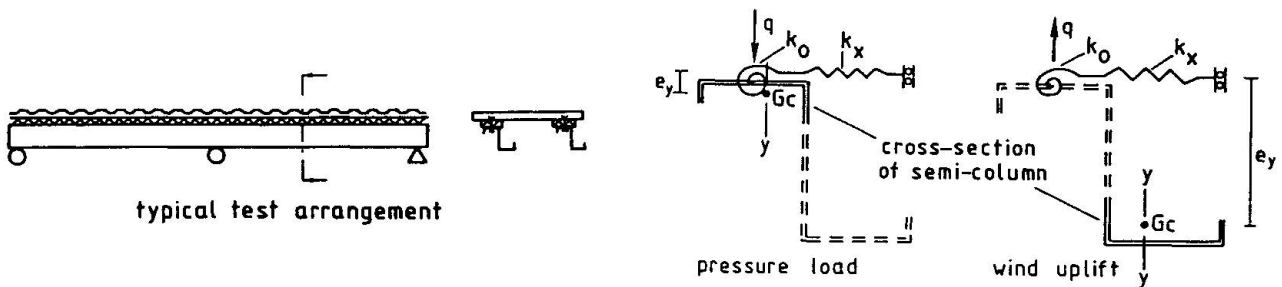
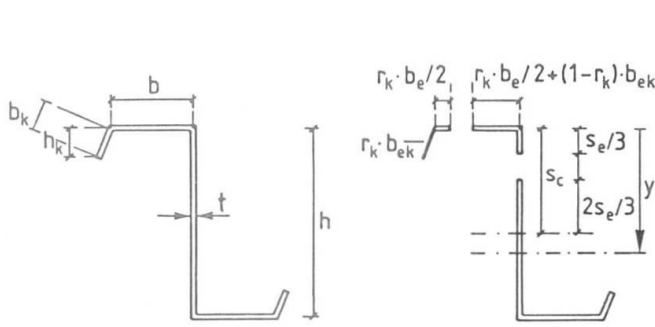


Fig. 2 Real structure and column for which critical stress is determined by means of calculations.



$$b_e = \frac{1}{\lambda_f} \left(1 - \frac{0.22}{\lambda_f} \right) \cdot b$$

$$\lambda_f = \frac{1.05}{\sqrt{4}} \cdot \frac{b}{t} \cdot \sqrt{f_y/E}$$

$$b_{ek} = 0.61 \cdot t \cdot \sqrt{E/f_y}$$

$$s_e = \frac{1}{\lambda_w} \left(1 - \frac{0.22}{\lambda_w} \right) \cdot s_c$$

$$\lambda_w = \frac{1.05}{\sqrt{7.81}} \cdot \frac{s_c}{t} \cdot \sqrt{f_y/E}$$

$$r_k = 1.49 - 0.6 \cdot \alpha$$

$$\alpha = 1.86 \cdot \sqrt{\frac{f_y \cdot b}{E \cdot t}} \cdot \sqrt{\frac{b + 2h}{h_k - 2t}}$$

Fig. 3 Calculation of the effective cross-section for a Z- and C-profile.

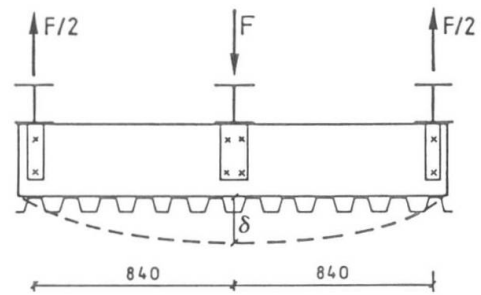
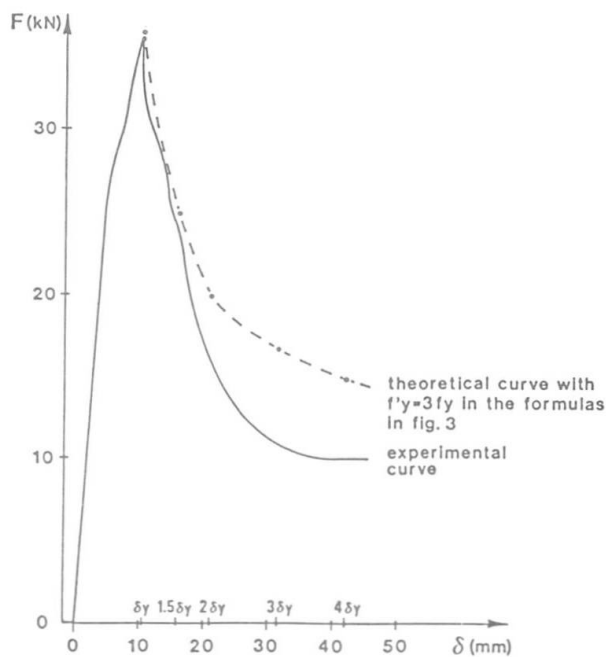


Fig. 4 Inelastic reserve for a Z-section 200/1.5 determined experimentally and theoretically.

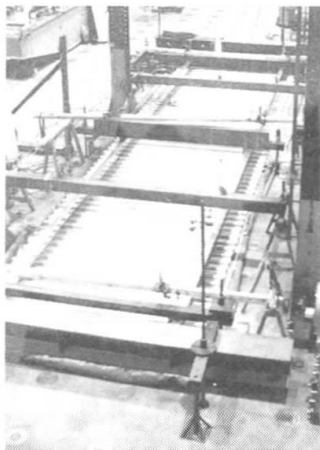


Fig. 5 Test no. 16 with air-bag system.

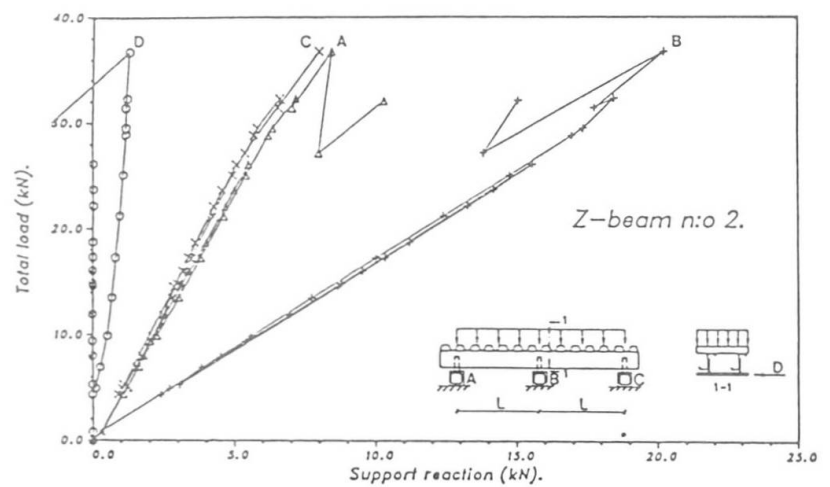


Fig. 6 Results for test no. 16.

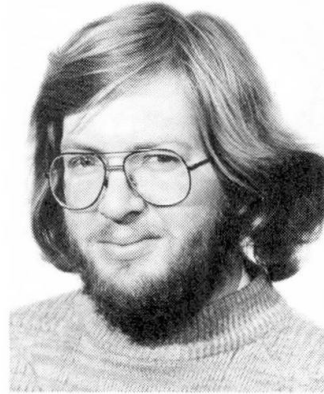
Non-Linear Behaviour of Thin-Walled Sections

Comportement non linéaire des profilés à parois minces

Nicht-lineare Verhalten von dünnwandigen Bauteilen

David MOORE

Senior Scientific Officer
Building Research Establishment
Garston, Watford, UK



David Moore, born 1956, earned his civil engineering degree at the University of Bradford and joined the Building Research Establishment in 1981. He is engaged in steelwork research and is currently investigating the stability of thin-walled members and the behaviour of beam-column connections.

SUMMARY

The paper examines theoretically and experimentally the influence of practical loading and warping restraint on the behaviour of thin-walled members. It is shown that loads which pass through the shear centre but which are not parallel to a principal axis do not produce pure bending. Furthermore, such loads can reduce the load at which instability occurs. It is also shown that warping restraint has a significant effect on instability.

RÉSUMÉ

Cette contribution concerne une étude théorique et expérimentale de l'influence des conditions réelles de mise en charge et d'appui résistant au gauchissement des profilés à parois minces. Il est montré que les charges qui sont appliquées au centre de cisaillement mais qui ne sont pas parallèles à un axe principal d'inertie ne provoquent pas une flexion uniaxiale. De plus, un tel chargement peut diminuer le niveau de la charge à laquelle l'instabilité se produit. Il est montré également que le gauchissement empêché a un effet déterminant sur la stabilité de l'élément.

ZUSAMMENFASSUNG

Der Einfluss der praktisch auftretenden Belastung und der Wölbbehinderung auf das Verhalten von dünnwandigen Bauteilen wird theoretisch und experimentell untersucht. Es wird festgestellt, dass Lasten, die durch den Schubmittelpunkt eines Bauteils gehen, aber nicht parallel zu einer Hauptachse sind, nicht nur reine Biegung verursachen. Solche Lasten können auch die kritische Last reduzieren (Instabilität). Es wird auch nachgewiesen, dass die Einschränkung der Wölbverformung eine bedeutende Einwirkung auf die Instabilität hat.



1. INTRODUCTION

Cold-formed, thin-walled members of open cross-section are now extensively used in building practice either as purlins or as sheeting rails. As these sections provide a more economical use of material than traditional hot-rolled sections their use as primary structural members is being investigated by some manufacturers. However, the thinness of the material used in manufacture and the process by which they are formed result in sections which have low torsional properties and only one or no axes of symmetry. The analysis of such sections is considerably more complex than that of traditional hot-rolled sections as they are prone to bi-axial bending and various modes of instability. Thus it is not surprising that very few reports have appeared on either the elastic behaviour or the stability of these sections.

There are many factors which influence the behaviour of cold-formed, thin-walled members, the major ones of which are:

- (a) The geometrical properties of the section.
- (b) The type and position of the boundary conditions.
- (c) The type and position of the applied load.
- (d) Material properties.

Of these, comparatively little work has been carried out on the type and position of both the applied load and boundary conditions. In particular the influence of load position, orientation of the load to the principal axes and the effects of warping restraint on the instability of mono-symmetric and asymmetric sections have received little attention.

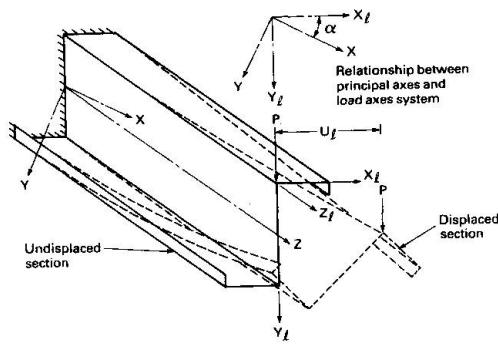
The effect of loads positioned above and below the shear centre has been investigated by Anderson and Trahair[1] for mono-symmetric sections. They concluded that loads positioned above the shear centre decrease the load at which instability occurs while those below increase it. However, in the case of asymmetric sections, the load is both eccentric to the shear centre and, in general, not parallel to a principal axis. The latter results in additional torsional moments in the member which increase with increased displacement and can have a significant effect on the behaviour and the stability of the section.

Nethercot and Rockey[2] investigated the effects of different boundary conditions on the stability of thin-walled members and concluded that for light-gauge sections warping restraint has a significant influence on the buckling load. Furthermore, they showed that its stabilizing influence lies between that of a simple support and a fully fixed support. They also showed that warping restraint has a more pronounced effect on stocky sections. This work, however, was derived for sections with one or more axes of symmetry and little experimental work exists for asymmetrical members.

This paper, therefore, presents a theoretical and experimental investigation into the effects of load orientation and warping restraint on the behaviour of cold-formed, thin-walled asymmetrical sections of different length.

2. THEORY

When considering the behaviour of a member it is usually assumed that the line of action of the loads relative to the principal axes of the member remains unaltered, even under loading.



If, as shown in Figure 1, the line of action of the load is inclined to the principal axes then the load moves relative to both the supports and the displaced principal axes. This generates additional torsional forces in the member which increase with increased deflection and have a marked influence on the behaviour of the member. By defining an additional axes system (X_1, Y_1, Z_1) which is coincident with the direction of the applied loads, as shown in Figure 1, Moore[3] derived the following equations which include the additional torsional moments:

Fig. 1 Typical movements of the applied load

$$EI_x \cdot V_{,zz} = -M_x(\cos\alpha + \beta \cdot \sin\alpha) - M_y(-\sin\alpha + \beta \cdot \cos\alpha) + T_z \cdot U_{,z}$$

$$EI_y \cdot U_{,zz} = M_x(-\beta \cdot \cos\alpha + \sin\alpha) + M_y(\beta \cdot \sin\alpha + \cos\alpha) - T_z \cdot V_{,z}$$

$$GC \cdot \beta_{,z} - EI \cdot \beta_{,zzz} = M_x(U_{,z} \cdot \cos\alpha + V_{,z} \cdot \sin\alpha) + M_y(-U_{,z} \cdot \sin\alpha + V_{,z} \cdot \cos\alpha) + T_z + T_d$$

Where M_x, M_y and T_z are the applied loads with respect to the principal X, Y and Z axes and T_d is the additional torsional moment. α is the angle between the principal axes of the member and the additional loading axes system and is shown in Figure 1. All the other terms have their usual meaning.

These equations represent the general expressions for the small displacement behaviour of a beam subject to combined bending and torsion. It is evident that U, V and β are all non-linear functions of the applied load and because of the inclusion of T_d , application of the load through the shear centre is not a sufficient condition to produce pure bending. Indeed pure bending can only occur if the right-hand side of the third equation vanishes. For this to occur, the resultant of the loads must pass through the shear centre and be parallel to a principal axis. When these conditions are fulfilled these equations become uncoupled and reduce to the usual differential equations for bending and torsion.

Expressions for the additional moments, T_d , have also been developed by Moore[3] for a simply supported beam subject to different load distributions and these are quoted below.

(a) eccentric u.d.l

$$T_d(g) = -q/2 \int_0^l (U(z) \cdot \cos\alpha + V(z) \cdot \sin\alpha + e \cdot \beta(z)) dz + q \cdot L (U(z) \cdot \cos\alpha + V(z) \cdot \sin\alpha) \\ + q \int_0^g (U(g) \cdot \cos\alpha + V(g) \cdot \sin\alpha - U(z) \cdot \cos\alpha - V(z) \cdot \sin\alpha) dz$$



where q is the applied load, $U(z)$ and $V(z)$ the displacements of the shear centre in the X and Y directions respectively, β is the rotation of the shear centre and, e , the vertical distance of the load above the shear centre.

(b) central point load

$$T_d(z) = P((U_c - U(z))\cos\alpha + (V_c - V(z))\sin\alpha + e.\beta(z))/2$$

Where P is the applied load and U_c and V_c the displacements of the shear centre in the X and Y directions respectively at mid-span.

(c) point loads at the quarter and three-quarter points

$$T_d(z) = P((U_q - U(z))\cos\alpha + (V_q - V(z))\sin\alpha + e.\beta(z))$$

Where P is the applied load at each of the quarter and three-quarter points and U_q and V_q the displacements of the shear centre in the X and Y directions respectively at the quarter points.

3. EXPERIMENTAL WORK

To assess the influence of the inclination of the load (with respect to the principal axes) and the warping restraint on the behaviour of thin-walled members, and to provide experimental data to verify the proposed theory, a series of tests were carried out on thin-walled cold-formed steel zed sections. A zed section was specifically chosen as its principal axes are naturally inclined to gravity loads. The test rig used for the experiment was designed by Salford University[4] to satisfy, as closely as possible, the following boundary conditions:

- (1) Simple supports about both principal axes
- (2) Restraint from twisting
- (3) Free and fixed warping

This test rig is shown in Figure 2. Because of the inclination of the principal axes of a zed section, it is difficult to devise a system which applies all the boundary conditions. However, by simply supporting any two axes at right-angles, any other two axes at right-angles which lie in the same plane will themselves have simple supports. Thus simply supporting the horizontal and vertical axes is equivalent to applying simple supports to the principal axes. These conditions were achieved by mounting the zed section through its shear centre on a steel bar supported at each end by frictionless bearings and mounting this assembly on a turntable. This arrangement is shown in Figure 3. Rotational fixity and free warping were achieved by attaching light gauge steel brackets to the top and bottom flanges of the section at each support. These brackets restrained the end rotations but allowed the section to warp. Fixed warping was achieved by clamping the section between 12mm thick mild steel plates. These plates were themselves restrained against twisting by the light-gauge steel brackets and are shown in Figure 3.

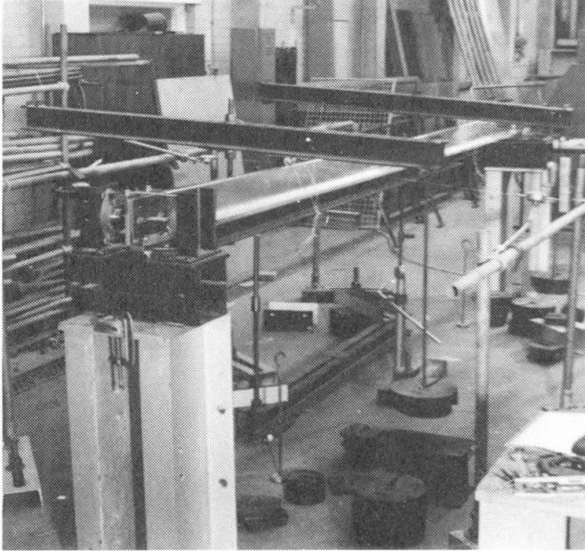


Fig. 2 General view of test rig

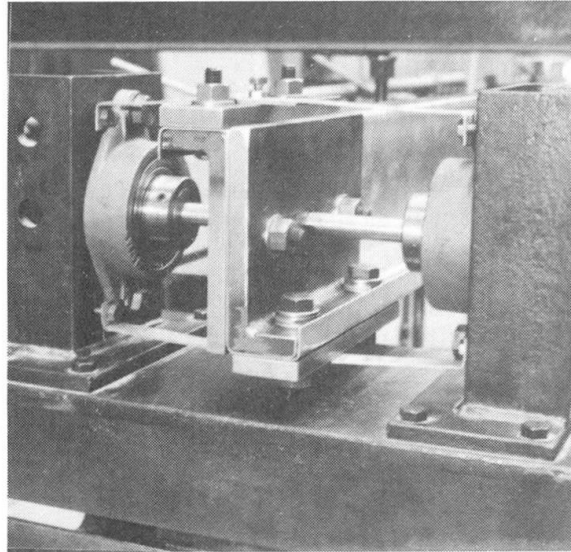


Fig. 3 Boundary conditions

The load was applied to the top flange of the section by means of a lever-arm system as shown in Figure 2. To ensure free movement of the load a roller bearing was placed between the underside of the lever-arm and the load points. With this system the lever-arm changes as the section moves, however, this was allowed for by measuring the horizontal movement of the section at each load point. In this way the actual load applied to the section can be determined from the following equation:

$$\text{applied load} = P \cdot (L_1 + L_2) / (L_1 + \delta)$$

where P is the weight applied to the lever-arm, L_1 and L_2 are the initial distances from the pivot point to the section and from the section to the load respectively and δ is the measured horizontal movement of the section.

Two dial gauges positioned parallel to the top and bottom flanges were used to monitor the horizontal displacement and the rotation of the section at each of the quarter, half and three-quarter points. Additionally a dial gauge was positioned at mid-span to monitor vertical displacement.

Nine tests were carried out on three different lengths (1000mm, 2500mm and 4500mm) of 140*50*1.6mm zed section subject to loads applied at the quarter and three-quarter points with eccentricities of -25mm, 0mm and 25mm from the shear centre. In each case the boundary conditions were simply supported about both principal axes, torsionally fixed and free to warp. Additionally, all three tests on the 2500mm length zed sections and two tests on the 4500mm length zed sections with eccentricities of -25mm and +25mm were repeated but with the warping restrained. In each case the load was incremented at the quarter and three-quarter points until failure occurred.



4. DISCUSSION OF RESULTS

4.1 The effect of load position and inclination

The load deflection characteristics shown in Figure 4 are for a simply supported, torsionally restrained and free warping zed section subject to loads at the quarter and three-quarter points and are typical of those obtained for all the tests identified in section 3. For each test the proposed theory follows the same general trend as the experiment and gives reasonable results for the displacements in the U direction and the rotations β .

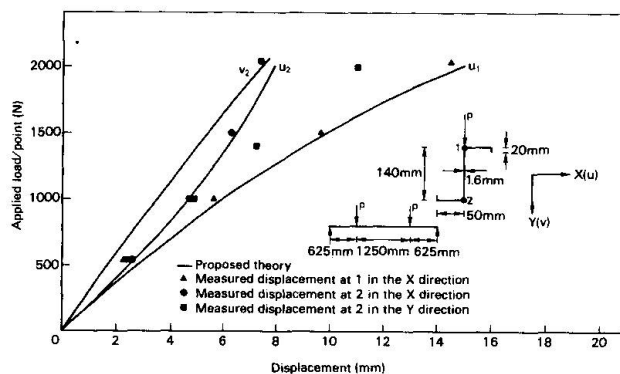


Fig. 4 Simply supported zed section subject to loads at the quarter and three-quarter points

However the theory is in poor agreement with the experimental displacements in the V direction. The reason for this is not clear but it is speculated that it is due to the rotation of the principal axes and the subsequent increase in displacement in the Y direction.

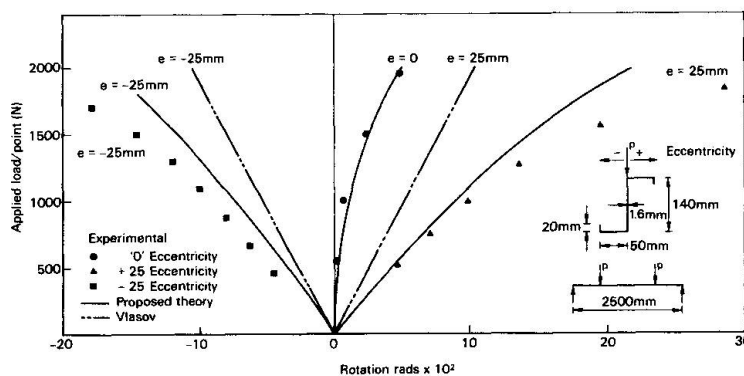


Fig. 5 Comparison between measured and computed rotations for different load eccentricities

Figure 5 shows the load rotation characteristics for the 2500mm long zed section with free warping subject to loads applied at the quarter and three-quarter points with eccentricities of -25mm, 0mm and 25mm. In each case both the

proposed theory and the experiment are non-linear and in good agreement. Also shown in Figure 5 is the theoretical solution of Vlasov[5] which is in poor agreement with both the experimental results and the proposed theory. It is also evident from Figure 5 that with the load through the shear centre ($e=0$) the section still twists.

It is interesting to note that both the proposed theory and the experiment give slightly smaller rotations when the load has a negative eccentricity than when the load has a positive eccentricity. This is due to the additional torsional moments, T_d , which act in the positive direction of β and therefore add to the torsional moments

produced by the loads with positive eccentricities and reduce those with negative eccentricities. This type of behaviour suggests that a combination of load orientation and positive eccentricity may result in a potentially more unstable condition than loads with the same orientation and a negative eccentricity. The experimentally obtained buckling moments for members with different

horizontal eccentricities are shown in Figure 6. Here positive eccentricity give consistently lower buckling moments than loads with negative eccentricities supporting the above argument. The exception to this is the 1000mm long section which gives marginally higher buckling moments for loads with positive eccentricities. It is also evident, from Figure 6, that eccentric loads generally reduce the load at which instability occurs and that this effect is most pronounced for members with low slenderness ratios.

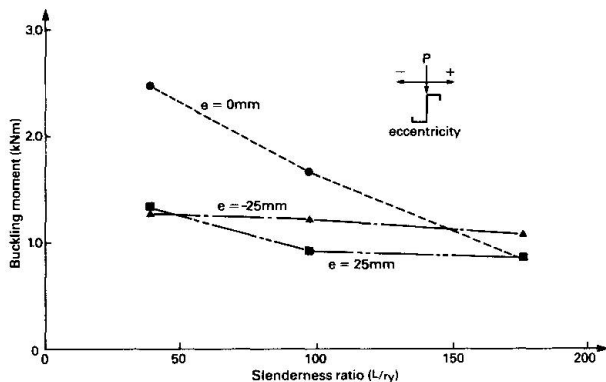


Fig. 6 Variation of buckling load with slenderness ratio and horizontal eccentricity.

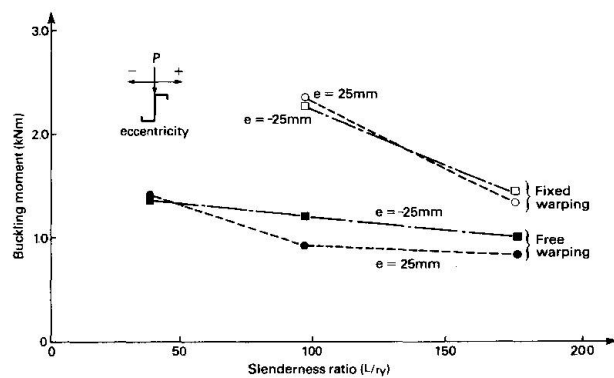


Fig. 7 Influence of warping restraint on buckling moment

4.2 The influence of warping restraint

Figure 7 shows the experimental values of buckling moment plotted against slenderness ratio for sections tested with and without warping restraint. From this limited number of tests it is evident that warping restraint has a significant effect on the buckling load. If the warping is fixed an increase in buckling moment of about 60% is obtained over the same section with free warping. It is also noted that the influence of warping restraint is more pronounced for beams with lower slenderness ratios. Thus an assessment of the warping restraint provided by practical boundary conditions must be made if structures which are either too conservative or unsafe are to be avoided. The Building Research Establishment is currently investigating the warping restraint provided by practical supports.



5. CONCLUSIONS

This paper proposes a non-linear theory for the behaviour of thin-walled members which includes the effect of load position and inclination. The theory is compared with experimental data in which the eccentricity of the load is varied. Additionally, a number of tests were carried out in which the effect of warping restraint on instability is investigated and the following conclusions applicable to unrestrained, simply supported thin-walled beams are drawn:

- (a) The proposed theory and experiment are in reasonable agreement for displacements and rotations.
- (b) Pure bending can only occur if the resultant load passes through the shear centre and is parallel to a principal axis.
- (c) The position and inclination of the load from the principal axes have a significant effect on the behaviour of thin-walled beams.
- (d) Loads above the shear centre, with a positive eccentricity and which are inclined to the principal axes decrease the critical load.
- (e) Warping restraint has a pronounced effect on buckling load.

6. ACKNOWLEDGMENTS

The work described in this paper forms part of the current programme of the Building Research Establishment (BRE). Experimental work forming part of this programme was carried out for BRE at Salford University. This paper is published by permission of the Director, BRE.

7. REFERENCES

1. ANDERSON J M and TRAHAIR N S., Stability of monosymmetric beams and cantilevers. Journal of the Structural Division, ASCE, 98(ST1), Proc paper 8646, 269-86, 1972.
2. NETHERCOT D A and ROCKEY K C., A unified approach to the elastic lateral buckling of beams. The Structural Engineer, July 1971, No. 7, Vol. 49, 321-30.
3. MOORE D.B., A non-linear theory for the behaviour of thin-walled sections subject to combined bending and torsion. In press.
4. LEACH P., Buckling behaviour of light gauge steel beams. Private report for the Building Research Establishment, 1985.
5. VLASOV V Z., Thin-walled elastic beams. Israeli programme for scientific translations, Jerusalem, 1961.

New British Code for the Design of Aluminium Structures

Nouveau code britannique pour le dimensionnement des structures en aluminium

Neue britische Vorschrift für die Bemessung von Aluminiumkonstruktionen

Philip S. BULSON

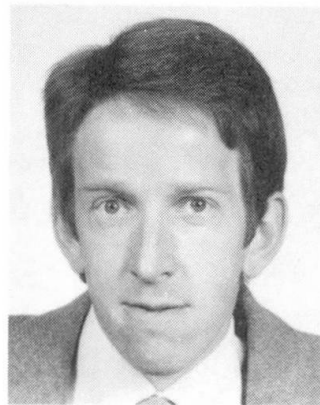
Director
Mott Hay & Anderson
Winchester, UK



Philip Bulson was a postgraduate at Bristol before he began his career in research, development and management of military engineering. Much of his work has dealt with military aluminium structures, and he is chairman of the codes of practice committee for structural aluminium.

David A. NETHERCOT

Senior Lecturer
Univ. of Sheffield
Sheffield, UK



David Nethercot, born 1946 obtained his degree at University College Cardiff where he was also an ICI Fellow. He has been active in research, teaching and code drafting in steel and aluminium structures at Sheffield since 1971.

SUMMARY

The procedures for the determination of the static strength of thin-walled members in BS 8118, the new UK code for the structural use of aluminium are summarised. Attention is concentrated on the various forms of instability that must be considered, with particular attention being given to those special aspects of aluminium construction which distinguish it from structural steelwork.

RÉSUMÉ

Les procédures utilisées pour déterminer la résistance statique des éléments à parois minces, qui figurent dans le nouveau règlement britannique «British Standard 8118», concernant l'emploi structurel de l'aluminium, sont résumées. Une attention particulière est accordée aux diverses formes d'instabilité qu'il faut prendre en compte, en soulignant surtout les aspects propres aux structures en aluminium qui les distinguent des constructions en acier.

ZUSAMMENFASSUNG

Die Verfahren zur Bestimmung der statischen Festigkeit von dünnwandigen Bauelementen nach BS 8118 (die neue englische Vorschrift für die konstruktive Verwendung von Aluminium) werden zusammenfassend beschrieben. Die verschiedenen zu berücksichtigenden Instabilitätsformen werden im Detail behandelt. Besonders hingewiesen wird auf diejenigen Merkmale der Aluminiumkonstruktionen, die sie von den Stahlkonstruktionen unterscheiden.



1. INTRODUCTION

The current British Code of Practice for Structural Aluminium (CP 118) was published in 1969, and although aimed at general engineering structures of most types (but not aircraft or aerospace structures), its roots lay in earlier Reports by the Institution of Structural Engineers on the structural use of aluminium alloys in building. CP 118 acknowledged that in pursuit of structural efficiency thin-walled structural members were part of a designers tool-kit, and the problems of local and torsional instability, and of lateral buckling, were pursued in depth.

The British Code is now under revision, and a new version, BS 8118, is due in late 1986 or early 1987. It has been written in limit state format, and as well as the changes that result from this, there has been a considerable extension of the treatment of static strength, fatigue life and joint analysis. The problem of heat affected zones in welded structures has received attention in the light of British research, and in addition new design rules for the ultimate strength of structural components subjected to loads that induce buckling have been established. These use the results of research and testing in many countries during the 1970's and early 1980's.

The purpose of this paper is to summarise the important developments incorporated in the new code, with particular reference to thin-walled structures. There are several areas that need discussion here: design principles; heat affected zones; the static strength of struts, ties, beams, plates, beam-columns and plate girders.

2. DESIGN PRINCIPLES

It is recognised that all structures must be checked for static strength, deformation and corrosion. In addition, certain structures will also need to be examined for overturning, fatigue and vibration.

For static strength the procedure is to check that for a component the factored resistance is not less than the Action under the factored loading $\times \gamma$, where λ_c is a partial factor to take account of the consequences of failure. The factored resistance is the calculated resistance $\div \gamma_m$, where γ_m is the material partial factor. This factor takes account of differences between the strength of material test specimens and the strength of the actual material in the structure as manufactured.

The load factor, γ_f , is the product of two components γ_{f1} and γ_{f2} . Factor γ_{f1} will be given by the relevant British structural loading standard, where one exists, but to check the strength of a structure where no guidance is available, BS 8118 suggests a set of factors to take account of dead loading, imposed loads (other than wind loads), wind load, and forces due to temperature effects. The load factor γ_f , to take account of the low probability that the severest loading actions will occur simultaneously, can be found analytically if enough statistical information exists, but for preliminary designs the code gives simple values (1.0, 0.8, 0.6 etc.) that are known to give reasonable agreement with more exact probability analysis. In certain codes γ_c is incorporated in γ_f or γ_m , but because of the wide-ranging use of BS 8118 separate values are given in this Code.

3. HEAT-AFFECTED ZONES (HAZ)

The treatment of Heat-affected zones in BS 8118 represents a notable step forward from earlier codes. Recent research at Cambridge University (1) has thrown a new light on the extent and strength of these zones, and much of this work has been incorporated in the design rules.

Thus detailed guidance is given for a variety of weld types, welding procedures and alloy classes. This will frequently lead to smaller strength reductions than those obtained with the old "one inch" rule.

4. STATIC STRENGTH OF STRUCTURAL MEMBERS

Almost one half of the Code is devoted to the detailed procedures required for the determination of the resistance of ties, struts, beams etc. The form of these may best be appreciated by considering the clauses for one particular type of element in some detail; the material covering the design of laterally unrestrained beams has been selected as representative of the general style.

4.1 Unrestrained Beams

The resistance moment M_{max} is determined from:

$$M_{max} = M_S C_{LT} / \gamma_m \quad (1)$$

in which M_S = basic moment capacity

C_{LT} = reduction factor for lateral buckling

γ_m = material factor (1.2 for extruded beams, 1.25 for welded beams)

Presentation of the design expression in this way provides explicit recognition of the various phenomena that influence beam strength. Thus M_S , which does, of course, represent the resistance for a beam not susceptible to lateral-torsional instability such as a box-section or a closely braced or continuously restrained I-section, is obtained as:

$$\begin{aligned} M_S &= f_{0.2} Z_p && \text{for a compact section} \\ f_{0.2} Z_p > M_S &\geq f_{0.2} Z_e && \text{for a semi-compact section} \\ M_S &= f_{0.2} Z_{eff} && \text{for a slender section} \end{aligned} \quad (2)$$

Since section classification depends upon the extent to which local buckling affects its capacity, the class of a particular section will depend principally upon the width/thickness ratio of its most slender plate element. Account is also taken of alloy strength, stiffeners and the presence of any weakened HAZ material through the use of a plate slenderness parameter defined as:

$$\frac{hb}{t} \sqrt{sf_{0.2}/250} \quad (3)$$

in which b = plate width

t = plate thickness

h = factor to allow for the effect of stiffeners

s = reduction factor for HAZ effects

$f_{0.2}$ = 0.2 percent proof stress in N/mm^2

Fig. 1 illustrates the dependence of M_S on b/t for two particular alloys for an unstiffened box section. This also shows how the practice in CP 118 of requiring separate design curves for each alloy has been simplified to consideration of two groups, the division between which is made solely on the basis of the ratio $f_u/f_{0.2}$, in which f_u is the ultimate tensile strength of the material. Since this is related to the parameter n used in the Ramberg-Osgood representation of the stress-strain curve, it distinguishes between material with a very rounded stress-strain curve for which $f_u/f_{0.2} \geq 1.4$ and more sharply yielding material for which $f_u/f_{0.2} < 1.4$. For the former Z_p is not used because of the large strains and thus excessive deformations needed to reach ' M_p '. In determining Z (plastic, elastic or effective) it is, of course, necessary to allow for the presence of HAZ material whose strength is less than $f_{0.2}$. Inclusion of when calculating plate slenderness recognises the lower stresses present in the unaffected zones of welded members that results from the use of these lower Z values.



The lateral buckling reduction factor C_{LT} is given in terms of a beam slenderness λ_{LT} which is based directly on the fundamental parameter $\sqrt{M_S/M_{Cr}}$, in which M_{Cr} is the elastic critical moment. This follows the practice of several recently published steel codes - notably EC3 - but in line with recent U.K. practice considerable assistance is given with the calculation of λ_{LT} for the more common structural shapes. Thus for I's, channels and tees λ_{LT} is given by

$$\lambda_{LT} = u v (\ell/\rho_y) \sqrt{f_{0.2}/250} \tag{4}$$

in which $u = 0.85$ for symmetrical I's, 0.75 for symmetrical channels and 1.0 for tees

$v = f(\frac{\ell}{\rho_y} \times \frac{t}{D_b}, N)$ is obtained from a graph

- ℓ = effective length
- ρ_y = radius of gyration about the weak axis
- t = mean flange thickness
- D_b = overall depth
- $N = I_c/(I_c + I_t)$ is a measure of the degree of monosymmetry

Explicit expressions for λ_{LT} are also provided for solid and hollow rectangular sections. All of these assume $M_S = f_{0.2} Z_p$.

Positioning of the actual $C_{LT} - \lambda_{LT}$ design curve was based largely on test data (2) since no complete theoretical solution embracing the combined effects of inelastic material behaviour, initial geometrical imperfections etc. is presently available. Tests from 4 types of cross-section under 5 different patterns of loading were employed. Fig. 2 compares the resulting design curve with these data. Following the approach taken with the strut curves, as well as that employed generally for buckling problems in recent U.K. codes, this may be represented by a modified Perry equation of the form

$$(M_{Cr}/M_S - C_{LT})(1 - C_{LT}) = \eta C_{LT} M_{Cr} \tag{5}$$

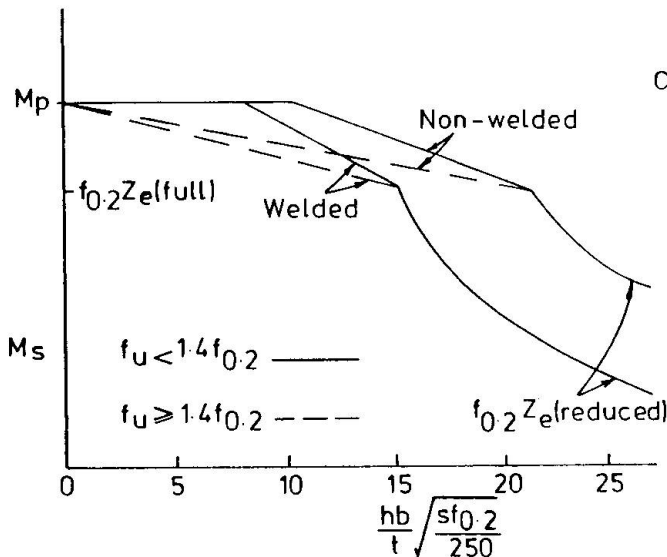


Fig. 1 Moment Capacity M_S - plotted for a beam with $f_u = 1.2f_{0.2}$ or $f_u = 1.4f_{0.2}$ with capacity controlled by an internal element

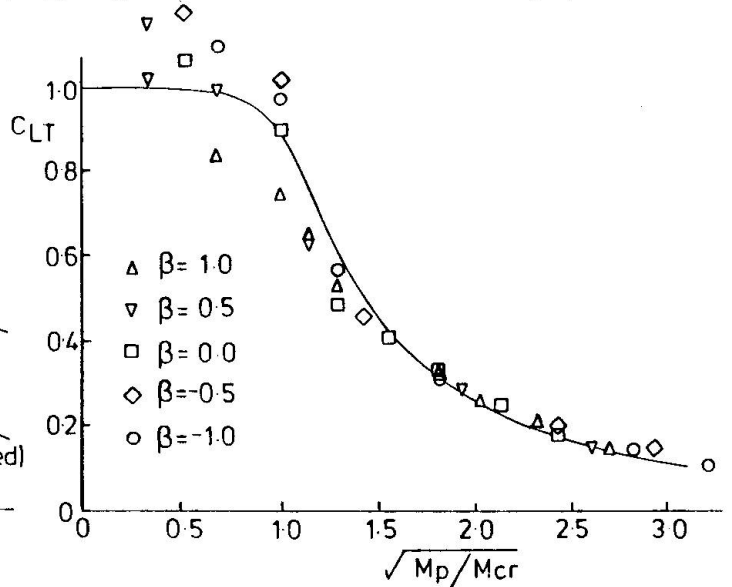


Fig. 2 Values of C_{LT} for lateral-torsional buckling, β = ratio (smaller end moment)/(larger end moment)

In the absence of either a comprehensive theoretical treatment or a sufficiently large and well structured body of test data, differentiation between classes of section in the manner of multiple column curves (which are used in this Code)

was not possible. A particular difficulty was caused by the absence of test data for welded beams, where evidence for steel (3) demonstrates the lower lateral buckling strength of such members. Although the reduction in basic cross-sectional strength is allowed for in the determination of M_5 , the existence of a further deleterious interaction of HAZ and residual stresses on overall buckling is a possibility. A single design curve has therefore been given corresponding to

$$\eta = 0.001 (\lambda_{LT} - 10.6) / \sqrt{f_{0.2}/250} \quad (6)$$

Whether or not this gives lower safety margins in the case of welded beams will have to await the production of the necessary data. For the 80 test results on extruded members the mean of the ratio (predicted strength)/(test strength) is 1.013 with a standard deviation of 0.11. In making these comparisons actual measured cross-sectional dimensions and material properties (including the compressive 0.2 per cent proof stress where possible) were used.

Fortunately 27 of these tests (4) were conducted under unequal end moment loading, thereby providing an opportunity to check the suitability of the equivalent uniform moment concept as a means of recognising the generally less severe effects of a non-uniform moment on lateral stability. Fig. 2 shows how the Code's provision for using

$$\bar{M} = m M_1 \quad (7)$$

in which $m = (0.6 + 0.4 M_2/M_1) \leq 0.40$

M_1, M_2 = larger and smaller end moments respectively

in place of M_1 causes these results to plot with those for uniform bending. The use of m -values of less than unity does, of course, mean that an additional check that M_1 does not exceed M_5 is also necessary.

Guidance is also provided, through the use of effective length factors, on the approximate effects of end fixity and destabilising loads i.e. those applied above the level of the shear centre in such a way that they are free to move sideways with the beam as it buckles. In the case of cantilevers, factors previously included in recent U.K. steel codes recognise the importance of restraint of the tip and, in the case of cantilevers formed by overhanging spans, at the vertical support.

The enterprising designer is given the opportunity to use research data for M_{cr} by giving the basic expression for λ_{LT} as

$$\lambda_{LT} = 53 \sqrt{M_5/M_{cr}} \quad (8)$$

This approach should also prove advantageous for beams containing slender plate elements for which M_5 should be determined using Z_{eff} . Using some of the test data obtained by Cherry (5), Fig. 3 shows how the use of the simplified Eq. 4 for the full section leads to very conservative allowances for the interaction of local and overall buckling. Cherry's tests were conducted on specimens with extremely thin compression flanges for which the Code gave t_e/t values of around one fifth, leading to values of M_5 of approximately one half of $f_{0.2} Z_p$. For sections just requiring the use of Z_{eff} the difference would, of course, be substantially less. An improved, but still conservative, result may be obtained if the approximate λ_{LT} is reduced in the ratio $\sqrt{Z_{eff}/Z_p}$.

4.2 Other Types of Member

Strut design is based on an expression analogous to Eq. 1 with the important difference that C_c , the reduction factor for flexural buckling, is defined by the 5 column curves shown in Fig. 4 with the allocation of a particular member being on the basis of cross-section, alloy and method of manufacture as given in Table 1. Because of the multiplicity of shapes possible with the extrusion process, torsional buckling is more likely than is the case for conventional steel sections. Accordingly a separate check that the reduction factor for



torsional buckling C_T , the value of which is obtained using $\lambda_t \sqrt{E_{0.2}/250}$ in which $\lambda_t = 830/\sqrt{E_{cr}}$ and f_{cr} is the elastic critical stress for torsional buckling, is not less than C_c , will often be required. Procedures to assist with the rapid determination of λ_t (or f_{cr}) are provided for several structural shapes. The particular values of C_T given are largely based on 2 large series of tests (6, 7).

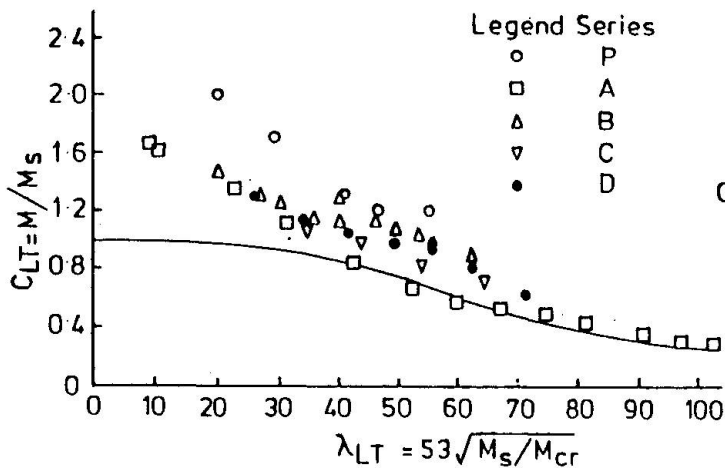


Fig. 3 Lateral-torsional buckling of beams containing slender plate elements

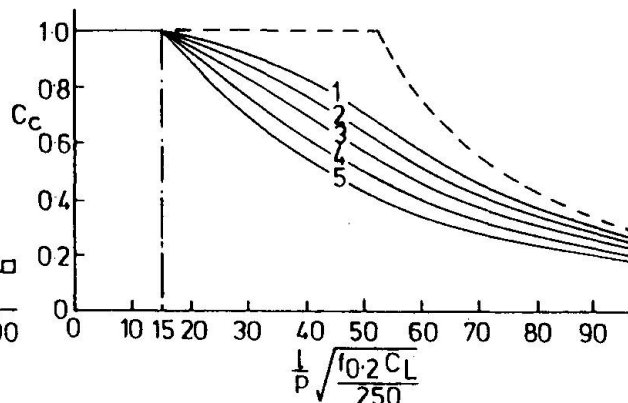


Fig. 4 Values of C_c for flexural buckling

Cross-Section		$f_u/f_{0.2}$ < 1.2	$f_u/f_{0.2}$ > 1.2
symmetric	non-welded	1	3
	welded	2	4
asymmetric	non-welded	2	4
	welded	3	5

symmetric $Y_1 / Y_2 < 1.2$
 asymmetric $Y_1 / Y_2 > 1.2$
 where Y_1 and Y_2 are extreme fibre distances

Table 1 Column curve selection

Members subject to combined bending and compression (or tension) are treated by means of interaction formulae. These are similar to those of the new U.K. steelwork code careful checking against several series of test data (2) having confirmed their suitability. Thus for the most general case of biaxial bending, buckling failure is checked using

$$\frac{\bar{M}_x}{M_{ax}} + \frac{\bar{M}_y}{M_{ay}} > 1 \tag{9}$$

in which M_{ax} is the lesser of

$$M_{ax} = M_{max} (1 - P/P_{cy}) \quad \text{for weak axis failure}$$

$$M_{ax} = \frac{(1 - P/P_{cx})}{(1 + P/P_{cx})} \frac{M_{sx}}{\gamma_m} \quad \text{for strong axis failure}$$

and M_y is obtained from the second expression by replacing x with y .

Treating the biaxial problem in this two stage fashion enables potential difficulties over factors such as different effective lengths for strong and weak axis column buckling, uncertainty over the governing mode under strong axis bending etc. to be avoided.

Plate girder design (8) is based on the type of interaction diagram for combined moment and shear shown as Fig. 5, which is similar to that used in the U.K. steel bridge code. Since V_{CF} and M_{CF} represent the shear capacity of the web alone and the moment capacity of the flanges alone, girders may be designed relatively simply for V_{CF} and M_{CF} in situations where M and V are both significant or for full moment and $V_{CF}/2$ or full shear and $M_{CF}/2$ where one type is dominant. Tension field action is utilised for vertically stiffened girders when determining the reduction factor C_{5T} on full shear capacity. When combined with longitudinal stiffeners the latter are assumed to affect only the initial buckling of the web. Thus C_{5T} is given by

$$C_{5T} = v_1 + v_2 + m^* v_3 \quad (10)$$

in which v_1 = represents initial buckling resistance

v_2 = contribution due to tension field action anchoring on the transverse stiffness

v_3 = additional contribution due to flanges

m^* = measure of flange strength

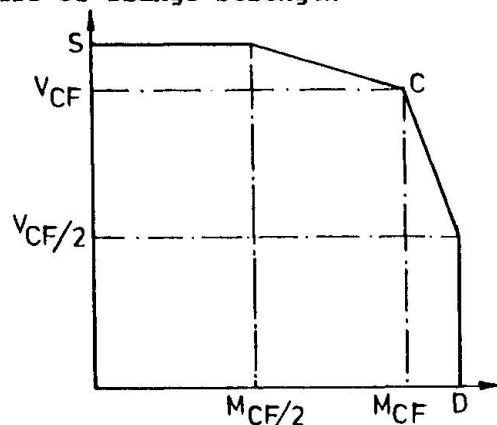


Fig. 5 Moment/shear interaction diagram

Graphs for determining each of these 4 quantities in terms of web slenderness d/t and panel aspect ratio a/d are provided.

The topics of joint design and fatigue have been treated in broadly the same fashion as in recent U.K. steel codes but noting any special features present in aluminium. Interested readers are referred to the appropriate papers (9, 10) of the draft code symposium for a brief account of the most important developments and to the forthcoming book (11) on the background to the Code for a lengthier treatment.

4.3 Topics Identified as Requiring Further Study

Although the Code incorporates the findings of much recent research, in several areas the drafting was hampered by insufficient data. On this basis the following are noted as requiring some attention:

1. Ultimate strength of members containing HAZ, particularly when these are due to transverse welds.
2. Ultimate strength of sections containing slender plate elements, particularly when these elements are subject to non-uniform stress.
3. Ultimate strength of members subject to biaxial bending and torsion.



Of course no code can cover every considerable situation adequately and it is for this reason that an important section of the Code is that covering the conduct of physical testing as a basis for design.

5. CONCLUSIONS

Certain aspects of the new British Code for the structural use of aluminium, BS 8118, have been summarised. Calibration studies against the previous document, CP 118, suggest that the new Code is more economic in terms of material usage and more rational in its coverage.

6. ACKNOWLEDGEMENTS

The authors are grateful to the many people who have assisted with the development of the Code and whose work forms the basis for the material contained therein. The contribution of Mr J.B. Dwight to the formulation of design clauses is particularly acknowledged.

REFERENCES

1. Robertson, I. and Dwight, J.B., "HAZ Softening in Welded Aluminium", 3rd International Conference on Aluminium Weldments, Munich, 1985.
2. Mazzolani, F.M., "Aluminium Alloy Structures", Pitman, London, 1985.
3. Fukumoto, Y., and Kubo, M., "A Survey of Tests on Lateral Buckling Strength of Beams". Preliminary Report, Second International Colloquium on Stability of Steel Structures, Liege, 1977.
4. Clark, J.W. and Jombock, J.R., "Lateral Buckling of I-beams Subjected to Unequal End Moments", J. Eng. Mech. Div., ASCE, EM3, 1957.
5. Cherry, S., "The Stability of Beams with Buckled Compression Flanges", The Structural Engineer, Sept. 1960.
6. Baker, J.F. & Roderick, J.W., "The Strength of Light Alloy Struts", Aluminium Development Association Report No. 3, 1948.
7. Smith, R.E., "Column Tests on Some Proposed Aluminium standard Structural Sections", Report B-IR-241-54-30/2, Aluminium Laboratories, Banbury, 1954.
8. Evans, H.R., "Design of Plates and Plate Girders", Symposium on The Structural Use of Aluminium, Institution of Structural Engineers, October 1985.
9. Cullimore, M.S.G., "Joints", Symposium on the Structural Use of Aluminium, Institution of Structural Engineers, October 1985.
10. Ogle, M., "Fatigue", Symposium on the Structural Use of Aluminium, Institution of Structural Engineers, October 1985.
11. Bulson, P.S. ed., "Aluminium Structures", Elsevier Applied Science Publishers, 1987.

Postcritical Behaviour of Thin Aluminium Plates

Comportement postcritique des tôles minces en aluminium

Überkritisches Verhalten dünner Aluminiumbleche

Sándor FERNEZELYI

Civil Engineer
Hungalu Eng. and Dev. Centre
Budapest, Hungary



S. Fernezelyi, born 1942, received his civil engineering degree and Ph.D. at the Technical University of Budapest. For eighteen years he was involved in problems of load-bearing aluminium structures. He is the designer of several large span aluminium roofs. S. Fernezelyi is now responsible for the engineering activity of the Hungarian Aluminium Co.

SUMMARY

According to our experiments, the structural components made of thin plates and loaded in unidirectional and uniform compression, lose their load-bearing capacity so that a plastic mechanism develops within which the lines of the plastic hinges are curved. Assuming a crushing profile that adequately approximates to the reality and considering the difference between the patterns of both the elastic and the plastic deformations, and also, considering the initial curvature of the plate, the value of ultimate load can be determined as a function of the plate's slenderness.

RÉSUMÉ

Nos essais ont montré que les éléments en tôle mince soumis à une compression uniforme perdent leur capacité portante par formation d'un mécanisme de ruine dans lequel les lignes de rupture plastique sont courbes. A l'aide d'un modèle de rupture proche de la réalité, en tenant compte des différences entre les valeurs élastique et plastique des déplacements et en considérant aussi les déformations initiales de l'élément, la valeur de la charge ultime de la plaque peut être déterminée en fonction de son élancement.

ZUSAMMENFASSUNG

Unsere Versuche haben gezeigt, dass die durch gleichmässigen Druck in einer Richtung belasteten dünnen Blechelemente ihre Tragfähigkeit verlieren, indem sich ein plastischer Mechanismus ausbildet, dessen Fliesslinien gebogen sind. Wenn wir ein der Wahrheit nahe stehendes Bruchbild annehmen und den Unterschied zwischen den elastischen und plastischen Verformungsmustern sowie die Anfangskrümmung des Bleches berücksichtigen, kann der Wert der maximalen Last als Funktion der Blechschlankheit bestimmt werden.



1. INTRODUCTION

Corrugated sheets being of wide use in building construction are made of substantially thinner material than that used in load-bearing structures in general. In spite of the fact that increased attention has been focused on post-critical behaviour of plates [1], [2], rather limited experimental and theoretical knowledge is still available concerning such ranges of width-to-thickness ratio. This is particularly true in the case of aluminium plates.

In order to establish the ultimate load, the form of collapse, the shape of the plastic mechanism should previously be determined. Most of the authors [3], [4], [5] assume that lines of the plastic hinges are straight, so that the shape of the plastic mechanism involves two triangles and two trapezoids (See Fig. 3/a). It is also assumed [5] that ultimate strength of the plate can be found as the intersection of a post-buckling loading curve with a plastic unloading line. However, experimental data have not fully confirmed the theoretical results [6].

2. DESIGN OF EXPERIMENTS

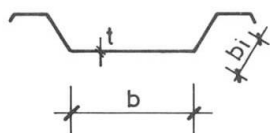


Figure 1.

In order to expand our data base, a far-flung experimental project has been recently accomplished. Characteristic cross-section of the samples are shown on Fig.1. Eccentric compression was used for loading. The samples were prepared with the use of standard corrugated sheets manufactured by the Hungarian Aluminium Corporation. For the trial runs, samples of various length, width, thickness and alloy were used. In all, 78 samples representing 22 types, were tested. Thus, our results are considered fairly appropriate to draw conclusions of general character.

Our investigations included testing of:

- initial imperfections;
- critical buckling load experienced during the tests;
- post-critical behaviour, and the ultimate load of the plate;
- interaction between the general and local buckling, in order to determine the ultimate load of the entire structural component.

The results were given in detail elsewhere [7], therefore, we shall herein use only experimental results concerning initial imperfections and the ultimate load of the plate.

We consider our experimental result a substantial one, namely that, in all cases, the shape of the plastic mechanism is as shown on Fig.2, i.e. the lines of plastic hinges are curved!

3. RANGE OF INVESTIGATIONS AND THE INITIAL ASSUMPTIONS

For comparison with previous experiments we have limited the field of investigations and made the following initial assumptions (for the applied notes, see Fig.1):

- (i) the sections are cold formed, their thickness is constant, i.e. $t = \text{const.}$;
- (ii) the plates are "extremely" thin, where slenderness ratio of one component plate is: $b/t > 80$;

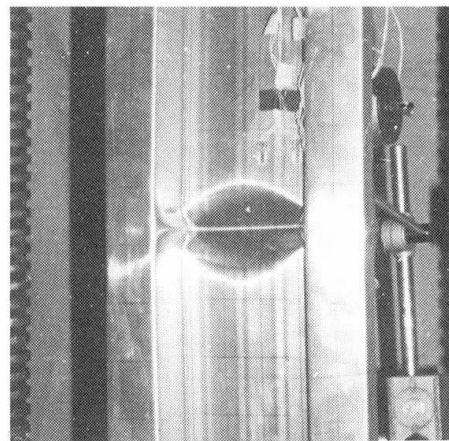


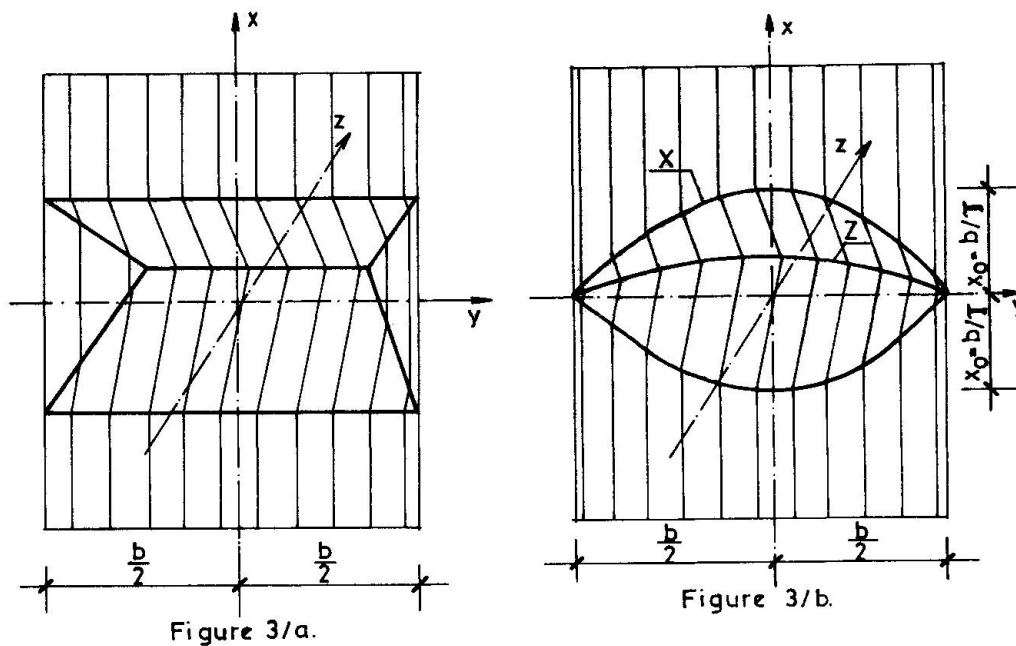
Figure 2.

- (iii) slenderness ratio of the connecting plates is much lower, i.e. $b_1 < 1/2 b$. Thus, buckling of such plates has no effect on the loading capacity of the entire section. Otherwise, the widest plate can be considered being simple supported;
 - (iv) the load is such as to cause uniform displacement at the loaded edges;
 - (v) the unloaded edges are stress free, thus, they do not remain straight;
 - (vi) collapse of the section shall always take place through the collapse of the widest plate component;
 - (vii) local deformation of the unloaded edges has no significant effect on the collapse load.
- Our experiments demonstrated that collapse of the component plate is frequently associated with simultaneous collapse of the edges. The value of yield stress is assumed to develop at the unloaded edges.
- (viii) lines of the plastic hinges are curved.

4. SHAPE OF THE PLASTIC MECHANISM

Figure 3/a shows that shape of the plastic mechanism which has been normally assumed in the literature, compared to Fig. 3/b which in turn, shows the shape proposed by us in conformity with the experimental results.

The function that describes the surface (according to the co-ordinate system shown in Fig. 3/b) is the following:



$$\frac{x}{X} + \frac{z}{Z} = 1 \tag{1}$$

Herein, "X" and "Z" represent functions of the curves which describe the lines of the plastic hinges and determine the character of the buckled shape.

Perpendicular sections of the surface shall create straight lines. (This proposed shape is the product of an approximation since the line described by the "X" function does not lie in the reference plane, however, showed that the resultant neglect is of no significance.)



The "x" and "z" curves which determine the surface as well as the in-plane displacement (δ) are not independent.

$$x = \frac{z^2 - \delta^2}{2\delta} \quad (2)$$

The angle experienced at the lines of the plastic hinges shall be:

$$\varphi_V = \text{tg}^{-1} \frac{2\delta z}{z^2 - \delta^2} \quad (3)$$

Assuming existence of discrete angles in the plane of the other main curvature, its value can be given as:

$$\Delta\varphi_H = \left\{ 2\delta x_1 \left[2ZZ' \frac{z^2 - 3\delta^2}{(z^2 - \delta^2)^3} - z'' \frac{z^2 + \delta^2}{(z^2 - \delta^2)^2} \right] - z'' \right\} \cos \varphi_V \cdot \Delta x \quad (4)$$

where: x_1 gives the locality of the investigated horizontal section
 Δx distance between horizontal sections

With the use of the above findings and by taking notice of the yield conditions, we can determine the external and internal part of the plastic work effected during deformation.

5. STRESS DISTRIBUTION

Based on equal external and internal plastic work and after certain mathematical transformations, we can describe the distribution of stress:

$$\frac{n}{n_{pl}} = \frac{t}{4} \left\{ \left[1 - \left(\frac{n}{n_{pl}} \right)^2 \right] \frac{2}{\delta} \left[\text{tg}^{-1} \frac{2\delta z}{z^2 - \delta^2} \right] + \left[1 - \frac{1}{2} \left(\frac{n}{n_{pl}} \right)^2 \right] \frac{1}{2} \left[2ZZ' \frac{z^2 - 3\delta^2}{z^2 - \delta^2} - \frac{z''}{2} (3z^2 - \delta^2) \right] \right\} \quad (5)$$

where: $n = \sigma \cdot t$ normal stress
 $n_{pl} = \sigma_y \cdot t$ yield stress

It can be seen that stress distribution depends solely on the rate of in-plane compression (δ) and the function which determines the shape of the yield mechanism (Z).

If we consider a model of plastic-rigid material then the resultant in-plane compression in the plastic mechanism, i.e.

$$\delta = \delta_0 = \text{constant}$$

shall be identical with the total compression (δ_0). Assuming a constant cross-section throughout (see condition iv.), this creates a geometric contradiction in the vicinity of the edges. We shall then obtain a solution well in conformity with the experimental results by taking into consideration the elastic compressions, as well:

$$\delta_0 = \delta_e + \delta = \text{constant}$$

where: δ_e elastic compression

Beyond the geometric data the elastic compression shall depend on the stress distribution and, if we consider proportions of the shape of the plastic mechanism, the plastic compression shall be:

$$\delta = \frac{W_{pl}^2}{2b} \frac{1-n/n_{pl}}{1-n_0/n_{pl}} \quad (6)$$

where: n_0 value of stress at the axis of symmetry
 W_{pl} highest value of out-of-plane displacement within the assumed plastic mechanism

If we consider the omissions that can be made concerning small angles, the relation (5) can be significantly simplified. Let's assume that function "Z" is described in the following form:

$$Z = W_{pl} \cdot \eta \cdot \left(\frac{\pi y}{b} \right) \quad (7)$$

This, and the substitution of the eqn. (6) into the eqn. (5) and having implemented the necessary reductions, we obtain an explicit function that describes the curve of stress distribution:

$$\frac{n}{n_{pl}} = \left[1 - \left(\frac{n}{n_{pl}} \right)^2 \right] \frac{t}{W_{pl} \eta} + \left[1 - \frac{1}{2} \left(\frac{n}{n_{pl}} \right)^2 \right] \cdot \frac{(1-n_0/n_{pl})^2}{(1-n/n_{pl})^2} \left(\frac{1}{2} \eta \eta'^2 - \frac{3}{4} \eta^2 \eta'' \right) \frac{t}{W_{pl}} \quad (8)$$

It is evident that by knowing the function η , we can determine the relation between the out-of-plane displacement and the stress distribution. Since the integral of the stresses constitutes the upper limit of the ultimate load, and according to the theory of plasticity, its minimum value approaches mostly the real value of load bearing capacity, we obtain the following variational problem:

$$\int_b \frac{n}{n_{pl}} dy = \min! \quad (9)$$

Since the exact mathematical solution of this task involves extreme difficulties, we resort to an approximation. We have investigated eight functions which met the requirements of boundary conditions and came to the following conclusions:

- a partial consideration of the elastic displacements as opposed to the purely rigid-plastic model shall cause only an insignificant change with respect to the ultimate load, however, the shape of yield mechanism becomes more realistic;
- in case of the curvilinear plastic mechanism (see Fig. 3/b) we obtain a significantly (i.e. by 22 %) lower value for the ultimate load than in case of the plastic mechanism containing straight lines. (See Fig. 3/a). Therefore, it stands closer to reality;
- the choice of curved line has a relatively small effect; the comparison of the different curves yields a variance lesser than 10 %;
- from among the considered trial-functions, the second order parabola, being of the form of

$$Z = 0,955 W_{pl} [1 - (2y/b)^2] \quad (10)$$

resulted in the minimum value. Thus, it describes the shape of the plastic mechanism with a grade of precision that meets the requirements of engineering calculations.



Having repeated the calculation concerning the eqn. (8) applying numeric approaches, the resultant curves of stress distribution illustrated in Fig.4, representing various kinds of different out-of-plane displacements. Also, with respect to the case of $W_{pl}/t = 5$, we demonstrate a stress distribution which can be calculated on the basis of a straight line plastic mechanism.

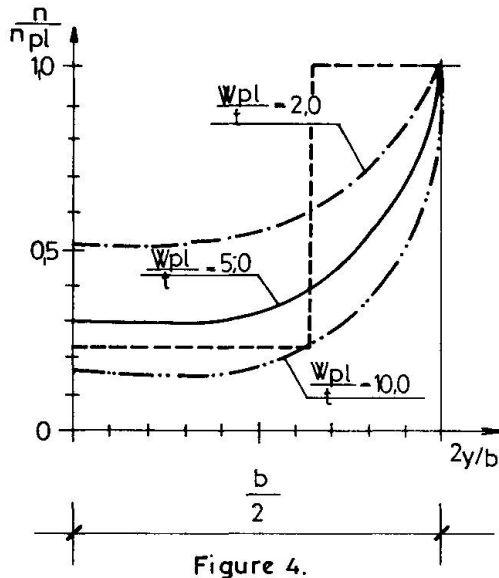


Figure 4.

6. PLASTIC UNLOADING LINE

By means of a repeated numeric integration, the values of the upper limit of the ultimate load could be determined, with respect to the values of out-of-plane displacement. Thus, we could develop the plastic unloading line (see Fig.5).

In order to find a more manageable form, we sought for an approximating function which should describe with sufficient precision the numerically determined values.

We found that:

$$\frac{P_u}{P_{pl}} = \frac{1}{1 + 0,3W_{pl}/t} \quad (11)$$

where: p_u ultimate load of the plate
 p_{pl} yield load of short plate

The formula shall provide the numerically determined values within a range of $\pm 1.7\%$.

7. ELASTIC DEFORMATION LINE

The relation between the load and elastic deformation is considered being in conformity with the literature and formulated according to our investigations:

- in case of initially flat plate:

$$\frac{P}{P_{pl}} = \frac{\sigma_{cr,p}}{\sigma_y} \left[\frac{1-\nu^2}{8} \left(\frac{W_e}{t} \right)^2 + 1 \right] \quad (12)$$

$\sigma_{cr,p}$ critical buckling stress
 ν Poisson's ratio
 W_e elastic out-of-plane displacement

- when the characteristic value of the eccentricity is:

$$\alpha = W_0/t$$

$$\frac{P}{P_{pl}} = \frac{\sigma_{cr,p}}{\sigma_y} \left\{ \frac{1-\nu^2}{8} \left[\left(\frac{W_e}{t} \right)^2 - \alpha^2 \right] \right\} + \frac{W_e/t + \alpha}{W_e/t} \quad (13)$$

8. ULTIMATE LOAD

The intersection of the plastic unloading line with the load/elastic displacement curve provides the upper limit of ultimate load (see Fig.5).

The real load/displacement path can be distributed to three phases:

- I. elastic phase;
- II. phase is where plasticity sets in. Here, the elastic pattern of displacements transforms in to the plastic pattern of displacements;
- III. plastic phase.

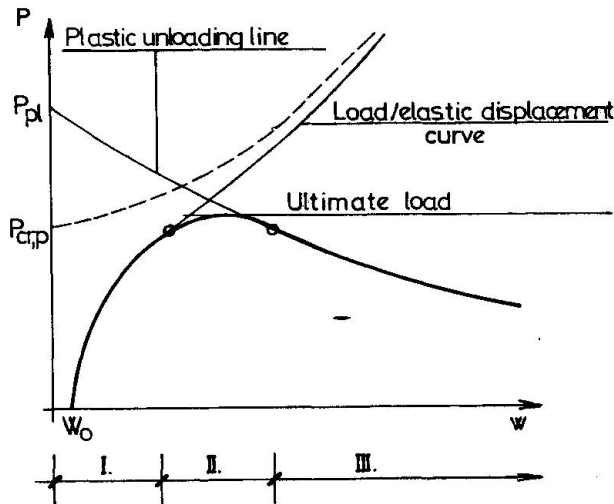


Figure 5.

Assuming that the transformation should take place at an identical value of in-plane displacement (and using the legend applied in Figure 6), we can determine the following relation between the characteristic values of out-of-displacement:

It can be seen that extremum of the real curve (which indicates the value of the ultimate load) is situated below the intersection. In order to assess this effect, we present a vertical cross-section of both the elastic pattern of displacements (Fig.6/a) and that of the plastic one, (Fig. 6/b).

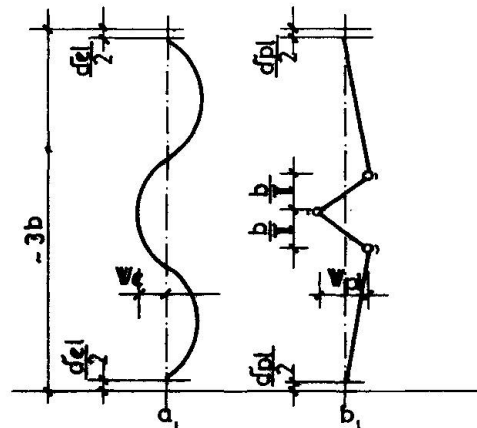


Figure 6.

$$W_{pl} = W_e \sqrt{\frac{3\pi/4}{\pi+1/(b+4/\pi)}} = 1,50W_e \tag{14}$$

While comparing the displacements, the above relation is used as a correction factor. Thus, by equating the plastic displacement calculated from the eqn. (11) with the elastic displacement derived from the eqn. (12), and taking into consideration the correction (14), we obtain the relation between the slenderness of the initially flat plate and its ultimate load:

$$\bar{\lambda}_{po} = \sqrt{\frac{(1-\bar{P})^2 + 1,78\bar{P}^2}{1,78\bar{P}}} \tag{15}$$

where: $\bar{\lambda}_{po}$ slenderness of the initially flat plate
 $\bar{P} = P_u/P_{pl}$ relative ultimate load

If we perform the same comparison using the formula of load/elastic displacement (13) which takes into consideration the initial eccentricity as well, furthermore, if we assume, in conformity with our experimental results, the value of the latter in the form of:

$$\alpha = \frac{w_0}{t} = A \left(\frac{b}{t}\right)^2 = A_1 \cdot \bar{\lambda}_p^2, \quad \bar{\lambda}_p = \sqrt{\sigma_y/\sigma_{cr}} \tag{16}$$



$$\text{where: } A_1 = A \frac{\pi E k}{12(1-\nu^2)\sigma_Y}$$

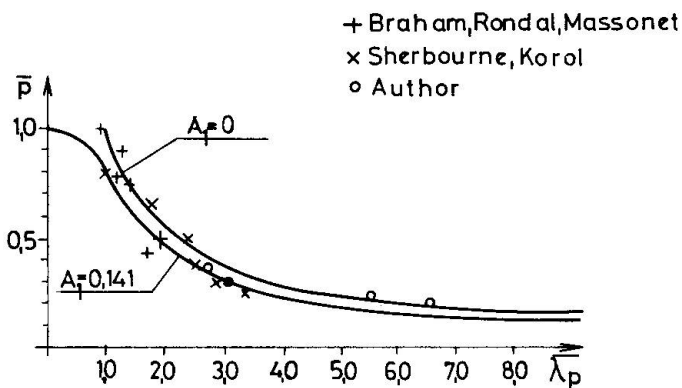
The relation between slenderness of the plate and the ultimate load shall be the following:

$$\bar{\lambda}_p^2 = \bar{\lambda}_{p0}^2 - \frac{A_1}{8,79\bar{P}} \bar{\lambda}_p^4 - \frac{0,45A_1}{1\bar{P}} \bar{\lambda}_p^2 \quad (17)$$

where: $\bar{\lambda}_p$ slenderness of the initially imperfect plate
 $\bar{\lambda}_{p0}$ slenderness of the plate of equal loadability which was, however, plane initially.

9. EXPERIMENTAL RESULTS

Fig.7 illustrates the curves calculated with the use of formulas (15) and (17). The latter was calculated with respect to the initial curvature being of a characteristic value of $A_1 = 0.141$. This value was obtained on the basis of results of evaluation of 62 samples.



The values of ultimate load obtained through experiments, were plotted in the figure, where several well-comparable measurement data can be observed, as well. It can be established that the theoretically determined curve fits quite well with the experimental results.

Figure 7.

10. IMPLEMENTED STRUCTURES

This process was used to control calculations concerning a roof structure of 30 meters span and manufactured from 1 mm thick plate. The roof structure was subjected to a full scale loading test. The difference of the measured and calculated values remained within a highly satisfactory range of 2.5 %.

REFERENCES

1. WILLIAMS, D.G., AALAMI, B., Thin Plate Design for In-plane Loading. Granada, London, 1979.
2. RHODES, I., WALKER, A.C., Thin-Walled Structures. Granada, London, 1980.
3. DAVIES, P., KEMP, K.O., WALKER, A.C., An Analysis of the Failure Mechanism of an Axially Loaded Simply Supported Steel Plate. Proc. ICE. Part 2. Vol. 59.
4. IVANYI, M. Yield Mechanism Curves for Local Buckling of Axially Compressed Members. Periodica Politechnica. C.E. Vol. 23. 1979.
5. KOROL, R.M., SHERBOURNE, A.N., Strength Predictions of Plates in Uniaxial Compression. I. ASCE. Vol. 98. St9. Sept. 1972.
6. SHERBOURNE, A.N., KOROL, R.M., Post-Buckling of Axially Compressed Plates. I. ASCE. Vol. 98. St9. Oct. 1972.
7. FERNEZELYI, S., Load-bearing capacity of thin aluminium plates. Experimental Investigation. Magyar Aluminium. (Prepared for publication, in Hungarian.)

From Thick to Thin or from Thin to Thick?

De l'épais au mince ou du mince à l'épais?

Von dick zu dünn oder von dünn zu dick?

René MAQUOI

Chargé de Cours
Université de Liège
Liège, Belgique



René Maquoi, born in 1942, graduated in Civil Engineering and Doctor in Applied Sciences. He teaches statics and steel construction at the University of Liège. He is a member of several international technical committees and is the author of more than 100 scientific papers.

Jacques RONDAL

Chargé de Cours
Université de Liège
Liège, Belgique



Jacques Rondal, born in 1944, graduated in Civil Engineering and is Doctor in Applied Sciences. His field of scientific activity is the stability and the optimisation of structures. He has written more than 100 scientific papers.

SUMMARY

Because thick-walled and thin-walled sections are not actually two different families, it should be aimed at having consistent rules which would apply to the whole range of sections. Based on a parametric study of uniaxial compression plates – the basic case – the authors suggest values of the parameters that are worthwhile being accounted for and they present a general format for plate buckling curves as well as the corresponding analytical expressions.

RÉSUMÉ

Il est nécessaire de disposer de règles de calcul homogènes qui couvriraient sans discontinuité tant les profils à parois épaisses que ceux à parois minces. Les auteurs ont procédé à une étude paramétrique du cas fondamental constitué par les plaques en compression uniaxiale. Sur cette base, ils proposent les paramètres à retenir et présentent une formulation générale des courbes de voilement ainsi que les expressions analytiques correspondantes.

ZUSAMMENFASSUNG

Es drängt sich immer mehr auf, über gleichwertige Berechnungsregeln zu verfügen, die kontinuierlich sowohl für dick- als auch für dünnwandige Profile gelten. Aufgrund des Studiums des grundlegenden Falles – einachsigen Druck ausgesetzte Platten – schlagen die Autoren die zu berücksichtigenden Parameter vor und geben eine allgemeine Formulierung der Beulkurven sowie die entsprechenden analytischen Ausdrücke an.

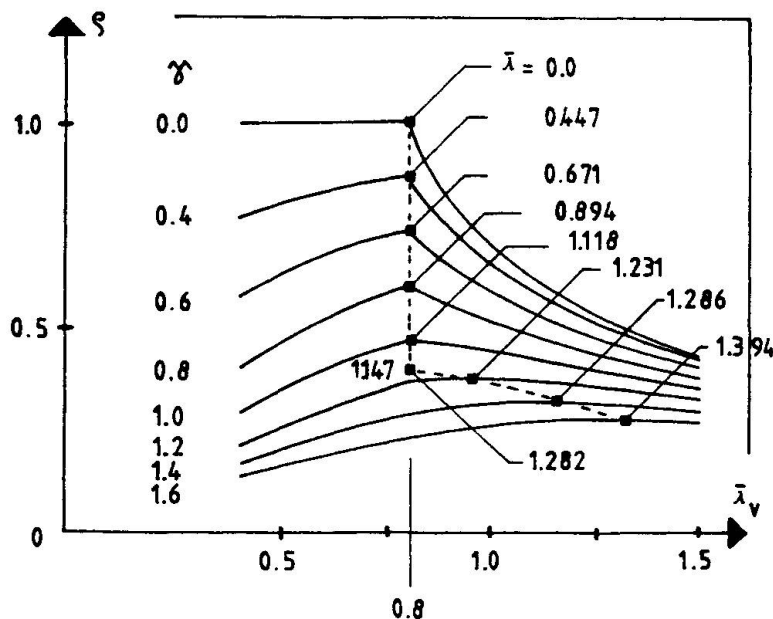


1. INTRODUCTION.

The codes and standards for steel construction have been first written with the hot-rolled sections in mind. At that time these sections can be called thick-walled because no local plate buckling can generally occur in the walls before the yield stress be reached there. That means that the wall slenderness is lower than a limiting value, beyond which local stability phenomena would prevail on yielding.

At a time when elastic design has been of regular use, the carrying capacity was supposed to be exhausted when the maximum stress, without account taken of any eventual residual stress, was reaching the yield stress. A section that is just able to comply with such a requirement is now called "semi compact". When the plastic design has been more in favour, yielding of the full cross-section became the collapse criterion of a section; a section that complies with such a condition is now called "compact". It has been then recognized that, at least in bending, the formation of a plastic hinge needed a large capacity of rotation. Thus a large amount of plastic deformation is required prior to the occurrence of any plate buckling, with the consequence that the limiting value of the plate slenderness is lower for compact sections than for semi-compact ones. Usual hot-rolled sections made with the most common steel grades, i.e. Fe 360 and Fe 510, belong to compact sections.

On the opposite to heavy steel construction - structures made with hot-rolled sections belong to this range - the use of structural sheets and sections with very thin walls developed with view to special applications or as sheathing (roofs, façades,...) of heavy constructions. These sections and sheets are most often cold formed. Specific design rules have been established especially for such structural components, that were produced using light gage steel. In this respect, most of the theoretical and experimental developments came from the United States and the first wide-spread book on the topics was the "Light Gage Cold-Formed Steel Design Manual" [1]. It is obvious that in the range of large plate slenderness values, plate buckling is elastic; it benefits usually from an appreciable postcritical strength reserve and is only slightly affected by the now well-known detrimental effect of the geometrical - and structural imperfections. These imperfections consist mainly in an out-of-flatness of the plate elements and in residual stresses due to cold forming.



The attention has been drawn on the intermediate range of plate slenderness values, that lies between thick walls and thin walls, when a special effort was namely produced to promote slender sections, as most welded beams or thin walled hollow sections are. An investigation of square hollow sections that are currently used as columns or beam-columns, and have thus to sustain mainly compressive loads has been conducted by the authors [2]. For cold-formed sections, it yielded figure 1, that is an efficiency chart the original idea of which

Figure 1 : Efficiency chart for square cold-formed hollow sections.

is due to USAMI and FUKUMOTO [3]. The efficiency ρ is measured by the ratio of the mean collapse stress σ to the material yield stress f_y , i.e. :

$$\rho = \frac{\sigma}{f_y} \quad (1)$$

The reduced plate slenderness $\bar{\lambda}_V$ of the walls of breadth b and thickness t is given by :

$$\bar{\lambda}_V = \frac{b}{1.9t} \sqrt{\frac{f_y}{E}} \quad (2)$$

The reduced column slenderness $\bar{\lambda}$ is defined as:

$$\bar{\lambda} = \lambda/\pi \sqrt{E/f_y} \quad (3.a)$$

and can be easily expressed in terms of the cross-sectional area A and of the length l as :

$$\bar{\lambda} = 2 \sqrt{6} l/\pi \sqrt{EA/btf_y} \quad (3.b)$$

Both above slenderness ratios may be connected according to :

$$\bar{\lambda} = \gamma/\sqrt{\bar{\lambda}_V} \quad (4)$$

where the dimensionless factor γ is equal to :

$$\gamma = 1.131 (1/\sqrt{A}) (f_y/E)^{0.75} \quad (5)$$

Interesting conclusions can be drawn from figure 1 :

- The optimum efficiency is never reached for a thick-walled tube, i.e. for $\bar{\lambda}_V < \bar{\lambda}_{V0}$, the limiting value $\bar{\lambda}_{V0}$ being chosen equal to 0.8 in accordance with the ECCS Recommendations [4];
- For small values of γ ($\gamma < 1.147$ in figure 1), the optimum efficiency corresponds to the limiting plate slenderness $\bar{\lambda}_V = \bar{\lambda}_{V0} = 0.8$;
- For larger values of γ , the optimum efficiency corresponds to thin walls, i.e. walls having $\bar{\lambda}_V$ larger than $\bar{\lambda}_{V0} = 0.8$.

For a specified wall breadth b , the efficiency ρ may be plotted against the wall thickness t for several values of the length l . The slope of the curves is larger in the region of thin walls than in that of thick walls ; in addition, all the curves are rather flat in the vicinity of the maximum efficiency. Figure 2 [5] illustrates the results for $b = 100$ mm and $f_y = 360$ MPa.

In the range of intermediate plate slenderness values, i.e. when $\bar{\lambda}_V$ is close to 1, plate buckling is elasto-plastic and because the critical plate buckling stress and the yield stress are close each other, the detrimental effect resulting from yielding-buckling interaction is there the most dependent on the magnitude of the structural and geometrical imperfections. That justifies the large scatter of the experimental results in this range and thus the discrepancy between the numerous proposals for plate buckling curves (fig. 3).

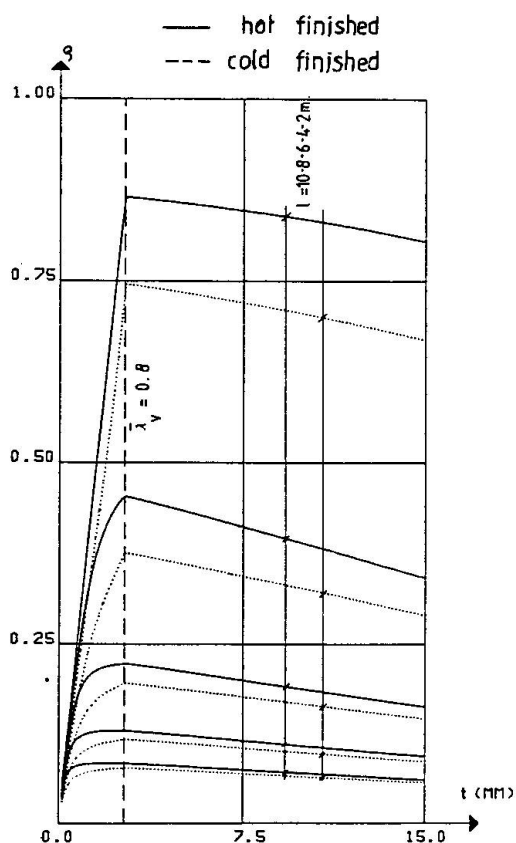


Figure 2 : Efficiency ρ against wall thickness t
($f_y = 360$ MPa, $b = 100$ mm)

2. PARAMETRIC STUDY.

The authors are of the opinion that standardized European buckling curves for compression plates, ought to be suggested as it has been successfully done for the European column buckling curves. Such a goal is sensible to be reached by performing numerical simulations by means of a reliable computer program that takes account of initial structural and geometrical imperfections and allows for large deflections and plasticity. Therefore, such a study has been launched at the University of Liège with the so-called Live Energy Method, developed by LITTLE [6]. The displacements are approximated by finite series as in the RAYLEIGH-RITZ method; each term of the series has to fulfil the boundary conditions. The axial shortening of the compression plate is successively incremented from the state of equilibrium that is known in displacements and stresses; the increments in the coefficients of the displacement series are determined by minimising the live energy according to a standard optimisation procedure. At each step strains and stresses are updated and the load is compared with that of the previous step in order to detect the maximum load, that will be the ultimate carrying capacity.

Calculations have been conducted with the aim of investigating the influence of the main parameters, which are :

- the aspect ratio of the buckled pattern, α ;
- the material steel grade, f_y ;
- the initial out-of-flatness f_0 , measured as a portion of the breadth b , f_y ;

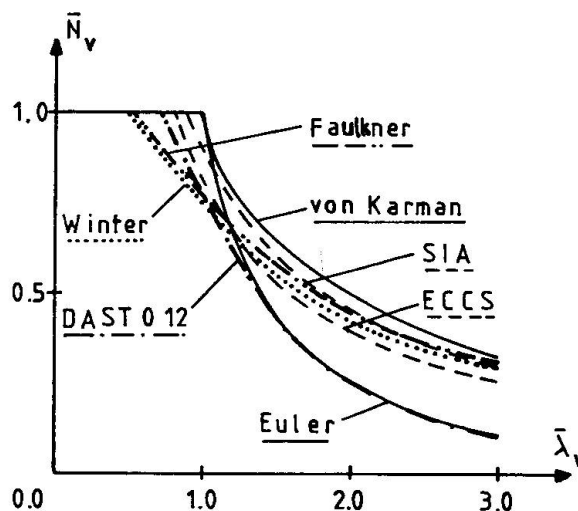


Figure 3 : Several proposals for plate buckling curves.

- the distribution and the amplitude of the residual stresses ;
- the membrane boundary conditions.

All the edges are assumed to be simply supported and the loaded edges are kept straight.

From the lot of numerical results, following conclusions have been drawn :

- a) The ultimate load is slightly increasing with the aspect ratio α of the buckled pattern in the vicinity of $\alpha = 1$;
- b) This increase is larger when the edges are constrained to remain straight, than when they are free to pull in ;
- c) There is no significative difference between the results obtained for Fe 360 and Fe 510, so that dimensionless coordinates may be used within this range of material yield stresses ;
- d) For a usual magnitude of initial out-of-flatness (from $b/200$ to $b/400$), the carrying capacity is increasing when the relative out-of-flatness is decreasing; this effect is only observed when the unloaded edges are free to pull in ;
- e) A bi-triangular distribution of residual stresses is more favourable than a bi-rectangular one, the relative value of peak stresses at the edges being the same ;
- f) Compressive residual stresses at the unloaded edges do not provide a significative drop of the carrying capacity of a similar plate that would be free from residual stresses ;
- g) Tensile residual stresses at the unloaded edges have a detrimental effect, which is increasing with the amplitude of these stresses ; this evolution tends to become independent of this amplitude when the plate slenderness is increasing.

Consideration of these results incited the authors to adopt following data with view to define standardized plate buckling curves :

- an aspect ratio of 0.9 in order to comply with experimental evidence, on the one hand [7] [8], and with the actual kinematics of a long plate during plate buckling, on the other hand ;
- an initial out-of-flatness of $b/200$ in accordance with a previous statistical study on tolerances in steel plated structures [9] ;
- a bi-rectangular distribution of residual stresses, that is found to be safer and more in agreement with measurements ;
- residual stresses with peak tensile values at the edges equal to 0 and f_y , respectively.

Last, it is worth-while distinguishing between unloaded edges that are free to pull in and those that are kept straight.

The results of dimensionless plate buckling curves calculated in accordance with the aforementioned data are plotted in figures 4.a for unloaded edges free to pull in and in figure 4.b for unloaded edges that are kept straight.

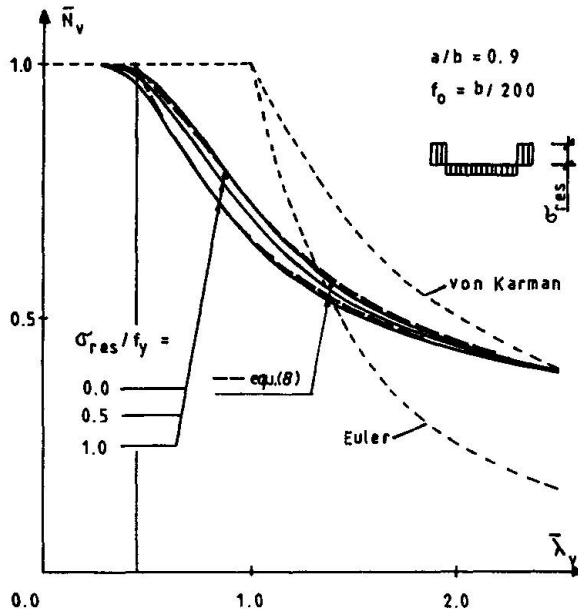


Figure 4.a.

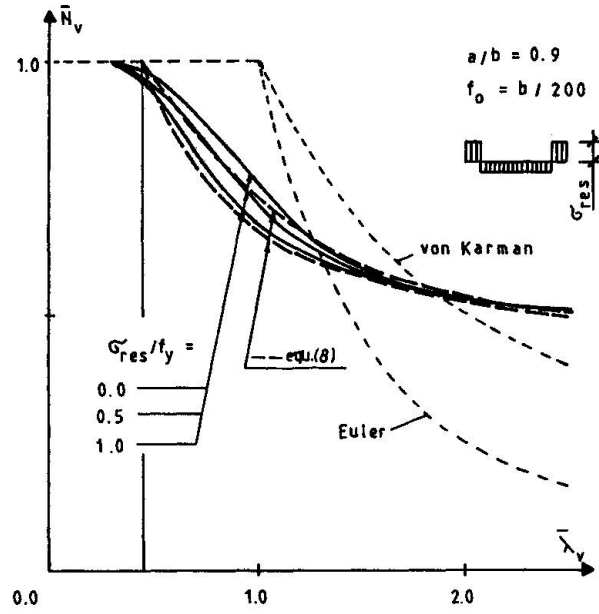


Figure 4.b.

3. PROPOSAL FOR COMPRESSION PLATE BUCKLING CURVES.

Considering that any plate buckling curve results from an interaction between the yield plateau $\bar{N}_v \equiv \sigma/f_y = 1$, for small plate slenderness ratios, and the buckling curve $\bar{N}_v = 1/\bar{\lambda}_v^\gamma$ of a perfect plate for large ones, a general format for plate buckling curves can be written as :

$$(1 - \bar{N}_v) (1 - \bar{N}_v \bar{\lambda}_v^\gamma) = n \bar{N}_v \quad (6)$$

γ is depending mainly on the membrane boundary conditions, n is an imperfection parameter that is depending on the plate slenderness ratio $\bar{\lambda}_v$, provided the latter be larger than a limiting value $\bar{\lambda}_{v0}$, that measures the length of the yield plateau $\bar{N}_v = 1$:

$$n = \beta (\bar{\lambda}_v - \bar{\lambda}_{v0}) \quad (7)$$

β is characterizing a specified plate buckling curve.

The solution of (6) is written, account taken of (7) :

$$\bar{N}_v = \frac{1}{2\bar{\lambda}_v^\gamma} [1 + \beta(\bar{\lambda}_v - \bar{\lambda}_{v0}) + \bar{\lambda}_v^\gamma] - \frac{1}{2\bar{\lambda}_v^\gamma} \sqrt{[1 + \beta(\bar{\lambda}_v - \bar{\lambda}_{v0}) + \bar{\lambda}_v^\gamma]^2 - 4\bar{\lambda}_v^\gamma} \quad (8)$$

To the authors' opinion, four plate buckling curves would be necessary but sufficient to describe the full set of conditions : unloaded edges free to pull in or constrained to remain straight, and, for each case, either zero residual stresses - covering cold formed edges - or tensile residual stresses with peak values $\sigma_{res}/f_y = 1$ at the unloaded edges - allowing for welded edges.

Experimental results and numerical simulations are comforting the idea that a same length $\bar{\lambda}_{vo}$ of the yield plateau can be reasonably accepted for both kinds of membrane boundary conditions along the unloaded edges.

By curve fitting to the results of the numerical simulation, following values of the parameters, that are describing the four aforementioned plate buckling curves, can be suggested :

Unloaded edges	$\bar{\lambda}_{vo}$	$\sigma_{res}/f_y = 0$ (cold formed edges or virgin edges)		$\sigma_{res}/f_y = 1$ (welded edges)	
		β	γ	β	γ
Free to pull in	0.45	0.19	0.75	0.34	0.45
Kept straight	0.45	0.20	0.25	0.28	0.00

The general format and the numerical values attached of the several plate buckling curves, as they are given hereabove, have only to be considered as a proposal. It would be the task of an international working group to investigate further and to search for a general agreement on what could be called European plate buckling curves.

4. REFERENCES.

- [1] American Iron and Steel Institute : Light Gage Cold-Formed Steel Design Manual. AISI, New-York, 1962.
- [2] RONDAL, J. and MAQUOI, R.: On the Optimum Design of Square Hollow Compression Members. IUTAM Symposium ; Collapse, The Buckling of Structures in Theory and Practice. Cambridge University Press, 1983, pp. 333 - 344.
- [3] USAMI, T. and FUKUMOTO, Y. : Local and Overall Buckling of Welded Box Sections. Proceedings ASCE, Jl. of the Structural Div., Vol.108,1982,pp.525-542.
- [4] European Convention for Constructional Steelwork : European Recommendations for Steel Construction, ECCS - EG77-2E.
- [5] RONDAL, J. and MAQUOI, R. : Etude d'une gamme optimale de profils creux carrés et rectangulaires. Annales de l'Institut Technique du Bâtiment et des Travaux Publics, Série Construction Métallique, 91, n° 409, Nov.1982,pp.63-72.
- [6] LITTLE, G.H.: Rapid Analysis of Plate Collapse by Live-Energy Minimisation, International Journal of Mechanical Sciences, Vol. 19, 1977, pp. 725-744.
- [7] DWIGHT, J.B. and RATCLIFFE, A.T.: The Strength of Thin Plates in Compression, Proceedings of the International Symposium on Thin-Walled Structures, Crosby Lockwood, 1969, pp. 3 - 34.
- [8] MOXHAM, K.E.: Buckling Tests on Individual Welded Steel Plates in Compression. Technical Report CUE D/C-Struct. TR3, Cambridge University, Dpt. of Civil Engineering, 1971.
- [9] MASSONNET, Ch.: Tolerances in Steel Plated Structures. IABSE Surveys, S 14/80, 1980.

Leere Seite
Blank page
Page vide

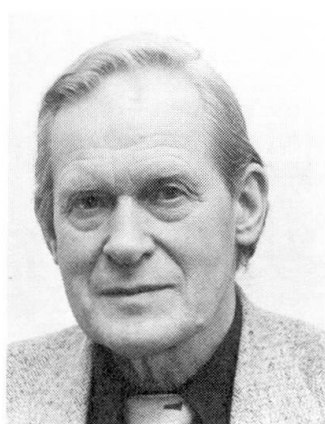
Buckling of Trapezoidally Corrugated Webs and Panels

Voilement de panneaux et d'âmes de poutres en tôle profilée
de forme trapézoïdale

Beulen von trapezförmig profilierten Stegen und Blechen

Allan BERGFELT

Professor Emeritus
Chalmers Univ. of Technology
Göteborg, Sweden



Allan Bergfelt, born 1915, graduated from Royal Inst. of Technology, Stockholm in 1937. After several years as a structural engineer, he was head of the design department, Gothenburg Harbour Authorities. Professor of Structural Engineering, Chalmers Univ. of Technology 1957 – 1981.

Luis LEIVA-ARAVENA

Research Assistant
Chalmers Univ. of Technology
Göteborg, Sweden



Luis Leiva-Aravena, born 1949, received his degree of Civ. Eng. (M.Sc.) at Chalmers Univ. of Technology in 1981. He is a research and teaching assistant at the Dep. of Structural Engineering, Div. of Steel and Timber Structures. His research work deals with buckling of thin-walled steel structures.

SUMMARY

Some test series on trapezoidally corrugated webs and panels are briefly presented. Local buckling seems to be governing for shear failure if the critical buckling stress is below or in the vicinity of the shear yield stress of the material. This seems to be valid for shear buckling for girder depths up to the region where global buckling calculated with common formulas may become critical. For combined axial and shear stress the best interaction curve seems to be a circle.

RÉSUMÉ

Des séries d'essais effectuées sur des panneaux et des âmes de poutres en tôle profilée de forme trapézoïdale sont brièvement présentées. La résistance ultime au cisaillement semble être gouvernée par un voilement local si la contrainte critique de voilement se trouve sous ou au voisinage de la contrainte limite de cisaillement du matériau. Cela semble valable au moins pour une hauteur de poutre qui se trouve en dessous de la limite de voilement global calculée avec les formules usuelles. Lorsque l'on combine contrainte normale et contrainte de cisaillement, la meilleure courbe d'interaction semble être l'arc de cercle.

ZUSAMMENFASSUNG

Einige Versuche mit trapezförmig profilierten Stegen und Blechen werden kurz beschrieben. Für die Schubbruchlast scheint das örtliche Beulen entscheidend zu sein, wenn die kritische Beulspannung unter oder in der Nähe der Schubfließspannung des Materials liegt. Dieses Verhalten scheint bei Trägerhöhen bis zu dem Bereich für das Schubbeulen gültig zu sein, bei dem das globale Beulen massgebend werden kann. Beim kombinierten Lastfall (Normal- und Schubspannung) wird eine kreisförmige Interaktionskurve vorgeschlagen.



1. INTRODUCTION

The type of welded steel girders with extremely thin, flat webs ($h/t \approx 220$) without any intermediate stiffeners, which were used in Sweden since the first years of the 1960's, met from the mid 60's a competition from girders with trapezoidally corrugated webs. These girders increased their part of the market and since the mid 70's they dominate the Swedish market for small and medium-span steel roofs.

The main reason for this situation is that it was possible to design the flat parts of the web with such a limited width, that no consideration to buckling of these parts had to be taken. Instead shear yield was governing for the dimensions ($\tau_{cr} \geq \tau_y$). The increase in allowable shear stress made it possible to use a thinner web and this compensated for the "longer" web plate, for the work of corrugating, and even for the loss of the possibility for the web to contribute to the bearing of bending moment of the girder. An extra advantage was that the specifications admitted one-sided welding, whilst flat webs were allowed with double-sided fillet welds only. The girders also had the advantage to be stiffer during handling than girders with flat webs.

As there was, of course, an interest to increase the span of the girders and thus their depth, there might be an influence of global buckling of the web and not only buckling of the individual plates between the folds. Research into this field was started in the first years of the 80's at the Division of Steel and Timber Structures at Chalmers University of Technology (CTH) as a part of a general research program within the field of thin-walled structures. Some preliminary reports on tests at CTH regarding this type of girders have been published [1], [2] and now some results are summarized here and supplemented with results from new tests.

Some of the new tests were mainly concerned with the problems of stiffening walls or "webs" in ships and in off-shore structures, where such walls may be designed as trapezoidally corrugated panels.

2. CALCULATIONS

2.1 Shear buckling

At the calculations the shear stress is presumed to be evenly distributed over the total depth of the web, $\tau = V/th \dots(1)$, see Fig.1b.

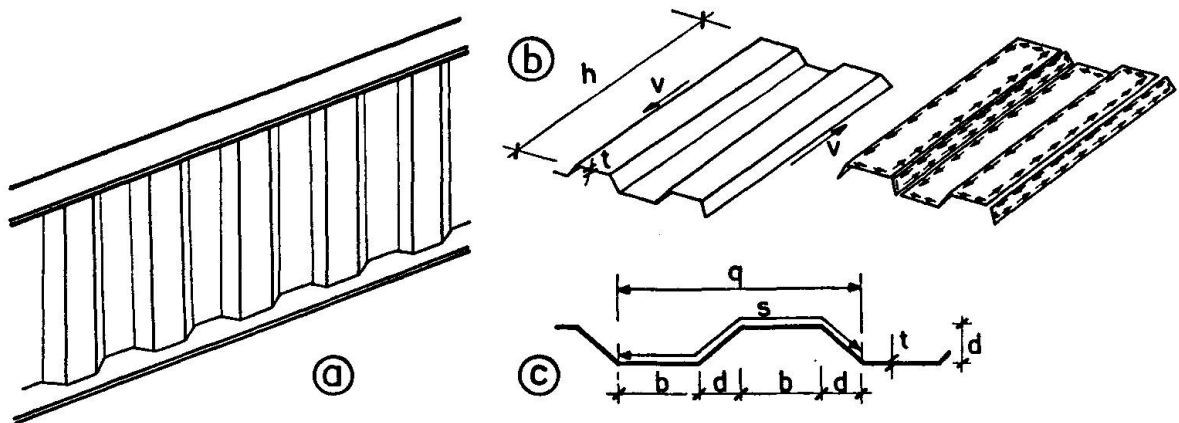


Fig. 1 Girder with corrugated web.

This stress must theoretically be smaller than the yield stress in shear τ_Y .

$$\tau \leq \tau_Y = \sigma_Y / \sqrt{3} = 0.577\sigma_Y \quad \dots(2)$$

The ideal (local) buckling of a plate of the web corresponds to

$$\tau_{cr} = \frac{k\pi^2 \cdot E}{12(1-\nu^2)(b/t)^2} \quad \dots(3)$$

Notations, see Fig.1c. Assuming ideal buckling and hinged edges (which gives a minimum value) you will have

$$\tau_{cr} / \sigma_Y = 4.83 / \lambda_w^2 \quad \text{where} \quad \lambda_w^2 = (b/t)^2 \cdot \sigma_Y / E \quad \dots(4)$$

However, there might be another type of buckling, too.

When the depth and length of the web are very large compared to the widths of single plates in the trapezoidal folded plate structure it might be possible that a long-wave buckle occurs over a larger portion of the web. This phenomenon is called "Global buckling".

Theoretical calculations, Ref. [3], [4], result in a formula for the critical shear force for global buckling N_{cr} (per unit length), that may be written:

$$N_{cr} = k_u \cdot (D_x \cdot D_y^3)^{1/4} / h^2, \quad \text{where} \quad D_x = \frac{q}{s} \cdot \frac{Et^3}{12} \quad \text{and} \quad D_y = \frac{EI_y}{q} \quad \dots(5a,b)$$

with $I_y = 2bt(d/2)^2 + 2\sqrt{2} \cdot d^3t/12$ for a symmetrical trapezoidal shape with 45° folds, c.f. Fig.1c.

The results of a calculation of k_u , given in Ref. [3], is $k_u = 32.4$ for hinged edges and 60.4 for fixed edges. (In most of the formulas given E is used instead of $E/(1-\nu^2)$ even for the plate stiffness D_x .) For a panel with fixed edges the critical shear stress for global buckling thus may be written

$$\tau_g = N_{cr} / t = 60.4 \cdot (D_x \cdot D_y^3)^{1/4} / h^2 t \quad \dots(6)$$

or with D_x and D_y inserted:

$$\tau_g = N_{cr} / t = \frac{60.4}{\sqrt[4]{96}} \underbrace{\left[\frac{q}{s} \cdot \left(\frac{\sqrt{2}}{3} + \frac{b}{d} \right)^3 \cdot \left(\frac{d}{q} \right)^3 \right]^{1/4}}_{p_g} \cdot \frac{d\sqrt{td}}{h^2} \cdot E \quad \dots(6b)$$

Here a factor p_g , "the global buckling product", is defined in formula (6b) for a web shape like Fig.1c, which is intended to make it easier to directly see the influence of the geometry of the web as p_g varies rather little. It was $p_g = 0.52$ and 0.54 respectively for the ideal shape of the tested webs and $p_g = 0.48-0.53$ for various imperfect waves.

2.2 Combined axial and shear stress

In a girder with a transversally corrugated web the normal stresses due to bending are produced mainly in the flanges. Any "horizontal" normal stress σ_x is produced in the web, only locally and in the vicinity of the flanges. A "vertical" stress σ_y may be introduced locally at the supports and at the points of loading.



In bulkheads or "webs" used as stiffening panels in ship structures and offshore structures there may, however, occur large forces introduced in the direction of the folds in a trapezoidally corrugated panel, all over the length of the panel.

The critical buckling load for these stresses σ_y ought to be σ_{cr}^y for the folded web seen as a column and σ_{cr}^{yp} for the individual plates

$$\sigma_{cr}^y = c \cdot \frac{\pi^2 EI_y}{A \cdot h^2} ; \quad \sigma_{cr}^{yp} = \frac{k\pi^2 E}{12(1-\nu^2)(b/t)^2} \quad \dots(7a,b)$$

With a general shape of the interaction formula you may write

$$\left(\frac{\sigma_y}{\sigma_{cr}^y}\right)^2 + \left(\frac{\tau}{\tau_{cr}}\right)^2 \leq 1 \quad \dots(8)$$

3. TESTS

3.1 Shear buckling, local and global

In order to obtain optimal economy of trapezoidally corrugated girder webs it is often convenient to choose the geometry of the corrugation in such a way that local buckling shear stress (eq.3) will be about the same as shear yield stress ($\tau_{cr} \approx \tau_y$). In Sweden such girder webs with standardized geometry have been used since the 1960's ($b = 140$ mm, $d = 50$ mm). In order to find the limit to which it is possible to increase the girder depth without making global buckling (eq.5a,b) the governing mode, i.e. making local buckling occur first, some test series have been performed, which were published in ref. [2].

Now a further test series has been performed and the former survey figure is supplemented with the new results. The new figure, Fig.2, is drawn in a way, which is thought to be more illustrative (and at the same time some misprints in the old material are corrected). At the horizontal axis the girder depth is represented as h/h^* , where h^* is the depth at which the theoretical critical global buckling stress τ_g (from eq.6) will coincide with the shear yield stress τ_y . Thus the formula for h^* is

$$h^* = \left[60.4 \cdot (D_x \cdot D_y^3)^{1/4} / \tau_y \cdot t \right]^{1/2} \quad \dots(9)$$

The calculated values of h^* for the different test girders are listed in Fig.2. The intention with the web geometry chosen in the specifications was to obtain $\tau_{cr} \approx \tau_y$. As this was not exactly the case for the test girders the ratios τ_d/τ_y are marked out in the diagram of Fig.2, too. Here τ_d is chosen to represent τ_{cr} , as a reduction is necessary when the buckling values are near the yield values. $\tau_d/\tau_y = \sqrt{3} \cdot 1.4 \frac{t}{b} \sqrt{E/\sigma_y}$ following the Swedish specifications for this region (when a value > 1 is obtained, the value 1.0 is denoted).

It is seen that even for the deepest of the girders tested local buckling was the phenomenon that started the buckling. Any obvious interaction between local and global buckling is difficult to observe even for girders with depth near to those where global buckling ought to dominate.

Any decrease of the load carrying capacity in the vicinity of the region where the curve for global buckling in Fig.2 passes under the level of τ_y , which was indicated by the first tests, c.f. ref. [2], thus is not confirmed. In connection to this it is to be observed that the high value of 60.4 corresponding to fixed edges is chosen for the constant k_u in the formula, eq. 5a and 6. With the value 32.4 for

hinged edges, the failure loads at the tests very clearly surpass any such "theoretical" global buckling.

When the deformations were driven further, however, the local buckling developed into "zonal" buckling and then into global buckling. The deformations ended into a very marked tension field as described in ref. [2].

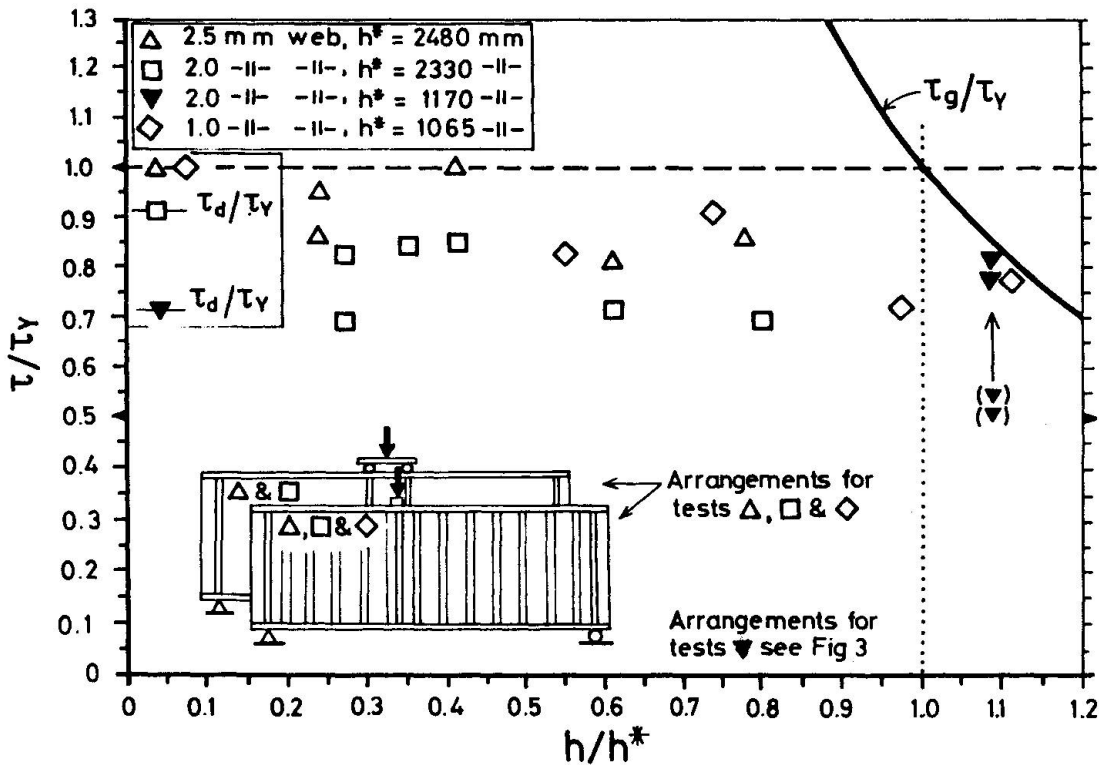


Fig. 2 Shear stress at buckling. Survey of test results.

3.2. Combined shear and normal buckling

3.2.1 General arrangement

The test series of elements under combined shear and normal stresses were made with elements of another geometry than that of the elements for girder tests. The reason was the intention to choose a geometry that could be seen as a model of what was thought to be a typical design for "walls" and panels in shipbuilding and off-shore structures.

The test arrangement was also different from that of the girders, and the loading giving vertical stresses were distributed all along the upper flange, while the horizontal force was introduced at one end of the upper flange, see Fig.3. The lower flange was vertically supported all along, but the horizontal reactions were taken by welding along about half the length of the flange. It was at first intended to take the horizontal reaction concentrated locally at the lower flange vertically under the horizontal load, but the welds then ought to be very large, and so the welding was spread out.

A weld all along the lower flange was not seen as necessary as the shear stress was relatively small. The reason of placing the weld at the same end as the horizontal force was, of course, to prevent lifting at this end at small vertical forces.

The test results of a pure shear loading is introduced in Fig.2. However, the flat



parts of the wall panel had a largest width of 171 mm for a 2 mm thick plate and thus local buckling was dominating. In order to make a comparison with the webs in Fig.2 directly possible, the test results are enlarged in proportion $(171/140)^2$. The original results are given, too, but these points are put within brackets.

All the results for the walls, both at combined loading, at purely shear loading and at purely vertical loading are collected into Fig.6.

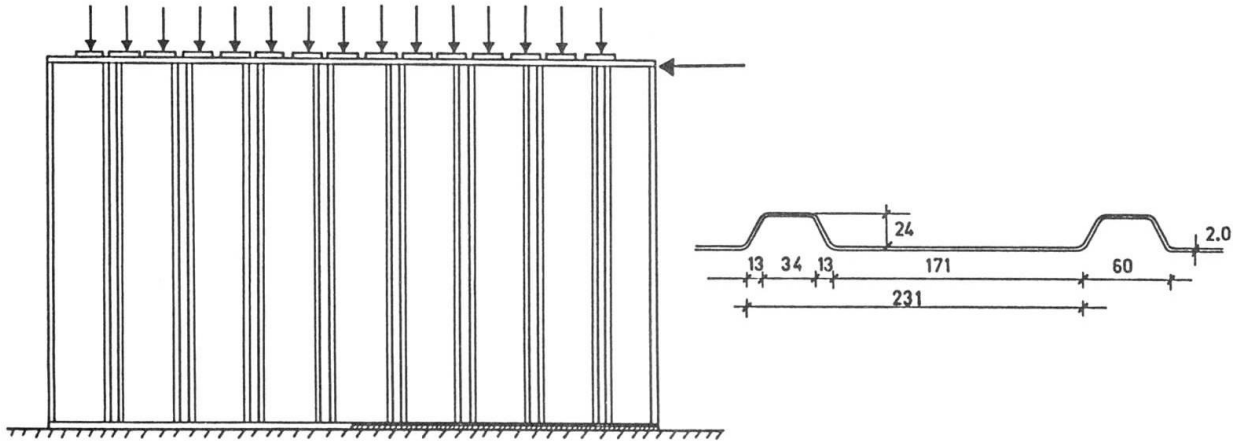


Fig. 3 Arrangement of panel testing. Section of the panel.
(Panel $h = 1270$ mm, $l = 1995$ mm.)

3.2.2 Testing performance

The vertical load resulting in buckling is to be calculated as for a column, and thus is obtained from eq.(7a). The global buckling load is calculated from eq.(6). As the geometry is unsymmetrical it is not possible to utilize the simplified eq.(6b).

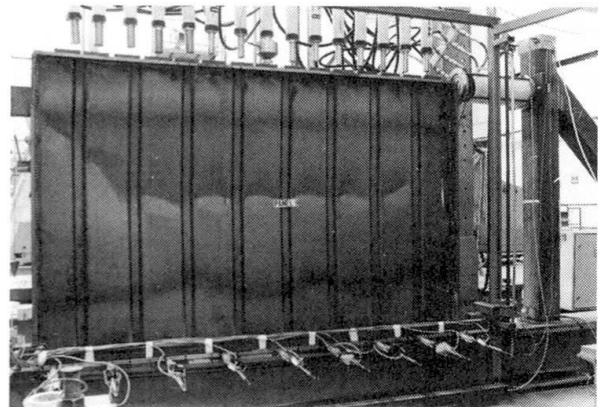
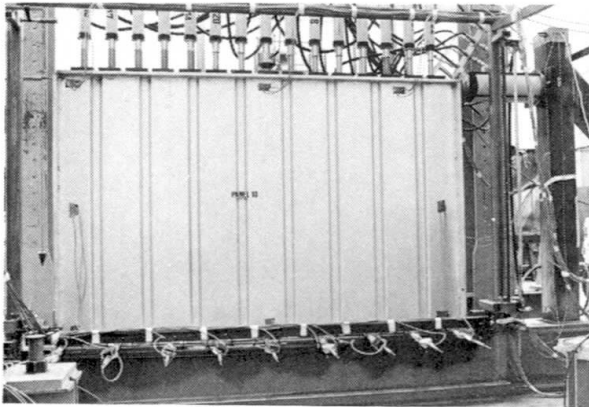
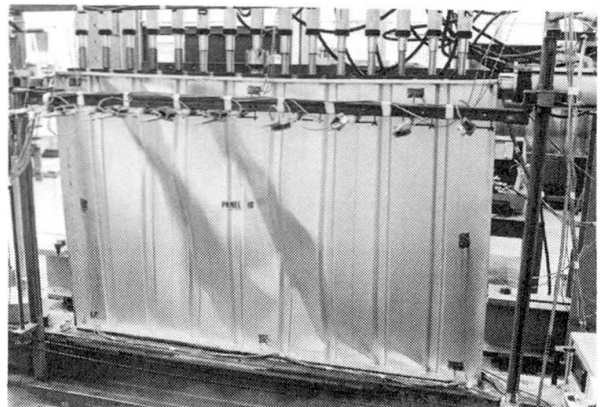


Fig. 4 Panel testing, arrangement.

Fig. 5 Buckling pattern after testing. Panel P9 and P10 resp.



The first experiments checked the two extreme points, that is buckling at pure vertical load and buckling at pure horizontal (shear) load. Further experiments were performed with such loading levels that the total vertical loading span was divided into six parts. The vertical load was introduced by 15 hydraulic jacks, coupled to give equal force.

Quite as for the girder tests the strains (stresses) were measured at several points of the web. The detailed result of these measures will be given in the detailed reports.

3.2.3 Test results

Two typical buckling modes at large deformations are illustrated in Fig.5. All buckling test results are given in Table 1 and are illustrated in Fig.6. The vertical stress σ_y in Table 1 is calculated as the sum P of all the vertical jack forces divided by the total section area. As there were vertical stiffeners at the ends taking part of the load, this means that the σ_y given are true only at the middle part of the web. The shear stress τ is calculated by dividing the force H of the horizontal jack by the projected length of the web times the web thickness. Even here some deviation may occur at the ends. A detailed calculation will be given in connection with the discussion of the strain gauges results.

The σ_{cr}^y from eq. (7a) calculated with $c = 1.8$ is 179 N/mm^2 (the coeff. c is calculated with consideration to end conditions and imperfections, by using the Swedish specifications). The σ_{cr}^P from eq. (7b) is 101 N/mm^2 with $k = 4$, τ_{cr} from eq.(3) is 135 N/mm^2 with $k = 5.34$ and σ_y for the material was 191 N/mm^2 . In Fig.6 the experimental values $\sigma_{cr}^{exp} = 156 \text{ N/mm}^2$ and $\tau_{cr}^{exp} = 101 \text{ N/mm}^2$ are used in eq.(8) for the curve of comparison. Even this choice will be discussed in connection to the strain gauges results.

It is seen that eq.(8) gives a fair picture of the interaction.

Table 1. Panel tests.

Test No	P_{\max} kN	H_{\max} kN	$\sigma_{\max}/\sigma_{cr}^{exp}$	$\tau_{\max}/\tau_{cr}^{exp}$
P4	0	388	0	0,97
P5	0	409	0	1,02
P8	195,0	430	0,28	1,08
P10	225,0	334	0,33	0,84
P6	375,0	303	0,55	0,76
P7	535,5	252	0,78	0,63
P9	592,5	166	0,86	0,42
P3	672,0	0	0,98	0
P2	700,5	0	1,02	0
P1	816,0	0	1,19	0

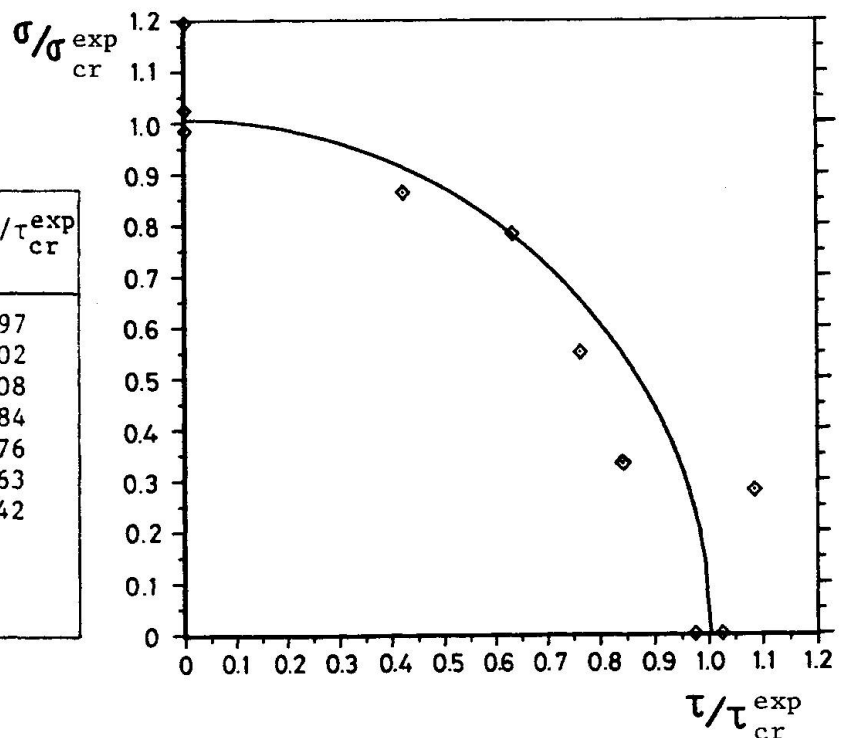


Fig. 6 Buckling stresses at combined axial load and shear load.



4. CONCLUSIONS

Any influence of global buckling on the shear buckling of the web of girders with the tested geometry seems very small. It seems necessary to extend the testing to deeper girders and also to girders with larger length-to-depth ratio in order to confirm any influence of global buckling.

The interaction curve for σ_y and τ followed principally the shape given by eq.(8).

REFERENCES

1. LEIVA L., *Skivbuckling hos plåtbalkar med trapetsprofilerat liv*. Delrapport 1. CTH, Stål-och Träbyggnad. Publ. S 83:1, Göteborg 1983. (In Swedish.)
2. BERGFELT A., EDLUND B., LEIVA L., *Trapezoidally corrugated girder webs*. Schweizer Ingenieur und Architect 1-2/85 s.22.
3. EASLEY J.T., *Buckling Formulas for Corrugated Metal Shear Diaphragms*. Journal of the Structural Div. ASCE, 1975, No ST 7, p.1403-1417.
4. PETERSON J.M., CARD M.F., *Investigation of the Buckling Strength of Corrugated Webs in Shear*. NASA Technical Note D-424. Washington 1960.

APPENDIX

TABLE

Test results plotted in Fig. 2. This is essentially table 1 in ref. [2] with some misprints corrected.

Girder	t mm	h mm	σ_y N/mm ²	λ_w	τ_d N/mm ²	R _{max} kN	τ_{max}^{exp} N/mm ²
L1A	1.94	1000	292	2.69	152	280	140
L1B	2.59	1000	335	2.16	217	502	201
L2A	1.94	1500	282	2.64	150	337	112
L2B	2.54	1500	317	2.14	207	564	150
L3A	2.01	2000	280	2.54	154	450	113
L3B	2.53	2000	300	2.09	201	775	155
B1	2.10	600	341	2.65	181	208	165
B4	2.11	600	363	2.72	187	183	145
B4b	2.11	600	363	2.72	187	217	171
B3	2.62	600	317	2.04	212	246	156
B2	2.62	600	315	2.04	211	273	174
M101	0.99	600	189	2.10	127	53	89
M102	0.99	800	190	2.11	126	79	99
M103	0.95	1000	213	2.23	134	84	85
M104	0.99	1200	189	2.10	127	101	88

Combined Axial Load and Bending in Cold-Formed Steel Members

Profilés formés à froid soumis à l'action combinée
de la compression axiale et de la flexion

Kaltverformte Stahlkonstruktionselemente unter Biegung mit Normalkraft

Teoman PEKOZ

Prof. of Struct. Eng.
Cornell University
Ithaca, NY, USA



Prof. Pekoz obtained his Ph.D. degree in 1967 at Cornell University where he has been involved in research on thin walled members since 1963. He has worked as a visiting Professor in Sweden and the Netherlands. He is active in consulting internationally as well as in the preparation of the American Iron and Steel Institute Specifications and the European Recommendations on Cold-Formed Steel Members.

SUMMARY

A general design approach for combined axial load and biaxial bending of singly and doubly symmetric open and tubular section is developed. The result is a unified design approach for the treatment of several problems. These include the treatment of plate elements, columns, beams and beam columns. The approach covers sections with plate elements that are locally stable as well as those in the post-local buckling range at overall failure. The overall failure modes include flexure and torsional-flexure. The approach developed was checked on the basis of analytical approaches and parametric studies. The results of 260 carefully conducted tests were also used in the verification of the proposed approach.

RÉSUMÉ

On développe une approche générale du dimensionnement de sections ouvertes et fermées à simple et double symétrie soumises à une charge axiale et à une flexion biaxiale. Le résultat en est une méthode unifiée pour le traitement de divers éléments tels que les plaques, les colonnes, les poutres et les poutres-colonnes. Cette approche couvre les sections comportant des éléments plans stables localement aussi bien que des éléments voilés localement lors de la rupture globale, qui se produit par flexion ou par déversement. L'approche développée a été vérifiée analytiquement et par étude paramétrique. Les résultats de 260 essais ont également été utilisés pour cette vérification.

ZUSAMMENFASSUNG

Eine Berechnungsmethode für zweiachsige Biegung mit Normalkraft von einfach- und doppelt-symmetrischen, offenen und rohrförmigen Querschnitten wurde entwickelt. Das Ergebnis ist eine einheitliche Methode für die Behandlung von verschiedenen Problemen (z.B. Plattenelemente, Stützen und Träger), die Querschnitte mit Plattenelementen umfasst. Die Versagenszustände schliessen einfache Biegung und Biegedrillknicken ein. Die neue Methode wurde anhand von analytischen und parametrischen Studien überprüft. Zusätzlich wurden Messresultate von 260 Versuchen für die Überprüfung der Methode ausgewertet.



This study deals with thin-walled doubly and singly symmetric open and tubular sections subjected to biaxial loading. Though singly symmetric open section cold-formed steel members are frequently subjected to biaxial loading, general design provisions do not exist. The design problem is often complicated because the plate elements making up such sections may buckle locally below loads causing overall failure. The subject is relevant to several practical applications including thin walled square or rectangular tubes, end wall columns in metal buildings, many typical industrial storage rack columns and purlins in the end bays of metal buildings.

The author has formulated [1] a unified design approach for beams, columns and beam-columns based on the data and conclusions reached in several research projects reported in [2] through [8] carried out by him and his collaborators. This approach also includes a unified treatment of plate elements making up such members. Due to length limitations, this paper will present only a brief summary of the details and supporting evidence reported in [1]. In each phase of the research, rigorous analytical models were developed and compared with the results of experiments conducted within the project as well as those conducted elsewhere. The results of tests on 51 locally stable columns and beam-columns, 102 locally unstable beams and 107 locally unstable column and beam-columns were used in this process [1].

The proposed unified design approach is being considered for the 1986 Edition of the AISI Specification for the Design of Cold-Formed Steel Structural Members and the ECCS European Recommendations for the Design of Light Gage Steel Members.

BEHAVIOR OF PLATE ELEMENTS

The post-buckling behavior of plate elements is represented by a generalization of the Winter effective width equation [9]. The Winter equation was derived for plate elements supported adequately along the two longitudinal edges. This concept has been extended in [3] through [6] to unstiffened elements (element supported only on one longitudinal edge) and to elements with an edge stiffener or an intermediate stiffener of any size.

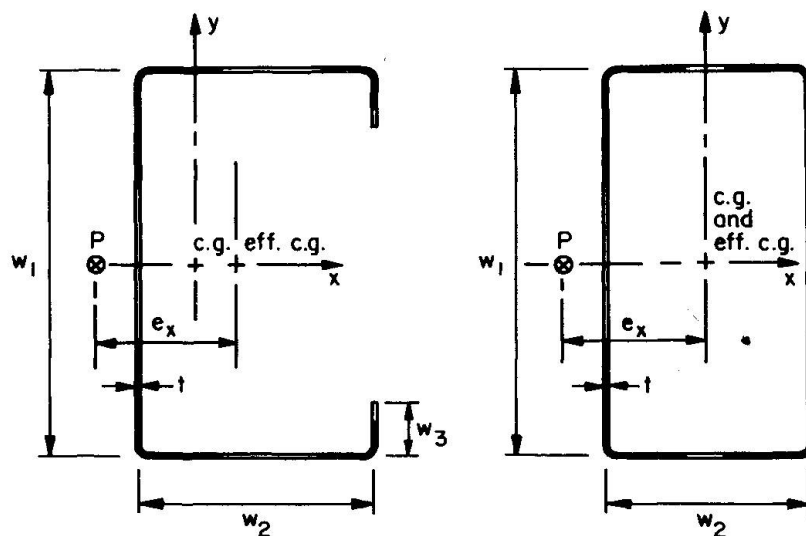


Fig. 1 Section geometry and generalized effective section

The expressions developed in [3] through [6] are the basis of the effective section properties calculated in the proposed approach with the exception of using the actual, rather than the effective moment of inertia in the equations of [5] to assess the stiffener adequacy. This gave improved results. A new approach for webs is also developed [1]. The cross-sectional geometry notation and the generalized effective section for a C and a tubular section is illustrated in Fig. 1.

LOCALLY STABLE BEAM COLUMNS OPEN SECTION

For sections with fully effective plate elements, the studies by the author [10] show that interaction equations can be used. This approach was adopted in the RMI Specification [11]. The validity of the approach was further confirmed in [8] on the basis of extensive analytical and experimental studies. The interaction equation is

$$\frac{P}{P_o} + \frac{M_x C_{mx}}{M_{xo} (1 - P/P_x)} + \frac{M_y C_{my}}{M_{yo} (1 - P/P_y)} = 1 \quad \text{Eq. 1}$$

P , M_x and M_y are the axial force and the moments about the x and y axes, respectively, due to the applied loading. P_o is the failure load in the absence of any moment. M_{xo} is the failure moment for bending about the x axis in the absence of an axial load or bending about the y axis. Similarly, M_{yo} is for the bending about the y axis. P_o , M_{xo} and M_{yo} are determined considering both flexural and torsional flexural buckling. C_{mx} and C_{my} are corrections to reflect the moment gradient in the member. P_x and P_y are the flexural buckling loads about the x and y axes, respectively.

INTERACTION OF LOCAL AND FLEXURAL COLUMN BUCKLING

The effect of local buckling on overall buckling behavior has been studied in several research projects at Cornell and elsewhere. On the basis of tests and analytical studies, [2] and [3] conclude that a satisfactory approach is to calculate the overall buckling load using the effective radius of gyration and the effective area, both calculated at the overall buckling stress. This results in an iterative procedure since the buckling stress depends on the effective section properties which in turn depend on the buckling stress. The iterative approach has been extended in [8] to the treatment of torsional flexural buckling.

The approach of [12] for flexural buckling is tried in [1] for a variety of sections and failure modes. This approach is very similar to the one proposed by the author [10] and adopted in the RMI Specification [11] for the treatment of perforated columns and beam columns subject to torsional flexural buckling. The buckling stress is found for an unperforated column and the allowable load is found by multiplying this stress by the net area.

The proposed approach consists of the following steps. First the elastic flexural buckling stress, F_e , is calculated for the full unreduced section:

$$F_e = \pi^2 E / (KL/r)^2 \quad \text{Eq. 2}$$

Then the failure stress, F_u , is determined:

$$F_u = F_e \quad \text{if } F_u < F_y/2 \quad \text{Eq. 3}$$

$$F_u = F_y (1 - F_y/4F_e) \quad \text{if } F_u > F_y/2 \quad \text{Eq. 4}$$



and the ultimate column load P_u is calculated as

$$P_u = A_e F_u \quad \text{Eq. 5}$$

where A_e is the effective area computed at stress F_u .

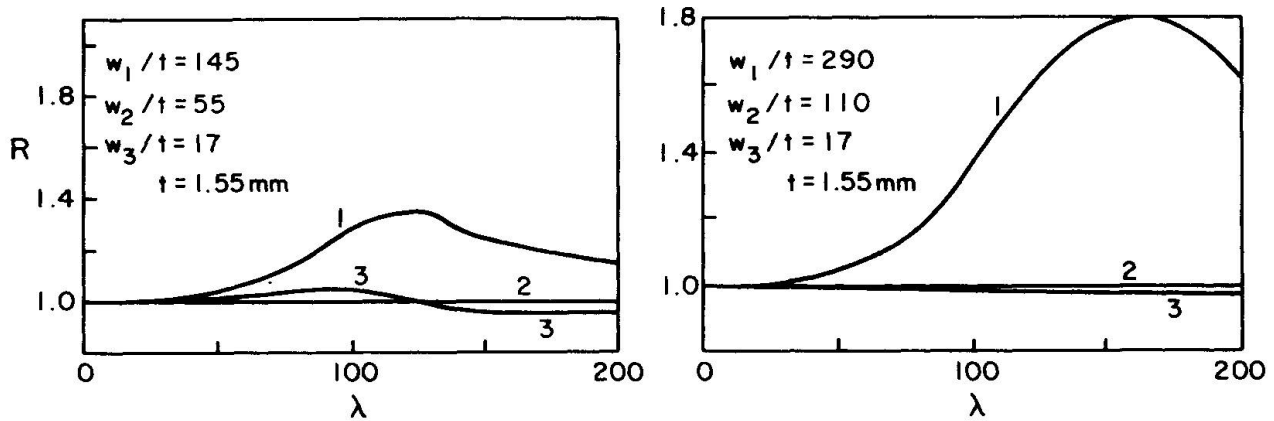


Fig. 2 Interaction of local and overall buckling - C sections ($F_y/E = .0017$)

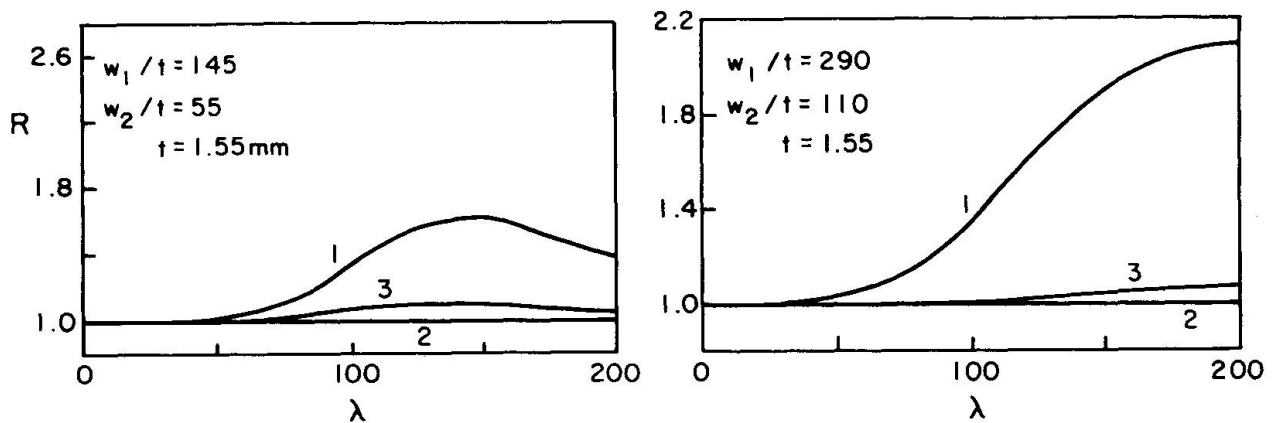


Fig. 3 Interaction of local and overall buckling - tubes ($F_y/E = .0017$)

The studies summarized in [1] show that proposed approach approximates the iterative approach very closely for flexural, torsional flexural and lateral buckling as discussed below. Figures 2 and 3 give some typical examples of the many comparisons presented in [1]. In these figures Curve 1 is for an approach using Eqs. 2, 3 and 4 taking the section to be fully effective and multiplying the yield stress by the ratio A_{eu}/A where A_{eu} is the effective area for yield stress and A is the full area. P_u is taken as $A F_u$. Curve 2 is for the iterative approach which is the best fit to the test data. Curve 3 is obtained with the proposed unified approach. R is the ratio of the P_u obtained by a particular approach to that obtained by the iterative approach. λ is the slenderness ratio KL/r_y .

The remarkable accuracy of the proposed approach can be explained as follows. The reduction in the value of the radius of gyration resulting from local buckling is rather small. For small slenderness ratios where the column buckling stresses are high compared to the yield stress, the buckling stress is quite insensitive to the changes in the radius of gyration. For small stresses, namely large slenderness ratios, the local buckling is not significant. However, the effective area gets influenced directly and significantly by local buckling. Therefore the behavior is well represented by ignoring the change in the radius of gyration and accounting for the reduction in the effective area in finding the ultimate load of the column.

For locally buckled C and other singly symmetric sections, concentric axial loading with respect to the centroid of the effective section is not typical in structures. The centroid of the effective section depends on the magnitude of loading. The location of the centroid moves as the load is increased. The allowable concentric loading is important as a parameter in the interaction equation.

INTERACTION OF LOCAL AND TORSIONAL-FLEXURAL COLUMN BUCKLING

An analytical model for the behavior of locally unstable open sections is developed in [8] on the basis of the torsional flexural theory for the effective section. The theory was confirmed by correlation with test results. As in the case of flexural buckling, the approach involves iterations. Again concentric buckling load is important for a locally buckled section only as a parameter in the interaction equation.

The proposed approach for the torsional flexural buckling of locally buckled columns is exactly the same as that for columns subject to flexural buckling. In the equations 2 through 5 above, only the determination of F_e changes. F_e is determined according to the torsional flexural buckling theory for the full unreduced section.

EVALUATION OF STUB COLUMN TEST RESULTS

The proposed approach necessitates an expression for the effective area A_e as a function of the stress on the effective area f . The stress f is taken as F_u in calculating column strength. When A_e cannot be calculated, such as when the column has dimensions or geometry outside the range of applicability of the generalized effective width equations, a functional relation between f and A_e can be obtained by stub column tests. A stub column is a short column that is long enough to reflect the local buckling behavior but preferably short enough so that the behavior is not affected by the overall buckling. The effective area, A_{eu} , at ultimate load, P_u is:

$$A_{eu} = P_u / F_y \tag{Eq. 6}$$

The effective area at any stress on the effective area f can be calculated as follows [1]:

$$A_e = A - (A - A_{eu}) (f / F_y)^{(A_{eu} / A)} \tag{Eq. 7}$$

where A is the full unreduced area of the section.

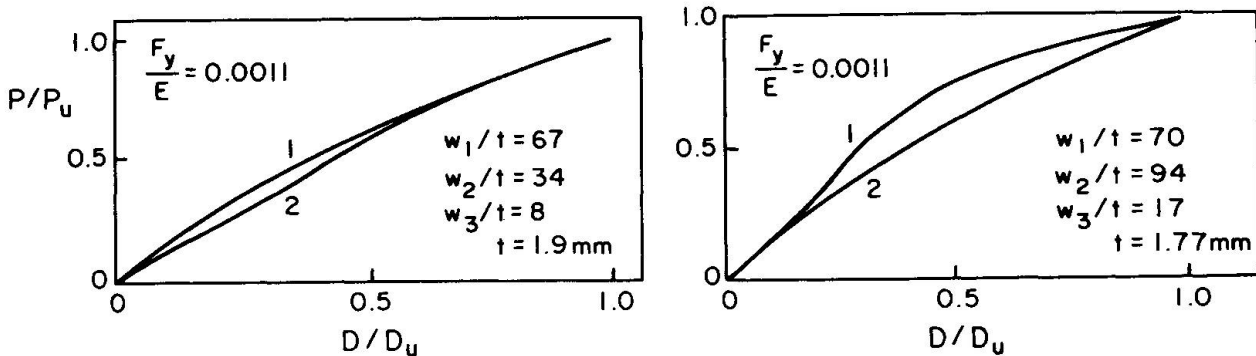


Fig. 4 Evaluation of stub column test results



The validity of the above equations is verified in [1] by a rather extensive parametric study. Many plots as those given in Fig. 4 are presented in [1]. In these figures D is the axial shortening of the stub column at an axial load P . D_u and P_u are the ultimate values of D and P . Curves 1 are based on actual tests. Curves 2 are calculated on the basis of Eqs. 6 and 7. It is seen that the equations are satisfactory and give conservative (low) values of the axial stiffness and consequently the value of A_e .

Approaches for determining an expression for A_e versus f from the measured axial shortening and for the treatment of the case when the stub column is not short enough are formulated in [1].

INTERACTION OF LOCAL AND LATERAL BEAM BUCKLING

The approach proposed in [1] for this case is consistent with the one proposed for columns. First, the elastic lateral buckling stress, F_e , is calculated on the basis of the torsional flexural buckling theory for the full unreduced section using the equations of [13]. Then the failure stress F_u is determined using Eqs. 3 and 4. The lateral buckling moment is determined by multiplying F_u by the effective section modulus calculated for an outer fiber stress of F_u .

The proposed design approach gives results virtually identical with those of the analytical approach developed in [8] on the basis of torsional-flexural buckling theory. There is no direct test data on the lateral buckling of cold-formed steel beams. However some data exists on the behavior of sections with eccentric axial loading. These test results show that the proposed approach is satisfactory [1].

BIAXIALLY LOADED LOCALLY UNSTABLE BEAM COLUMNS

The interaction equation given above was studied extensively and extended to locally unstable sections in [8] and [1]. The approach of [1] involves the use of Eq. 1 for singly or doubly symmetric open sections and closed tubes with some of the terms redefined to account for locally buckled plate elements. P_0 is determined as described above for locally unstable columns. It may be governed by flexural or torsional flexural buckling. M_{x0} and M_{y0} are determined by the approach described above for lateral buckling. All eccentricities (for example e_x in Fig. 1) are taken with respect to the centroid of the effective section for the axial load alone. The parameters P_x and P_y are the elastic buckling loads for the full unreduced section.

The proposed formulation is confirmed in [1] by theory and 107 tests on simply supported, locally unstable C, channel and hat section beam columns. Correlation for angle and lipped angle sections is needed. The extension of the use of the interaction equations for frames is discussed in [1].

An example of the correlation with the test results is illustrated in Fig. 5. This figure presents the results of all the tests with loads with uniaxial or biaxial eccentricities. The figure on the left illustrates the presentation of the results. In this figure R_p , R_x and R_y represent the first, second and the third terms of Eq. 1. Eq. 1 defines the plane ABC. For a given test, the observed values of P , M_x and M_y are substituted into the equation and a point with the resulting R_p , M_x and M_y values is plotted. The results that fall outside the volume OABC indicate that the proposed interaction equation is conservative for those cases. This three-dimensional situation is represented in the figure on the right in two dimensions by plotting the projections of the test points on the R_p - R_0 plane. Thus from geometry R_0 is equal to $.707 (R_x + R_y)$. The points that fall outside the area OAD in the figure on the right show that the Eq. 1 is conservative. The few points that fall within this area have been mostly explained in [1] and the approach is judged satisfactory.

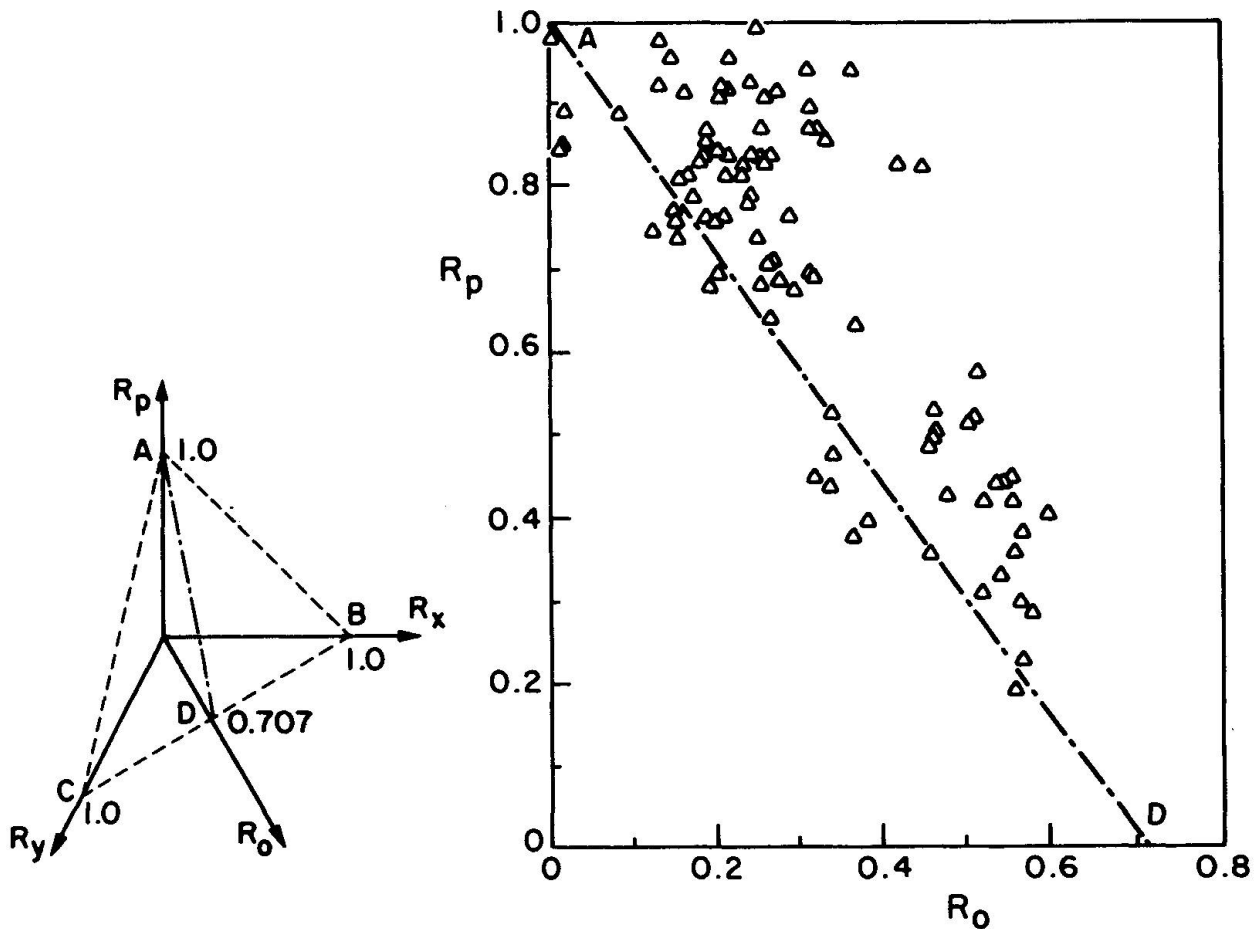


Fig. 5 Correlation of beam column test results with Eq. 1

ACKNOWLEDGEMENTS

The author is deeply grateful to Dr. S. J. Errera, Chairman of the AISI Specification Advisory Committee and the members of the AISI Task Group on Compression Members for their support, review, contributions and enthusiasm. The author would also like to acknowledge the contributions by the coauthors of references 2 through 8 and by Mr. C. C. Weng for his calculations for Fig. 5. The work was sponsored by the American Iron and Steel Institute.

REFERENCES

1. Pekoz, T., "A Unified Approach to the Design of Thin-Walled Steel Members", Department of Civil Engineering Report, Cornell University, 1985.
2. DeWolf, J. T., Pekoz, T. and Winter, G., "Local and Overall Buckling of Cold Formed Steel Members", Journal of the Structural Division, ASCE, October 1974.
3. Kalyanaraman, V., Pekoz, T. and Winter, G., "Unstiffened Compression Elements", Journal of the Structural Division, ASCE, September 1977.
4. Kalyanaraman, V. and Pekoz, T., "Analytical Study of Unstiffened Elements", Journal of the Structural Division, ASCE, September 1978.
5. Desmond, T. P., Pekoz, T., and Winter, G., "Edge Stiffeners for Thin-Walled Members", Journal of the Structural Division, ASCE, February 1981.



6. Desmond, T. P., Pekoz, T. and Winter, G., "Intermediate Stiffeners for Thin-Walled Members", Journal of the Structural Division, ASCE, April 1981.
7. Mulligan, G. P. and Pekoz, T., "Locally Buckled Thin-Walled Columns", Journal of the Structural Division, ASCE, November 1984.
8. Loh, T. S. and Pekoz, T. (Project Director), "Combined Axial Load and Bending in Cold-Formed Steel Members", Department of Structural Engineering Report, Cornell University, 1985.
9. Winter, G., "Strength of Thin Steel Compression Flanges", Transactions, ASCE, Vol. 112, 1947.
10. Pekoz, T., "Design of Cold-Formed Steel Racks", Thin-Walled Structures, Edited by J. Rhodes and A. C. Walker, 1979.
11. Rack Manufacturers Institute, "Specification for Design, Testing and Utilization of Industrial Storage Racks", February 1979.
12. Canadian Standards Association, "Cold Formed Steel Structural Members - A National Standard of Canada", 1984.
13. Pekoz, T. and Winter, G., "Torsional-Flexural Buckling of Thin-Walled Sections under Eccentric Load", Journal of the Structural Division, ASCE, May 1969.

Limit State of a Thin-Walled Rectangular Hollow Beam-Column

Etat ultime des profils creux, de section rectangulaire, à parois minces

Grenzzustand des dünnwandigen Druckstabes

Jerzy GOCZEK

Research Fellow
Techn. Univ. of Łódź
Łódź, Poland



Jerzy Goczek, born 1951, received his structural engineering M.S. and Ph.D. degrees from Technical University of Łódź in 1975 and 1984, respectively, where he is currently research worker.

Marian LUKOWIAK

Prof. of Structural Eng.
Techn. Univ. of Łódź
Łódź, Poland



Marian Lukowiak, born 1939, received his M.S. and Ph.D. degrees from Technical University of Łódź in 1961 and 1965, respectively, where he is currently Professor and Head of the Division of Steel Structures.

SUMMARY

A theoretical study of the behaviour of a thin-walled beam-column affected by plate buckling has been conducted. The moment-curvature-thrust relationships for a rectangular hollow cross-section are developed and the elastic response of a column segment subjected to compression combined with a bending moment is studied. The technical analysis known as the «Curvature Method» is used to obtain the solution for a symmetrically loaded beam-column.

RÉSUMÉ

Dans cet article, nous avons étudié le comportement des profils creux à parois minces en voilement local. Nous avons obtenu les relations entre le moment, la courbure de l'élément et l'effort normal pour les profils creux rectangulaires et analysé le comportement élastique d'une poutre-colonne soumise à une combinaison d'actions compression-moment de flexion. La «méthode de courbure» a été utilisée pour résoudre le cas d'une poutre-colonne chargée symétriquement.

ZUSAMMENFASSUNG

Im Aufsatz wurde das Verhalten des dünnwandigen Stabes mit lokal ausgebeulten Wänden analysiert. Die Abhängigkeit zwischen dem Moment (2. Ordnung) und der Krümmung wurden für den geschlossenen, viereckigen Querschnitt dargestellt. Auch das elastische Verhalten eines Stabstückes unter Druck und Biegung wurde analysiert. Für die Lösung des Problems des symmetrisch belasteten Druckstabes wurde die Krümmungsmethode verwendet.



1. INTRODUCTION

Local buckling is usually a governing mode of the behaviour of thin-walled steel structural elements. The basic concept underlying the design of these elements involves the utilization of the post-buckling strength of the compression plate elements which comprise the cross-section. As a steel column is a system of thin plates, its overall and local deformations are interconnected. The cause of collapse is usually an interaction between two different modes of buckling.

In case of compressed thin-walled columns, which are affected by plate buckling, a great deal of research has been carried out recently and a number of different design analysis procedures has been formulated, but they have proved impractical to apply. Most researchers assume ideal geometrical and structural conditions and calculate the bifurcation load of axially compressed thin-walled columns. However, it is known that local and overall buckling cannot occur in a strict theoretical sense. Since the bifurcation concept does not correspond to the behaviour of real columns it results in an overestimation of the critical load.

Only a few researchers have considered a column with unavoidable initial irregularities. Also the action of the combination of bending moments and a direct compression on a beam-column has received relatively little attention.

Hence, the relationships between generalized stress - generalized strain for a thin-walled rectangular hollow cross-section have been presented and the elastic response of a column segment subjected to compression combined with a bending moment has been studied. Next the analysis technique known as the "Curvature Method" has been used to obtain a solution for the beam-column loaded symmetrically.

2. OUTLINE OF THEORETICAL BACKGROUND

The basic equation of beam-column theory is generally expressed in terms of the lateral displacement of the center line $w(x)$. This approach, known as the "Deflection Method", resolves itself into the differential equation of the fourth order for the deflection curve. Analytical exact solutions in elastic range can be obtained in most cases because the basic relationship between the moment and the curvature is linear. When a beam-column is affected by plate buckling, the solutions cannot be obtained in a similar manner because of high nonlinearity which arises from local buckling.

It has been proved that the curvature of a beam-column can be more useful for the analytical solution than the deflection curve. The analysis technique which involves the curvature is known as the "Curvature Method" and has been developed for elastic-plastic beam-columns [1]. Since the "Curvature Method" requires a moment-curvature-thrust relationship, this has been studied in the paper first and foremost.

3. MOMENT-CURVATURE RELATIONS

Fig. 1 shows a column segment of a rectangular hollow section which is subjected to a bending moment, M , in the plane of symmetry and to an axial thrust P . Considering the deflected configuration of the beam-column, Bernoulli's hypothesis concerning plane cross-sections is assumed.

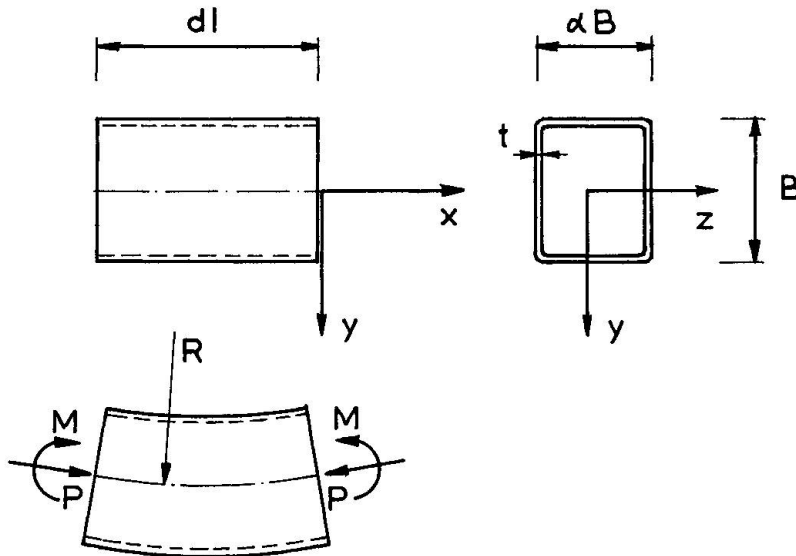


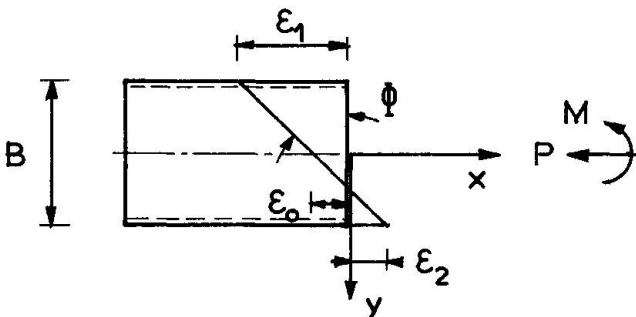
Fig. 1 Compression and bending of a segment

Deflection w of the beam-column is assumed to be of such order that the curvature can be determined by the expression

$$\Phi = -w'' \tag{1}$$

The strain ϵ in the fiber, which is away from the center line by distance y , can be expressed using the curvature Φ and the mean strain ϵ_0 .

$$\epsilon = \Phi y + \epsilon_0 \tag{2}$$



The strain distribution is shown in Fig. 2. If the material is ideally elasto-plastic the corresponding stress distribution is obtained directly from Hooke's law

$$\sigma = E (\Phi y + \epsilon_0) \tag{3}$$

Fig. 2 Strain distribution of a section

in which E is Young's modulus.



Formulations of the exact moment-curvature-thrust relationship are based on the assumption that von Karman's equation describes the post-buckling behaviour of plate elements. The effective widths B_{eff1} and B_{eff2} are uniquely determined by the edge strains ϵ_1 and ϵ_2

$$\frac{B_{\text{eff1}}}{B} = \sqrt{\frac{\epsilon_{\text{cr}}}{\epsilon_1}}, \quad \frac{B_{\text{eff2}}}{B} = \sqrt{\frac{\epsilon_{\text{cr}}}{\epsilon_2}} \quad (4)$$

in which ϵ_{cr} is the local buckling strain.

If it is assumed that local buckling occurs only in flanges subjected to a uniform shortening there are three possible modes of the cross-section behaviour as shown in Fig. 3.

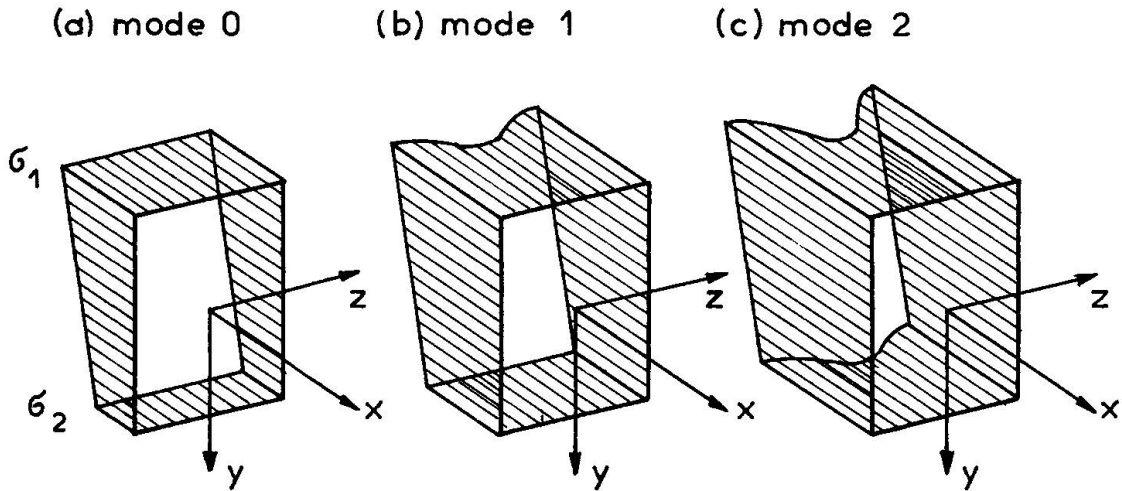


Fig. 3 Modes of the cross-section behaviour

On a cross-section at a distance x , from the end of the beam-column, the generalized stresses or stress resultants are obtained by integrating the axial stress over the entire area of the section, A ,

$$\text{Normal Force: } P(\Phi, \epsilon_0) = \int_A \sigma \, dA \quad (5)$$

$$\text{Bending Moment: } M(\Phi, \epsilon_0) = \int_A \sigma y \, dA \quad (6)$$

These are the relationships between generalized stresses, P and M , and the generalized strains, Φ and ϵ_0 . Next, the analysis is simplified using nondimensionalized quantities

$$p = \frac{P}{P_{\text{cr}}}, \quad m = \frac{M}{M_{\text{cr}}}, \quad \varphi = \frac{\Phi}{\Phi_{\text{cr}}}, \quad \bar{\epsilon} = \frac{\epsilon}{\epsilon_{\text{cr}}} \quad (7)$$

in which the dimensional quantities P_{cr} , M_{cr} and Φ_{cr} , ϵ_{cr} refer to local buckling of plate elements.

Relationships among the bending moment m , the curvature φ and the axial thrust p are derived in three different regimes 0, 1 and 2 according to three modes of the cross-section behaviour:

Regime 0

$$p = \bar{\varepsilon}_0 \quad (8)$$

$$m = \varphi \quad (9)$$

Regime 1

$$p = \frac{1}{2(1 + \alpha)} [2\bar{\varepsilon}_0 + \alpha \sqrt{\varphi + \bar{\varepsilon}_0} + \alpha (-\varphi + \bar{\varepsilon}_0)] \quad (10)$$

$$m = \frac{1}{2(1 + 3\alpha)} \left[\frac{3}{2} \varphi + \alpha \sqrt{\varphi + \bar{\varepsilon}_0} - \alpha (-\varphi + \bar{\varepsilon}_0) \right] \quad (11)$$

Regime 2

$$p = \frac{1}{2(1 + \alpha)} (2\bar{\varepsilon}_0 + \alpha \sqrt{\varphi + \bar{\varepsilon}_0} + \alpha \sqrt{-\varphi + \bar{\varepsilon}_0}) \quad (12)$$

$$m = \frac{1}{2(1 + 3\alpha)} \left(\frac{3}{2} \varphi + \alpha \sqrt{\varphi + \bar{\varepsilon}_0} - \alpha \sqrt{-\varphi + \bar{\varepsilon}_0} \right) \quad (13)$$

Fig. 4 shows the example of these $m - \varphi - p$ relationships for a beam-column of the square cross-section ($\alpha = 1.0$). The exact nonlinear moment-curvature-thrust relationships cannot be used directly in an analytical solution due to their complicated mathematical form. However the exact $m - \varphi - p$ relationships can be easily approximated by elementary functions.

4. LIMIT STATE, INTERACTION CURVES

The limit state is defined by means of the onset of yielding in the column. The limit state criterion can be expressed in form

$$\sigma_1 = \sigma_y \quad (14)$$

Hence, the yield strength of the material σ_y to the local buckling stress σ_{cr} ratio is indicated as n . The ratio n provides information about the range of the post-buckling

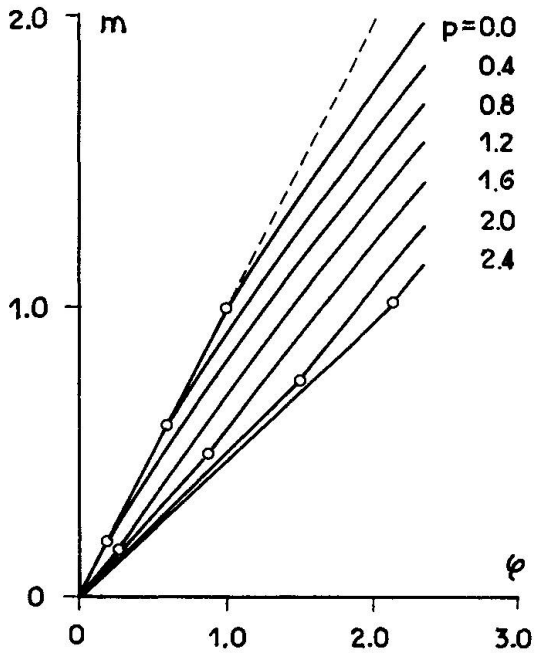


Fig. 4 Moment-curvature-thrust relationships

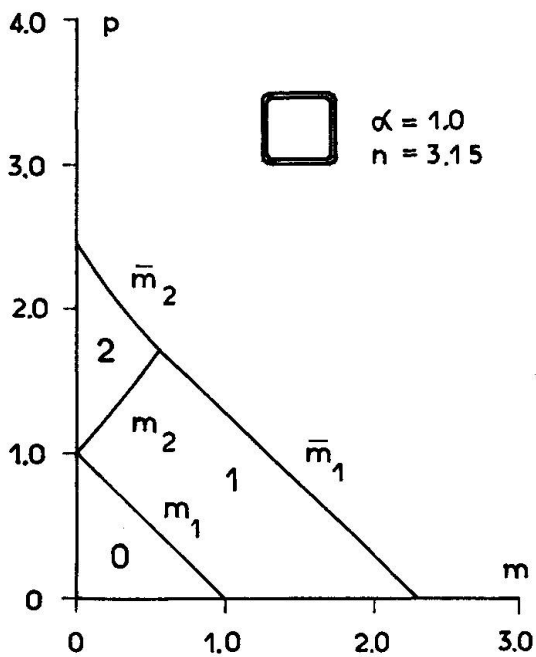


Fig. 5 Interaction curves

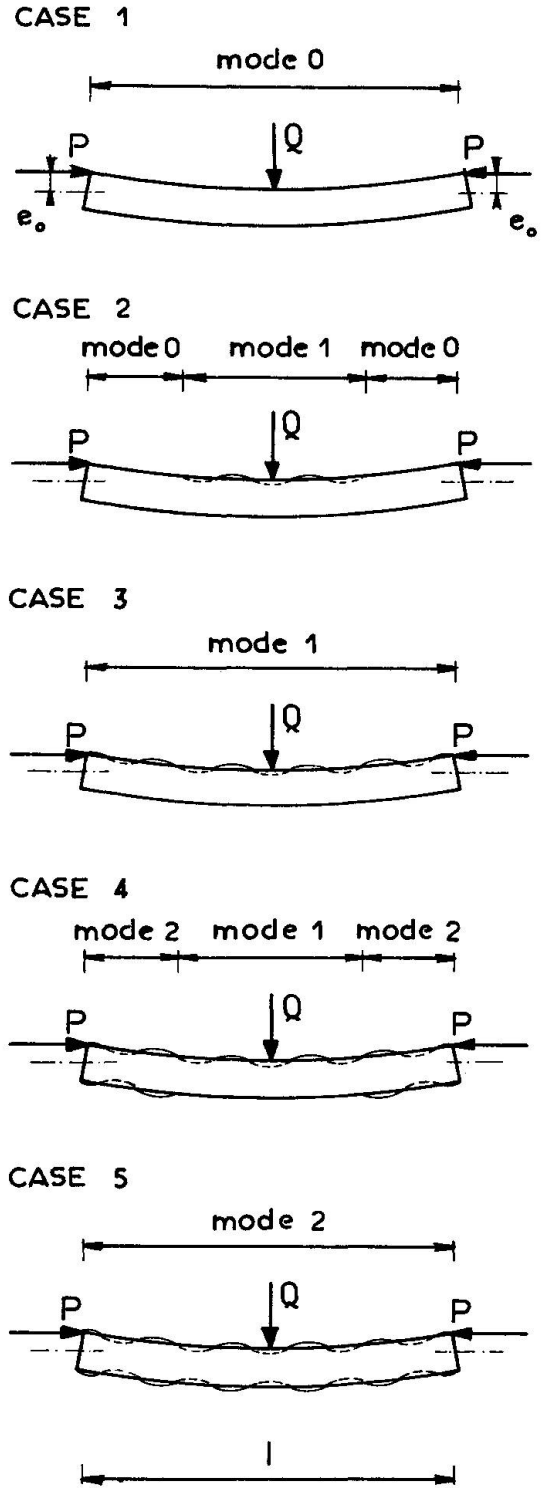


Fig. 6 An eccentrically loaded beam-column (possible cases)

behaviour.

By using $m - \varphi - p$ relationships and the limit state criterion the interaction equations are obtained. Fig. 5 shows the interaction curves.

5. CURVATURE METHOD

The deflection curve $w(x)$ of an elastic beam-column is governed by the following differential equation if there is no lateral load, $q = 0$,

$$M'' - P w'' = 0 \quad (15)$$

Substitution of Φ from Eq. (1) into Eq. (15) results in the basic differential equation as follows

$$[M(\Phi, P)]'' + P \Phi = 0 \quad (16)$$

Combining the equilibrium equation with the $m - \varphi - p$ relationships the basic differential equation for the curvature Φ is obtained.

The concave or both flanges may be buckled locally. Depending on the extent of the local buckling zones, the state of the beam-column is categorized into five possible cases as shown in Fig. 6.

The boundary conditions at the ends of the column and continuity conditions at the boundaries between two adjacent regimes are needed. Since the location of the boundaries are not known, the formulation of these conditions cannot be stated in a routine way. The jump conditions for the derivate of the curvature must be obtained for the determination of the integration constants.

If the $m - \varphi - p$ relationships are approximated by linear functions the solution has a closed form.

5. EXAMPLE OF ANALYSIS

An eccentrically and symmetrically compressed beam-column is studied herein as the particular case of the general solution. Since the analytical $m - \varphi - p$ relationships are linearized, the closed-form solution has a simple form. The results obtained from the analysis are valid for a wide range of cross-section proportions due to the nondimension form.

Fig. 7 shows the relationships between the slenderness ratio and the limit load for the beam-columns of the square hollow section ($\alpha = 1$). The ratio n defines properties of the material and



proportions of the cross-section.

The eccentricity ratio $e/r = 0.05$ is assumed to obtain the limit loads for various values of the slenderness ratio l/r . In Fig. 7 the curve with the eccentricity ratio $e/r = 0.05$ is compared with the exact curve determined for beam-columns of the same parameters but not affected by local buckling ($n = 1.0$). The computed results show a very significant influence of local buckling on the limit state of thin-walled steel columns of small and medium slenderness ratios.

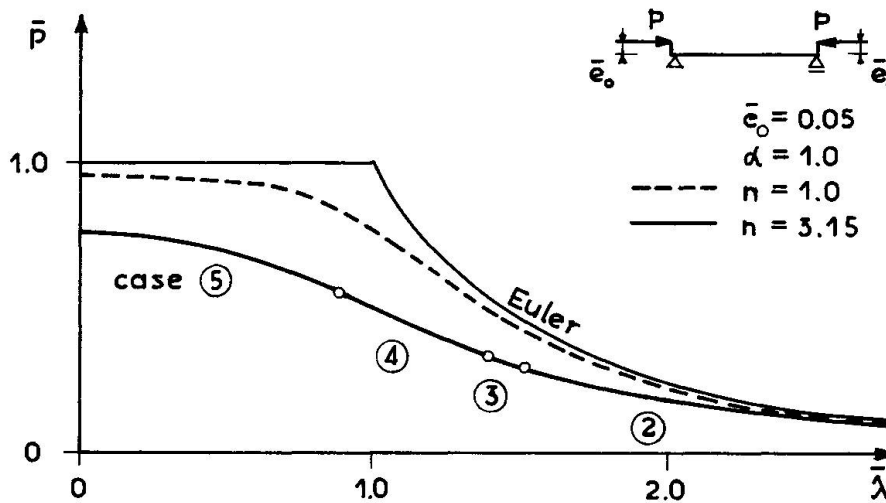


Fig. 7 The effect of local buckling, illustrated by a comparison of the two curves $n=3.15$ and $n=1.0$

6. SUMMARY AND CONCLUSIONS

The Curvature Method, applied for the analysis of thin-walled beam-columns affected by local buckling, permits to solve one of the most difficult problems in the field of structural stability. This method enables designers to assess the limit load of these columns in a simple manner. It is quite general in its applicability to any cross-sectional shape though only the rectangular hollow cross-sections have been considered in this paper.

The moment-curvature-thrust relationships, which play the key role in the study, have been based on the von Karman's expression. The modification to the expression for the effective width and the consideration of local buckling of webs under stress gradient will make for greater accuracy.

REFERENCES

1. CHEN W. F. and ATSUTA T., Theory of Beam-Columns. Vol 1 - In-Plane Behaviour and Design, McGraw-Hill, New York, N.Y., 1976.

Torsional-Flexural Buckling of Partially Closed Thin-Walled Columns

Flambement par flexion et torsion de colonnes à parois minces
partiellement caissonnées

Biegedrillknicken von teilweise geschlossenen dünnwandigen Stützen

Shi-Ji WANG

Professor
Hunan University
Changsha, Hunan, China



Shi-Ji Wang, born 1924, received his BS at Zhong-Zheng University in 1947. For thirty years he has been engaged in teaching and research on steel structures, and now he is the vice-chairman of the Technical Group of the Chinese National Specification Committee for the Design of Cold-Formed Thin-Walled Steel Structures.

SUMMARY

This paper discusses the buckling behavior of partially closed thin-walled sections, i.e. thin-walled open sections with battens, under concentric or eccentric load. A rational method for determining the torsional-flexural buckling load of such members is presented. The influence of prebuckling displacements due to end couples is included in the analysis of instability for both open and partially closed sections. Theoretical results are compared with experimentally obtained buckling loads.

RÉSUMÉ

Cette contribution concerne l'étude du flambement de colonnes dont la section droite est constituée de sections ouvertes à parois minces reliées par des diaphragmes et soumises à des charges centrées et excentrées. On y présente une méthode rationnelle permettant de déterminer la charge de flambement par flexion et torsion de tels éléments. L'influence des déformations dues aux moments d'extrémités est prise en compte dans l'analyse de l'instabilité des sections ouvertes ou partiellement caissonnées. Les résultats de cette analyse sont comparés avec les charges de flambement obtenues expérimentalement.

ZUSAMMENFASSUNG

Dieser Beitrag behandelt das Knickverhalten des teilweise geschlossenen, dünnwandigen Stabes und zwar des offenen dünnwandigen Querschnittes mit Versteifungsblechen unter Axialdruck und exzentrischem Druck. Eine Berechnungsmethode für die Ermittlung der Verzweigungslast bei Biegedrillknicken des Stabes wird vorgestellt. Bei der Analyse der Instabilität wird der Einfluss einer Verschiebung des offenen und des teilweise geschlossenen Querschnitts, die durch Endmomente entsteht, berücksichtigt. Theoretische Ergebnisse werden mit experimentellen Knicklasten verglichen.



INTRODUCTION

It is well known that when torsional-flexural buckling occurs, the critical load of thin-walled open sections will always be less than the in-plane buckling or collapse load. However, if some batten plates are attached along the open side of such members so that there exist several intermittent closed sections, their load-carrying capacity will be increased, and it is possible to transform the mode of failure from torsional-flexural buckling to in-plane instability provided the spacing of battens is short enough to prevent the member from warping and twisting. This problem has been studied by the writer in another paper [1], in which the effect of prebuckling deflection was ignored.

Owing to the fact that the torsional-flexural buckling load of an eccentric column is more or less influenced by its prebuckling deflection, especially for slender member under axial thrust and large terminal moment, the effect of prebuckling deflection has been investigated by Peköz and Winter [2], who assumed a parabolic curve to approximate the in-plane deflection. In this paper, an exact deflection curve is adopted to estimate the influence of prebuckling deflection on torsional-flexural buckling load.

1. ELASTIC TORSIONAL-FLEXURAL BUCKLING OF SINGLY SYMMETRIC OPEN SECTIONS

The total potential energy of a singly symmetric section under axial thrust and equal terminal moments applied in the plane of symmetry as shown in Fig.1 is

$$\Pi = \frac{1}{2} \int_0^L [EI_y u''^2 + EI_x v''^2 + EC_w \varphi''^2 + (GJ - Pr_o^2 + M\beta_y) \varphi'^2 - P(u'^2 + v'^2) + 2(Px_o + M)v'\varphi'] dz \tag{1}$$

where x,y= symmetric and unsymmetric axis of the cross-section, respectively;

E = modulus of elasticity; G = shear modulus; I_x, I_y = moments of inertia with respect to x- and y-axis; J = St Venant torsion constant C_w = warping constant; x_o = abscissa of the shear centre; u,v = displacements of the shear centre in the x and y direction; φ = angle of rotation of the cross-section about the shear centre; P = axial thrust; M = bending moment in the symmetric plane and

$$r_o^2 = (I_x + I_y) / A + x_o^2 \tag{2}$$

$$\beta_y = \frac{1}{I_y} \int_A x(x^2 + y^2) dA - 2x_o \tag{3}$$

For simply supported beam-columns subjected to equal end moments M_o and axial thrust P the deflection curve can be expressed by the following equation [3]

$$u = \frac{M_o}{P \cos(kL/2)} \cos\left(\frac{kL}{2} - kz\right) - \frac{M_o}{P} \tag{4}$$

from which

$$M = -EI_y u'' = M_o (\cos kz + \tan w \sin kz) \tag{5}$$

where

$$k = \sqrt{P/EI_y} \tag{6}$$

$$w = kL/2 \tag{7}$$

Since we are interested to obtain the torsional-flexural buckling load only, the expression for total potential energy can be

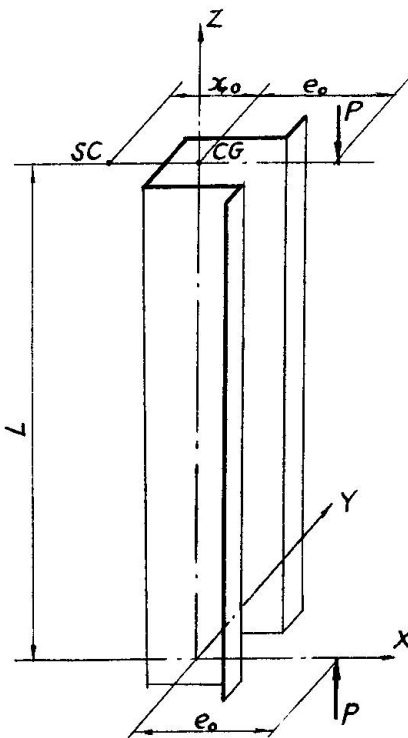


Fig.1 Singly symmetric open section under eccentric load

reduced to

$$\Pi = \frac{1}{2} \int_0^L \left[EI_x v''^2 + EC_w \varphi''^2 + (GJ - Pr_0^2 + M\beta_y) \varphi'^2 - Pv'^2 + 2(Px_0 + M)v'\varphi' \right] dz \quad (8)$$

1.1 Unbattened Open Sections

The deflection components v and φ under various boundary conditions are assumed as shown in Table 1, in which v_0 and φ_0 are undetermined parameters.

Boundary Conditions at $z=0, L$	v	φ
$U=v=\varphi=0, u''=v''=\varphi''=0$	$v_0 \sin(\pi z/L)$	$\varphi_0 \sin(\pi z/L)$
$u=v=\varphi=0, u''=v''=\varphi'=0$	$v_0 \sin(\pi z/L)$	$\varphi_0 [1 - \cos(2\pi z/L)]$
$u=v=\varphi=0, u''=v'= \varphi'=0$	$v_0 [1 - \cos(2\pi z/L)]$	$\varphi_0 [1 - \cos(2\pi z/L)]$

Table 1 Assumed deflection components

Substituting the appropriate deflection components v, φ and the in-plane moment given in eqn 5 into eqn 8, and using the Rayleigh-Ritz method an approximate value of the torsional-flexural buckling load can be obtained. The solution is expressed in a generalized form as follows

$$\begin{vmatrix} P_x - P & K'_{23} P(x_0 - C_1 e_0) \\ K'_{32} P(x_0 - C_1 e_0) & r_{ec}^2 (P_z - P) \end{vmatrix} = 0 \quad (9)$$

Expansion of eqn 9 leads to

$$r_{ec}^2 (P_x - P)(P_z - P) - K_{23}^2 P^2 (x_0 - C_1 e_0)^2 = 0$$

Solving this equation yields the torsional-flexural buckling load

$$P_{TF} = \frac{P_x + P_z - \sqrt{(P_x + P_z)^2 - 4DP_x P_z}}{2D} \quad (10)$$

where

$$P_x = K_{22} \pi^2 EI_x / L^2 \quad (11)$$

$$P_z = (K_{33} \pi^2 EC_w / L^2 + GJ) / r_{ec}^2 \quad (12)$$

$$r_{ec}^2 = r_0^2 + C_2 \beta_y e_0 \quad (13)$$

$$e_0 = M_0 / P \quad (14)$$

$$D = 1 - K_{23}^2 (x_0 - C_1 e_0)^2 / r_{ec}^2 \quad (15)$$

$$K_{23} = \sqrt{K'_{23} K'_{32}} \quad (16)$$

C_1, C_2 = amplification factors for eccentricity

Values of coefficients K_{ij}, K'_{ij} and amplification factors C_1, C_2 are given in Table 2.

Since C_1 and C_2 are functions of P , direct solution of eqn 10 would be either difficult or impossible, and method of successive approximation must be employed. The initial values for both C_1 and C_2 may be taken as unity, i.e., the member is assumed to be undeflected prior to buckling, thus a first approximation of the critical value of P can be found. This value is used to compute C_1 and C_2 and the second approximation of P can be obtained by substituting them into eqn 10. Repeat the procedure until a satisfactory accurate result is reached.



Boundary conditions at $z=0, L$	K_{22}	K_{33}	K'_{23}	K'_{32}	$K_{23} = \frac{K'_{23} K'_{32}}{\sqrt{K'_{23} K'_{32}}}$	C_1	C_2
$u = v = \varphi = 0$ $u'' = v'' = \varphi'' = 0$	1	1	1	1	1	$\frac{\pi^2 - 2w^2}{\pi^2 - w^2} \frac{\tan w}{w}$	$\frac{\pi^2 - 2w^2}{\pi^2 - w^2} \frac{\tan w}{w}$
$u = v = \varphi = 0$ $u'' = v'' = \varphi' = 0$	1	4	$\frac{16}{3\pi}$	$\frac{4}{3\pi}$	$\frac{8}{3\pi}$	$\frac{3\pi^2}{4} \left(\frac{3}{9\pi^2 - 4w^2} + \frac{1}{\pi^2 - 4w^2} \right)$	$\frac{4\pi^2}{4\pi^2 - w^2} \frac{\tan w}{w}$
$u = v = \varphi = 0$ $u'' = v' = \varphi' = 0$	4	4	1	1	1	$\frac{4\pi^2}{4\pi^2 - w^2} \frac{\tan w}{w}$	$\frac{4\pi^2}{4\pi^2 - w^2} \frac{\tan w}{w}$

Table 2 Values of K_{ij}, K'_{ij} and expressions of C_1, C_2

1.2 Open Sections with Battens

Since batten plates are employed to form several closed sections intermittently along the longitudinal axis of the member, we assume that the rate of change of twisting angle at these sections vanishes provided the shearing rigidity of the batten plates is large enough to prevent the sections from warping. Suppose that the centre lines of battens divide the length of the member into n equal segments, thus the centre-to-centre spacing of battens becomes $a = L/n$ as shown in Fig. 2.

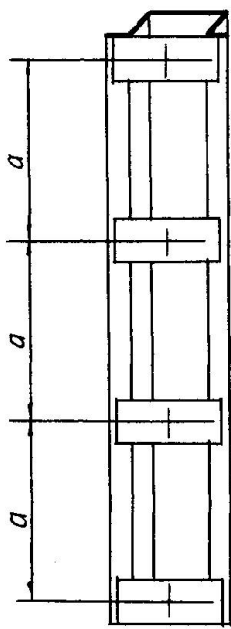
According to the assumption mentioned above, the deflection component φ must satisfy the following additional boundary conditions:

$$\varphi' = 0 \text{ at } z = ja \quad (j = 1, 2, 3, \dots, n-1)$$

Two cases are studied for singly symmetric open sections with battens.

1.2.1 The boundary conditions at both ends are: $u = v = \varphi = 0, u'' = v'' = \varphi' = 0$.

For battened members under this end conditions, the assumed deflection function φ given in Table 1 is replaced by



$$\varphi = \varphi_0 \left\{ \sin\left(\frac{i-1}{n}\right)\pi + \sin\frac{\pi}{2n} \cos\left(\frac{2i-1}{2n}\right)\pi \left[1 + (-1)^i \cos\frac{\pi z}{a} \right] \right\} \quad (17)$$

$(i = 1, 2, 3, \dots, n+1)$

where $i = j+1$ and n is an even number.

Applying the Rayleigh-Ritz method one obtains the same expression for P_{TF} as eqn 10 only if P_z, K_{23}, K'_{32} and K_{23} are replaced by

$$P_z = (\pi^2 EC_w/a^2 + GJ)/r_{eq}^2 \quad (18)$$

$$K'_{23} = \frac{2n^2}{(n^2-1)\pi} \sin\frac{\pi}{n} \sum_{i=1}^n \cos^2\left(\frac{2i-1}{2n}\right)\pi \quad (19)$$

$$K'_{32} = \frac{4n}{(n^2-1)\pi \tan\frac{\pi}{2n}} \quad (20)$$

$$K_{23} = \sqrt{K'_{23} K'_{32}}$$

When $n \geq 2$, the values of K_{23} vary from 0.8488 to 0.9003

If n is an odd number, eqn 17 is valid only for $0 \leq z \leq (n-1)a/2$ and $(n+1)a/2 \leq z \leq L$. For the mid-segment, i.e., when $(n-1)a/2 \leq z \leq (n+1)a/2$, the assumed function should be replaced by

$$\varphi = \varphi_0 \left[\cos\frac{\pi}{2n} + \frac{1}{2} (1 - \cos\frac{\pi}{2n}) (1 - \cos\frac{2\pi z}{a}) \right] \quad (21)$$

Fig.2 Open section with battens



Applying the same procedure as before, the coefficients K'_{23} and K'_{32} can be derived as follows

$$K'_{23} = \frac{4n^2}{\pi} \left[\frac{n}{4(n^2-1)} \sin \frac{\pi}{n} + \frac{2}{4n^2-1} \sin \frac{\pi}{2n} (1 - \cos \frac{\pi}{2n}) \right] \quad (22)$$

$$K'_{32} = K'_{23} / \left[\frac{n^2}{2} \sin^2 \left(\frac{\pi}{2n} \right) + n(1 - \cos \frac{\pi}{2n})^2 \right] \quad (23)$$

When $n \geq 3$, the values of $K_{23} = \sqrt{K'_{23}K'_{32}}$ vary between 0.8973 and 0.9003.

1.2.2 The boundary conditions at both ends are: $u = v = \varphi = 0$, $u'' = v'' = \varphi' = 0$.

In order to satisfy the boundary conditions at both ends and intermediate batted sections, the assumed function for φ should be replaced by

$$\varphi = \varphi_0 \left\{ \left[1 - \cos \frac{2(i-1)\pi}{n} \right] + \sin \frac{\pi}{n} \sin \frac{(2i-1)\pi}{n} \left[1 + (-1)^i \cos \frac{\pi z}{e} \right] \right\} \quad (24)$$

$$(n = \text{even numbers, } i = 1, 2, 3, \dots, n+1)$$

from which

$$K'_{23} = K'_{32} = 1 \quad (n = 2) \quad (25)$$

$$\left. \begin{aligned} K'_{23} &= \frac{n^3}{2(n^2-4)\pi} \sin \frac{2\pi}{n} \\ K'_{32} &= \frac{8n}{(n^2-4)\pi \tan \frac{\pi}{n}} \end{aligned} \right\} (n \geq 4) \quad (26)$$

When $n \geq 4$, K_{23} vary between 0.8498 and 0.9003.

In the cases when n are odd numbers eqn 24 is valid only for $0 \leq z \leq (n-1)e/2$ and $(n+1)e/2 \leq z \leq L$, in the interval $(n-1)e/2 \leq z \leq (n+1)e/2$ we use the following function instead:

$$\varphi = \varphi_0 \left[(1 + \cos \frac{\pi}{n}) + \frac{1}{2} (1 - \cos \frac{\pi}{n}) (1 - \cos \frac{2\pi z}{e}) \right] \quad (27)$$

from which

$$K'_{23} = \frac{1}{\pi} \left[\frac{n^2}{n^2-4} \sin \frac{2\pi}{n} + \frac{2}{n^2-1} \sin \frac{\pi}{n} (1 - \cos \frac{\pi}{n}) \right] \quad (28)$$

$$K'_{32} = K'_{23} / \left[\frac{1}{2} \sin^2 \left(\frac{\pi}{n} \right) + \frac{1}{n} (1 - \cos \frac{\pi}{n})^2 \right] \quad (29)$$

When $n \geq 3$, $K_{23} = \sqrt{K'_{23}K'_{32}}$ vary between 0.7839 and 0.9003.

1.2.3 Simplified approach for determining the torsional-flexural buckling load of partially closed members.

It should be noted that if there is only one intermediate batten plate attached at the mid-span of the member, i.e. $n=2$, its buckling behavior is identical to the unbattened member with the same dimensions. As a result, when $n=2$, the coefficient K_{23} will automatically coincide with that given in Table 2, and we can conclude that the buckling behavior of thin-walled open sections will not be improved if only one batten plate is used. So that at least two batten plates are required for battened members.

Summarizing the two cases of end conditions in 1.2.1 and 1.2.2, the values of K_{23} vary from 0.7839 to 0.9003 except for $n=2$. Fortunately, the range of variation is so small that we can use a definite value for K_{23} without regard to the number of battens. For this reason the writer suggests $K_{23} = 0.9$ for all the cases mentioned above, which yields a slightly conservative value of the theoretical buckling load. Thus, eqns 10, 11, 13 to 16, and coefficients K_{22}, C_1, C_2 given in Table 2 are also valid for partially closed sections, but eqn 12 should be replaced by eqn 19 and take $K_{23} = 0.9$.



2. INELASTIC TORSIONAL-FLEXURAL BUCKLING

For centrally loaded simple columns, the inelastic buckling load can easily be found by using the well known tangent modulus theory. However, when torsional buckling occurs, the problem becomes more complex because both E and G no longer remain constants, so that the elastic section rigidities EI_x, GJ and EC_w should be replaced by the tangent section rigidities $(EI_x)_t, (GJ)_t$ and $(EC_w)_t$, respectively. Bleich [4] presented a simplified treatment for inelastic torsional buckling, which was based on the assumption that E and G in the whole section will be reduced to E_t and G_t synchronously, where τ is the ratio of tangent modulus E_t to the elastic modulus E . In this paper, Bleich's suggestion is adopted to determine the inelastic torsional-flexural buckling loads. Thus eqn 10 is also valid for inelastic domain if E and G in eqns 11, 12 are replaced by E_t and G_t .

2.1 Equivalent Length for Torsional-Flexural Buckling

For design purposes, a new concept, the equivalent length for torsional-flexural buckling, is introduced herein.

From eqn 9

$$\frac{1}{P} = \frac{P_x + P_z}{2P_x P_z} + \sqrt{\left(\frac{P_x + P_z}{2P_x P_z}\right)^2 - \frac{r_{eq}^2 - K_{23}^2(x_o - C_1 e_o)^2}{r_{eq}^2 P_x P_z}} \quad (30)$$

The larger root of $1/P$ corresponds to the smaller root of P , thus

$$P_{TF} = \frac{K_{22} \pi^2 E I_x / L^2}{\frac{s^2 + r_{eq}^2}{2s^2} + \sqrt{\left(\frac{s^2 + r_{eq}^2}{2s^2}\right)^2 - \frac{r_{eq}^2 - K_{23}^2(x_o - C_1 e_o)^2}{s^2}}} \quad (31)$$

where

$$P_x = K_{22} \pi^2 E_t I_x / L^2 \quad (32)$$

$$P_z = (K_{33} \pi^2 E_t C_w / L_w^2 + G_t J) / r_{eq}^2 \quad (33)$$

$$\begin{aligned} s^2 &= \frac{r_{eq}^2 P_z}{P_x} = \frac{K_{33} \pi^2 E_t C_w / L_w^2 + G_t J}{K_{22} \pi^2 E_t I_x / L^2} \\ &= \frac{L^2}{K_{22} I_x} \left(\frac{K_{33} C_w}{L_w^2} + \frac{GJ}{\pi^2 E} \right) \end{aligned} \quad (34)$$

K_{22}, K_{33}, K_{23} and L_w are evaluated as follows:

For unbattened members: $L_w = L$; K_{22}, K_{33} and K_{23} are given in Table 2.

For battened members: $L_w = a$, $K_{33} = 1$, $K_{23} = 0.9$, K_{22} is given in Table 2.

Let

$$\mu = \sqrt{\frac{s^2 + r_{eq}^2}{2s^2} + \sqrt{\left(\frac{s^2 + r_{eq}^2}{2s^2}\right)^2 - \frac{r_{eq}^2 - K_{23}^2(x_o - C_1 e_o)^2}{s^2}}} \quad (35)$$

then

$$P_{TF} = K_{22} \pi^2 E I_x / (\mu L)^2 \quad (36)$$

in which μL is defined as the equivalent length for torsional-flexural buckling. Since the inelastic factor τ can be eliminated in eqn 34, so that the equivalent-length coefficient μ is valid for both elastic and inelastic buckling, and P_{TF} can be obtained by using the basic column curve.



Specimen	Dimensions (mm)					No. of batten plates	e_0 in mm	Axial load (KN)			P_{exp}	P_{exp}
	h	b	c	t	L			P_{yd}	P_{TF}	P_{exp}	P_{yd}	P_{TF}
H1-1-0	62.3	77.8	25.5	2.56		0		82.99	78.59	76.10		0.968
H1-1-2	62.0	77.2	25.8	2.52	2710	2	-10	81.08	90.73	86.00	1.061	
H1-1-3	63.1	77.8	25.9	2.42		3		79.84	112.80	95.32	1.194	
H1-2-0	62.9	76.6	26.0	2.53		0		129.04	49.65	50.50		1.017
H1-2-2	62.8	76.8	26.7	2.77		2		141.40	87.98	87.38		0.993
H1-2-3	62.8	77.7	25.7	2.61	2710	3	0	134.39	105.34	98.07		0.931
H1-2-4	63.1	78.1	25.9	2.66		4		137.87	126.90	116.70		0.920
H1-2-5	62.9	76.7	25.6	2.52		5		128.24	129.77	123.56	0.964	
H1-3-0	63.1	76.7	25.7	2.47		0		77.13	37.93	38.83		1.024
H1-3-2	62.5	77.9	25.5	2.55	2710	2	+10	80.63	62.08	62.76		1.011
H1-3-3	62.7	76.0	26.5	2.54		3		78.47	81.43	75.51	1.039	
H1-3-4	62.6	76.5	26.2	2.52		4		78.38	94.36	73.06	1.073	
H1-4-0	62.5	76.8	25.8	2.46		0		59.39	31.30	31.68		1.012
H1-4-2	63.0	77.2	25.8	2.53	2710	2	+20	61.45	52.71	56.00		1.062
H1-4-3	62.3	78.0	25.5	2.46		3		60.61	68.01	63.74	1.052	
H1-4-4	63.2	78.1	26.6	2.58		4		64.46	88.87	67.96	1.054	
H1-5-0	63.0	77.8	25.7	2.45		0		50.14	27.56	27.65		1.003
H1-5-2	63.3	76.8	27.5	2.53	2710	2	+30	52.00	48.49	48.15		0.993
H1-5-3	63.1	77.4	25.6	2.59		3		52.05	63.67	49.43	0.950	
H1-6-0	64.5	78.1	26.2	2.49		0		44.46	25.93	25.99		1.002
H1-6-2	63.2	79.5	25.6	2.49	2710	2	+40	44.98	42.19	39.23		1.075
H1-6-3	62.6	74.8	27.1	2.47		3		41.80	54.41	44.13	1.056	
H1-7-0	62.6	77.5	27.0	2.59	2710	0	+50	40.27	24.07	22.75		0.945
H1-7-2	63.0	76.9	26.8	2.50		2		38.52	37.87	36.28		0.959
H1-8-0	62.5	76.9	25.3	2.51	2710	0	+60	33.52	19.81	18.24		0.921
H1-8-2	62.2	77.5	25.8	2.68		2		36.14	35.75	34.03		0.952
H2-1-0	60.5	77.0	25.9	2.48	1890	0	-10	96.07	122.70	96.60	1.006	
H2-1-2	61.9	76.1	26.1	2.49		2		95.86	134.34	96.11	1.003	
H2-2-0	60.6	76.3	26.9	2.46		0		143.58	86.02	85.81		0.998
H2-2-2	62.8	76.1	25.6	2.46	1890	2	0	142.94	128.24	120.62		0.941
H2-2-3	60.4	77.6	25.2	2.52		3		146.37	191.83	129.94	0.888	
H2-3-0	61.2	78.3	25.9	2.44	1890	0	+10	94.74	67.33	60.80		0.903
H2-3-2	62.0	76.4	26.3	2.49		2		94.24	120.05	86.30	0.916	
H2-4-0	61.7	75.9	26.2	2.41	1890	0	+20	68.13	55.00	54.92		0.999
H2-4-2	61.8	76.3	26.5	2.47		2		70.44	100.84	71.59	1.016	
H2-5-0	61.5	76.6	26.2	2.45	1890	0	+30	56.76	48.67	45.60		0.937
H2-5-2	61.8	76.5	26.6	2.47		2		57.49	88.74	56.88	0.989	
H3-1-0	60.9	77.7	25.7	2.41	1480	0	-10	100.80	133.02	101.01	1.002	
H3-2-0	61.9	77.2	25.4	2.47	1480	0	0	150.75	124.01	115.72		0.933
H3-2-2	62.4	76.4	26.4	2.47		2		151.53	249.86	141.71	0.935	
H3-3-0	61.2	76.4	25.5	2.41	1480	0	+10	96.26	99.41	91.20	0.948	
H3-4-0	60.4	76.6	25.0	2.43	1480	0	+30	58.07	70.22	56.88	0.980	

Table 3 Theoretical and experimental failure load comparisons



3. EXPERIMENTS

In order to confirm the theory, a series of test were performed. The tests consisted of cold-formed thin-walled hat sections with various slenderness ratios under concentric or eccentric load. Two or more intermediate batten plates with equal spacing were welded on the open side of the member except those unbattened ones. The shape of the cross section is shown in Fig.3, and their dimensions are given in Table 3. A thick plate was welded to each end of specimens, and both ends were seated on the cruciform-knife supports, thus the boundary conditions of the test columns approach to $u = v = \psi = 0$, $u'' = v'' = \psi' = 0$ at both ends and $\psi' = 0$ at battened sections. The experimental ultimate loads P_{exp} and theoretical values of P_{TF} and the initial yield loads P_{yd} are also given in Table 3.

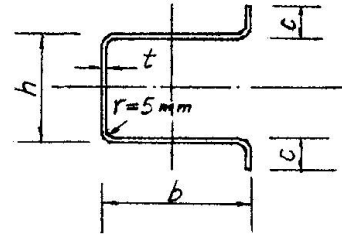


Fig.3 Cross section of specimens

4. CONCLUSIONS

A rational method for determining the torsional-flexural buckling load for thin-walled columns of open cross sections is presented. This method is valid for battened and unbattened members under concentric or eccentric load. The influence of prebuckling deflection is taken into consideration. For the convenience of design, the equivalent-length coefficient is introduced. This coefficient is applicable for both elastic and inelastic buckling. Comparing the theoretical values with experimental results the following conclusions may be drawn:

The torsional-flexural buckling load of an open thin-walled column can be increased by attaching batten plates on its open side.

It is possible to transform the mode of failure from torsional-flexural buckling into in-plane instability if sufficient number of battens are used.

When $P_{TF} \geq P_{yd}$ torsional buckling does not occur, more batten plate is unnecessary because the ultimate load of the member can not be further increased.

REFERENCES

1. WANG, SHI-JI, Torsional-Flexural Buckling of Open Thin-Walled Columns with Battens. Thin-Walled Structures, No.3,1985.
2. PEKÖZ, T.B. and WINTER, G., Torsional-Flexural Buckling of Thin-Walled Sections Under Eccentric Load, Journal of the Structural Division, ASCE, Vol.95, No.ST5, Proc. Paper 6571, May 1969.
3. TIMOSHENKO, S.P. and GERE, J.M., Theory of Elastic Stability, 2nd edn., McGraw-Hill, New York, 1961, p.14.
4. BLEICH, F., Buckling Strength of Metal Structures, McGraw-Hill, New York, 1952.

Single Load on Trapezoidal Steel Sheet

Charge concentrée appliquée sur une tôle profilée en acier
de forme trapézoïdale

Einzellast auf einem trapezförmigen Stahlblech

Germund JOHANSSON

Assist. Prof.
Chalmers Univ. of Technology
Göteborg, Sweden



Germund Johansson, born 1937, received his civil engineering degree at Chalmers Univ. of Technology in 1962. After some years at a consulting firm for geotechnical problems he joined the Dep. of Steel and Timber Structures at Chalmers Univ. of Technology. His research interests are, among others, steel structures, roofs, and structural damage (due to snow, wind).

SUMMARY

A simple model is presented for the calculation of moments and deflections for a trapezoidal steel sheet loaded by a single transversal load at mid-span. The theoretical calculations are compared with laboratory tests on nine different types of steel decks. Results from «in situ» tests are given.

RÉSUMÉ

Un modèle simple de calcul des moments et des flèches d'une plaque profilée de forme trapézoïdale soumise à une charge concentrée transversale à mi-travée est présenté. Les résultats théoriques sont comparés aux résultats d'essais effectués en laboratoire sur neuf types différents de tôles profilées. Des résultats d'essais «in situ» sont également donnés.

ZUSAMMENFASSUNG

Ein einfaches Modell für die Berechnung von Momenten und Durchbiegungen eines trapezförmigen profilierten Stahlbleches, das durch eine Einzellast in der Feldmitte belastet ist, wird beschrieben. Die theoretische Berechnung wird mit Laborversuchen von neun verschiedenen Stahlblechtypen verglichen. Ergebnisse von einigen Feldversuchen werden ebenfalls angegeben.



1. INTRODUCTION

The resistance against a single load on a thin-walled steel deck is very important as most of the steel decks are used as working platforms during the erection period. Two properties of structural behaviour are important - the distribution of deformation over the neighbouring profiles and the capacity to withstand a single load acting on one of the profile tops. If a load is applied on the steel deck near bonded insulation, it is easy to damage the bonding. What is the load magnitude that can be accepted without permanent local deformation of the flange or the web? Those two questions have been pretty much discussed during the last years.

The concepts of (a) "capacity to carry a single load" and (b) "walkability" are concepts partly overlapping each other. The assessment of "walkability" is mainly subjective. To exceed the load carrying capacity, without deformation restrictions, is very hard in practice. The steel sheet can buckle at a rather low load level but the load can be raised to several times the buckling load due to the "suspension" effect. "Walkability" means among other things that the steel sheet must carry a walking man without permanent indentation. In the Swedish standard it is stated that the residual deformation under the load must not exceed 3 mm.

2. THEORETICAL MODEL

Let us start with a simple model, the simply supported trapezoidal steel sheet with a single load applied in the middle. Of all the single profiles ("waves") only three waves are assumed to be active. The loaded wave is supposed to be supported by the two neighbouring waves via springs, c.f. fig.1.

The deflection for the mid-wave and for the side-waves are denoted y_m and y_s respectively. The spring force q acting between these two "beams" is

$$q = c(y_m - y_s) \quad (1)$$

where c is the spring stiffness.

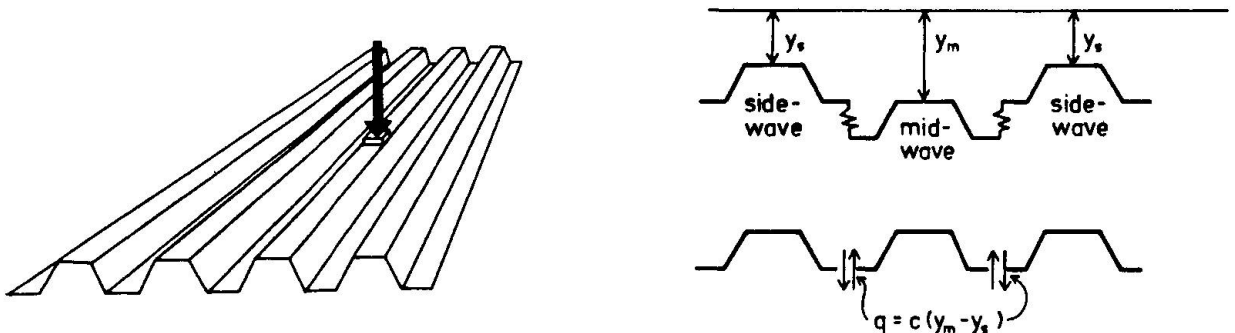


Fig.1 Model

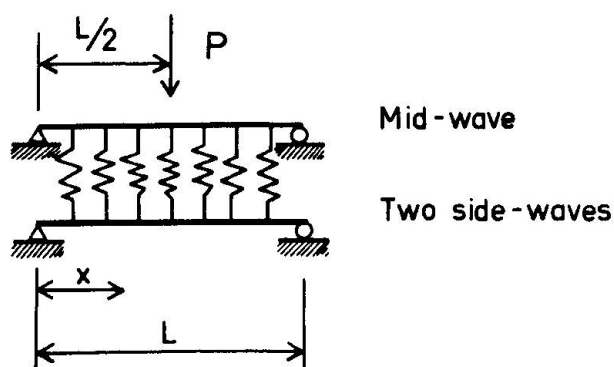


Fig.2 Model with springs

With the assumption that the bending stiffness EI does not vary along the length and that middle- and side-waves have the same stiffness the relationships between forces and deformations are

$$\frac{d^2 y_m}{dx^2} = -\frac{M_m}{EI} ; \quad \frac{d^2 M_m}{dx^2} = 2q \quad (2)$$

This gives

$$\frac{d^4 y_m}{dx^4} = -\frac{2c}{EI} (y_m - y_s) \quad (3)$$

and for the side beam

$$\frac{d^4 y_s}{dx^4} = -\frac{c}{EI} (y_s - y_m) \quad (4)$$

Instead of solving these two equations exactly, which leads to cosh·sinh terms - we will use a simple approximation for the form of the deflection curve. We assume that the deflection line can be approximated by the first term of a Fourier series.

$$y = \delta_0 \sin \frac{\pi x}{L} \quad (5)$$

where the boundary conditions $y = 0$ for $x = 0$ and $x = L$ are fulfilled. The approximation is rather good because it is known that the form of the deflection curves, both under a single load and a distributed load, is very close to the sinusoidal shape. With the sinusoidal deflection curves also the spring force distribution will be sinusoidal.

$$q = q_0 \sin \frac{\pi x}{L} \quad (6)$$

where q_0 is the intensity at $x = \frac{L}{2}$. At the midspan deflection due to the load q , eq (6), is

$$\delta_0 = \frac{q_0 L^4}{\pi^4 EI} \quad (7)$$

With the assumptions made above the deflection for the mid-wave, the deflection for the side-wave and the relationship between deflection and spring force are

$$\delta_m = \frac{PL^3}{48EI} - \frac{2q_0 L^4}{\pi^4 EI} ; \quad \delta_s = \frac{q_0 L^4}{\pi^4 EI} ; \quad q_0 = c(\delta_m - \delta_s) \quad (8)$$

where

δ_m = midspan deflection, mid-wave
 δ_s = midspan deflection, side-wave



3. SPRING STIFFNESS

One key point in this evaluation is the value of the spring stiffness c . The forces between the loaded wave and the supporting waves are transmitted through bending of the steel sheet in the transverse direction. It is difficult to decide exactly which part of the profile will be active to transmit forces. The length of the spring can be adjusted by introducing a correction factor.

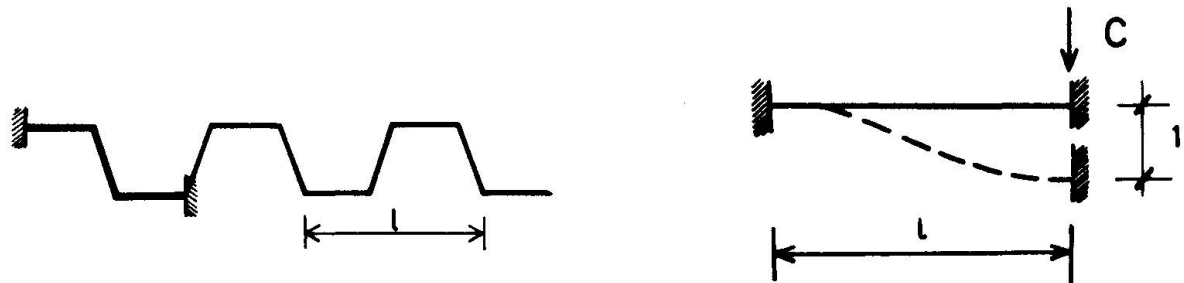


Fig.3 Model for the spring stiffness

Suppose that the spring action will be as shown in fig.3. The spring is assumed to be clamped at both ends. For a perfectly straight "spring beam", fig.3, the spring stiffness c will be

$$c = 12EI_f/\ell^3 \quad \text{where } I_f = t^3/12 \quad (9)$$

t = thickness of the steel sheet

The real spring will have the point of inflexion in the web and a different deformation length. However, usually the web deformation will not influence the total deformation more than a few percent. This justifies that we use the expression (9), which gives

$$c = E t^3/\ell^3 \quad (10)$$

4. FINAL EXPRESSIONS

4.1 Deflection

The expressions (8) together with (10) give

$$\delta_m = \frac{PL^3}{48EI} \cdot \frac{1}{1 + 2/(1+\alpha)} \quad (11)$$

$$\delta_s = \delta_m/(1 + \alpha)$$

where

$$\alpha = \pi^4 EI/cL^4 = \pi^4 \ell^3 I/t^3 L^4.$$

For $\alpha = 0$, which corresponds to an infinitely large stiffness of the spring, we get $\delta_s = \delta_m = 1/3 \cdot PL^3/48EI$ and for $\alpha \rightarrow \infty$ we get $\delta_m = PL^3/48EI$ and $\delta_s = 0$. The deflections as a function of α are shown in fig.4.

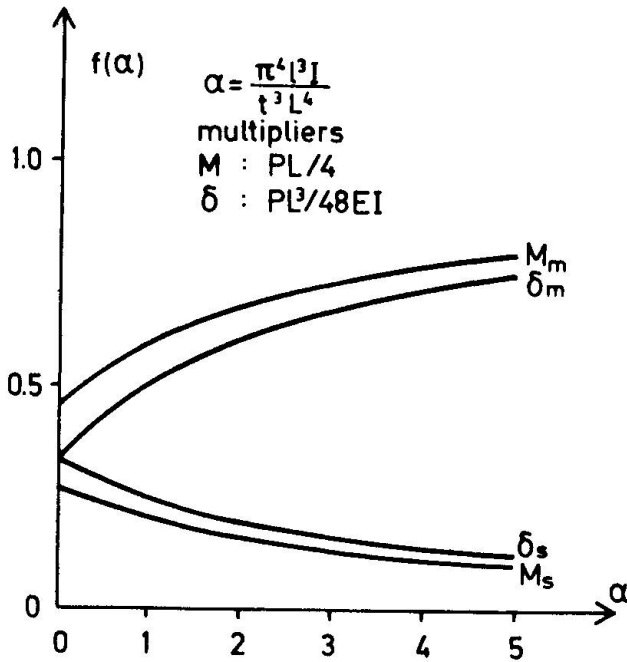


Fig.4 Deflections and moments as a function of α

4.2 Moment

The midspan moment for the loaded profile is

$$M_m = \frac{PL}{4} - 2 M_q \quad (12)$$

where

M_q = the moment in the mid-wave caused by the spring forces and at the same time the moment in the side-wave.

An expression for M_q is derived from (2), (6), and (11):

$$M_q = M_s = \frac{PL}{4} \frac{\pi^2}{12} \frac{1}{3+\alpha} \quad (13)$$

Then we get

$$M_m = \frac{PL}{4} \left(1 - \frac{\pi^2}{6} \frac{1}{3+\alpha} \right) \quad (14)$$

The variations of the moments are also shown in fig.4.

5. DIFFERENT MODELS - COMPARISONS

In the above model a section with three "waves" was studied. For a section with five waves we instead get the following expressions for the deformation.

$$\delta_m = \frac{PL}{48EI} \frac{1}{1 + \frac{2(2+\alpha)}{\alpha^2+3\alpha+1}} ; \quad \delta_s = \delta_m \frac{1+\alpha}{\alpha^2+3\alpha+1} ; \quad \delta_e = \delta_m \frac{1}{\alpha^2+3\alpha+1} \quad (15)$$

where δ_e is the mid-span deformation of the exterior wave.

A comparison between the two models shows that for the maximum moment and the mid-span deflection the results just differ slightly.



As an example we show the results for $\alpha = 1$:

	3 profile model	5 profile model	3 profile "exact"	mult
Deflection under load	0.50	0.46	0.51	* $\frac{PL^3}{48EI}$
Moment under load	0.59	0.55	0.59	* $\frac{PL}{4}$

In the table above results from an exact solution for the differential equation system (3) + (4) are also shown for comparison.

It may also be interesting to have an idea of the size of the parameter α for some commonly used steel sheets. The range of variation is approximately between $\alpha = 0.5$ and $\alpha = 4$.

6. CONTINUOUS CASE

In the continuous case, e.g. for a two span "beam", fig.5, we get

$$\delta_m = \frac{PL}{48EI} \cdot \frac{23}{32} \frac{1}{1 + \frac{2}{1+\alpha_k}}$$

$$M_{AB,m} = \frac{13 PL}{64} \left(1 - \frac{\pi^2 \cdot 23}{13 \cdot 12} \left(1 - \frac{3}{4\pi}\right) \frac{1}{\alpha + 3\left(1 - \frac{3\pi}{32}\right)}\right) \quad (16)$$

$$M_{B,m} = \frac{3PL}{32} \left(1 - \frac{23\pi}{48} \frac{1}{\alpha + 3\left(1 - \frac{3\pi}{32}\right)}\right)$$

where

$$\alpha_k = \alpha / \left(1 - \frac{3\pi}{32}\right)$$

$M_{AB,m}$ = mid-span moment for the loaded profile

$M_{B,m}$ = support moment for the loaded profile

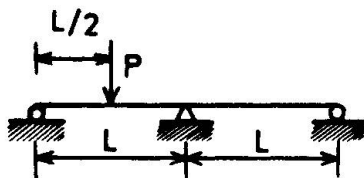


Fig.5 Continuous beam

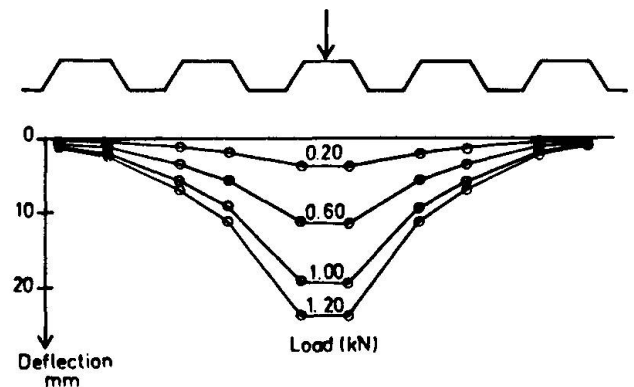


Fig.6 Measured deflections at mid-span for a 3 m span simply supported steel sheet



7. TESTS

7.1 In situ

Different test series have been conducted. In one interesting series roofers, insulation manufacturers and steel sheet manufacturers had to grade different types of steel sheets just by walking on small "test roofs".

In the test series 8 different types of steel sheets were used. The test roofs consisted of 2 steel sheets side by side (popped together) and continuous over three supports. The depth of the profiles used varied from 45 up to 110 mm. The results showed a very big scatter in the judgements - some roofs got both the marks 1 and 5, on the scale 1-5. Three very important points were found at this occasion:

1. The judgements were heavily influenced by the type of industry to which the judging persons belong.
2. Two of the steel sheets were judged "not acceptable" and both showed large deflections in a subsequent test with a load of 1.1 kN (37 and 42 mm respectively). The next roof on the scale had only 27 mm deflection.
3. The judgements also show that a small difference between the deflections of adjoining profiles often gave a good walkability mark.

7.2 Laboratory tests

In the laboratory some tests have been conducted, both simply supported and continuously supported sheets have been tested. Each specimen consisted of two adjacent sheets fixed with pop rivets. For each specimen two different spans were tested. Different load locations were also tested. Both deflections and strains were measured. Just as an example of deflection measurements the results of a simply supported profile having 50 mm depth, 0.6 mm thickness and a span length of 3 m are shown in fig.6. The result of strain measurements are shown in fig.7 both for a midspan section and for a support section.

The tests have confirmed that it is nearly only the loaded profile and the two adjacent profiles that are active in carrying the load.

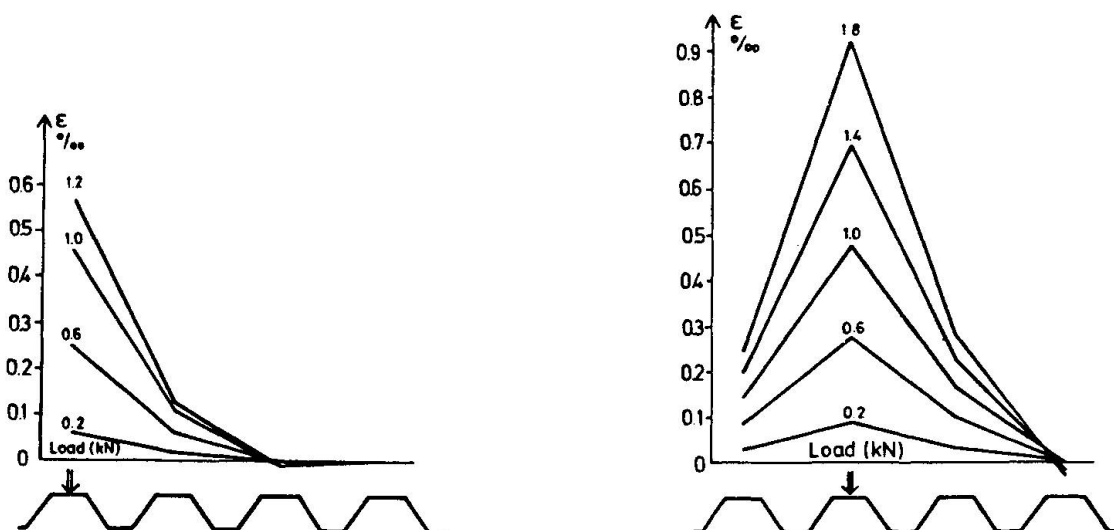


Fig.7 Measured strain distribution, midspan (left) and support section (right) for two different sheets



It is also interesting to see if the test results support the simple model. For this reason the quotients $\delta_m/\Sigma\delta$ and $\epsilon_m/\Sigma\epsilon$ are compared with the theoretical results. By comparing this kind of "relative" properties you "get rid" of variations in modulus of inertia, modulus of elasticity and the exact load level. The results from this comparison are shown in fig.8.

7.3 Deformations

Tests and theory agree very well for $\alpha < 1.5$ but for $\alpha > 1.5$ the model gives too big deflection share for the mid-profile. However, the parameter α is very sensitive to the size of the included parameters. If, for instance, we use 0.8ℓ instead of ℓ as a length of the spring there will be better agreement between tests and theory for $\alpha > 1.5$.

The absolute value of the midspan deflection is more influenced by the variations in span length than by a variation in α . A rather good estimate of the deformations under the load is obtained using the assumption that the deflection of the loaded profile is 50% of the total, or in other words, the loaded profile carries 50% of the load.

7.4 Strain

The strain measurements give an idea how the moment is shared between the waves. These measurements are shown in two different diagrams for the continuous sheets, Fig. 8b,c. As you can see there is a fairly good agreement between theory and tests for the mid-span moment but a big scatter for the support moment, up to 50% of the estimated moment. However, this does not matter, because the support moment due to a single load is just half the mid-span moment.

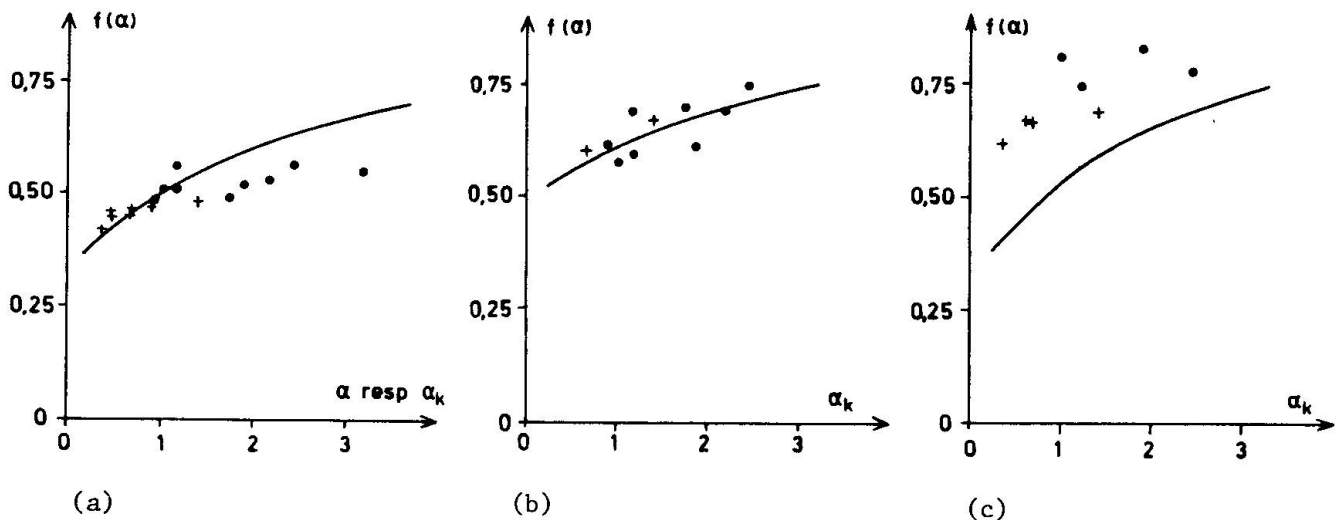


Fig.8 Measured $\delta_m/\Sigma\delta$ (left), $\epsilon_m/\Sigma\epsilon$ in midspan (middle) and $\epsilon_m/\Sigma\epsilon$ for support moment. The curves are theoretically calculated.

8. ACKNOWLEDGMENT

The author would like to thank Professor Bo Edlund, who has carefully read the manuscript and made valuable suggestions.

Moment Redistribution in Continuous Profiled Steel Sheeting

Redistribution des moments dans les tôles profilées continues

Momentenumlagerung in durchlaufenden Profilstahlblechen

Yung-Min TSAI

Ingénieur-doctorant
EPF Lausanne
Lausanne, Switzerland



Yung-Min Tsai, born 1954, received his B.Sc. at the National Taiwan University in Taipei. He has worked for two years in concrete construction and is presently at the Institute of Steel Structures (ICOM) of the Swiss Federal Institute of Technology in Lausanne.

Michel CRISINEL

Chef de section
EPF Lausanne
Lausanne, Switzerland



Michel Crisinel, born 1945, graduated from the Swiss Federal Institute of Technology in Lausanne in 1968 and worked for a consulting firm in Switzerland prior to his joining EPFL. He is now the research manager at ICOM for both composite and cold-formed thin-walled sheet steel structures.

SUMMARY

The load capacity of continuous sheeting calculated according to the ECCS European Recommendations is smaller than that obtained from testing. Understandably, manufacturers and designers prefer the use of testing rather than design. Research at EPFL has developed a simple test procedure which determines the load capacity of multispan cold-formed profiled sheeting. This procedure conservatively predicts the redistribution that occurs at interior supports.

RÉSUMÉ

La capacité portante d'une tôle profilée continue calculée à l'aide des recommandations européennes CECM est inférieure à la valeur déterminée par essai de charge. C'est pourquoi actuellement les fabricants et les ingénieurs préfèrent avoir recours aux essais plutôt qu'aux calculs. Une recherche entreprise à l'EPFL a conduit à l'établissement d'une procédure d'essais permettant de déterminer de façon précise la capacité portante d'une tôle continue, compte tenu de la redistribution du moment sur appui.

ZUSAMMENFASSUNG

Die nach den europäischen Empfehlungen EKS berechnete Traglast von Profilblechen ist kleiner als der durch Versuche ermittelte Wert. Hersteller und Ingenieure ziehen deshalb die Versuchsergebnisse den Berechnungen vor. An der EPFL wurde ein einfacher Test entwickelt, mit dem die Traglast von durchlaufenden Profilstahlblechen genau ermittelt werden kann. Der Momentenumlagerung über den Stützen wird dabei Rechnung getragen.



1. INTRODUCTION

The present ECCS European Recommendations for the Design of Profiled Sheeting [1] are based upon the effective width concept and empirically determined factors. The use of empirical factors is necessary in the design procedure due to difficulties in modelling :

- initial imperfections,
- residual stresses,
- elastic buckling of individual plate elements.

However, the empirical factors used in the ECCS design procedure are based upon tests which were performed on single span specimens only. Using similar factors to predict the flexural capacity of multiple span specimen yields overly conservative values. As a result, most manufacturers prefer testing to the ECCS design values when determining ultimate load capacities.

Research which better defines the reserve capacity of continuous span specimens has been conducted. The principal objectives of this research are :

- to determine the accuracy of the present ECCS design procedure,
- to compare the ultimate load capacity of similar single and multiple span specimens using a simple test procedure,
- to determine the increase in ultimate load capacity which occurs in multiple span specimens as a result of moment redistribution near interior supports.

2. EXPERIMENTAL INVESTIGATION

2.1 Test specimens

Profiled sheetings were chosen according to two criteria. Firstly, sections without embossments or intermediate stiffeners were used in order to reduce the number of assumptions necessary when calculating section properties and predicting behaviour. Secondly, profiled sheetings which have found common usage in composite cold-formed floors constructed in Switzerland were employed. As a result the following sections were chosen :

- Montana 57/0.80 mm (unsymmetric trapezoidal ribs),
- Hi-Bond 55/0.88 mm (trapezoidal ribs),
- Holorib 51/0.75 mm (dovetailed ribs).

These three sections are shown in Figure 1.

Three types of tests were performed on each sheeting; this enabled a comparison of behaviour with similar single and multiple span specimens. These tests are identified as series 1, 2 and 3. Load placement and span lengths were chosen such that test results could be directly compared with the ECCS design procedure. The coiled sheeting from which the specimens were formed was inspected both before and after the forming process. Each specimen was then marked prior to shipping. This minimised dimensional variation between test series on similar test specimens.

Test series 1 consisted of a single span simply supported profiled sheet, loaded symmetrically by two equal line loads. These tests determined the ultimate flexural strength of a single span specimen in pure bending. The static testing system for this test series is shown in Figure 2 a).

Test series 2 consisted of a single span profiled sheet, simply supported and loaded at midspan. This test series determined the influence of a concentrated load in the region of maximum moment. The line load at midspan simulates the effect of the interior support of a two span specimen . In Figure 2 b) the static system is shown.

Test series 3 consisted of a profiled sheet continuous over two equal spans. Each span length was the same as that used in test series 1. Two lines loads, of equal

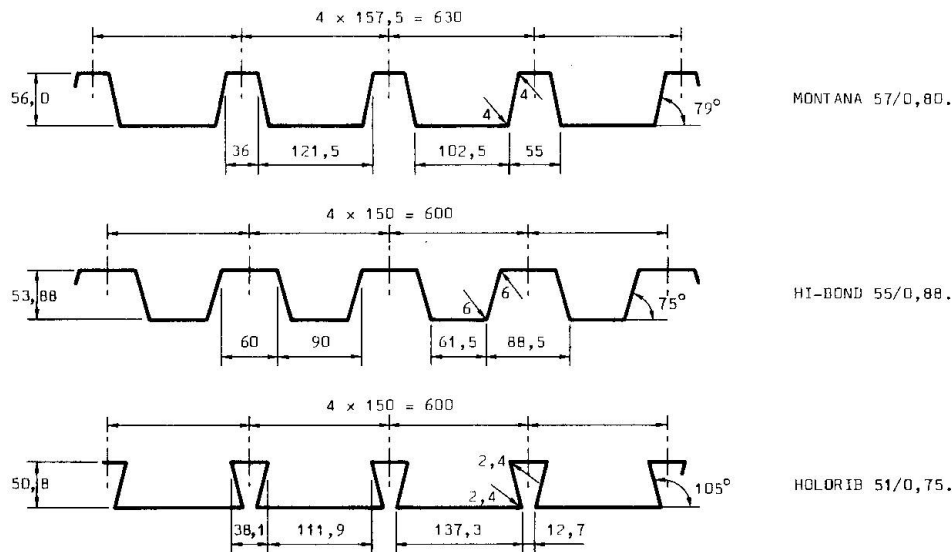


Fig. 1 : Profiled sheeting sections.

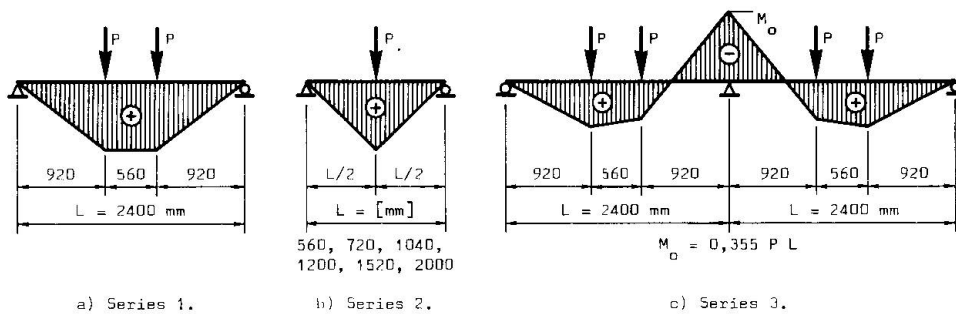


Fig. 2 : Static system for the tests.

magnitude, were applied to each span at the same location as in test series 1. The static system is shown in Figure 2 c).

For each sheeting, three series 1 tests, nine series 2 tests and two series 3 tests were performed.

2.2 Test Procedure

Before testing, the cross-sectional geometries and material thicknesses of all specimens were measured. All measurements were made in accordance with the ECCS Recommendations for the testing of profiled metal sheeting [2]. Six tensile test specimens were cut from the stock material used to form each profile. After the forming process six additional specimens were cut from the centre of flat plate elements and an additional six at the curved portion between these elements. All specimens were tested according to the standard ISO procedure [3]. A more detailed review of the test procedure and the test specimens is contained in [4].

Test series 1. The procedure adopted for conducting these tests was a modification of the ECCS Recommendations [2]. The blockings, required by ECCS between all ribs under concentrated loads, were provided only at exterior ribs. This change was made for two reasons. Firstly, it is difficult to determine the distribution of the applied load on the specimen with more than two blocks and secondly, using only two blocks, it is much easier to assemble the test.

Test series 2. The ECCS Recommendations were followed for this test series. Blocking is not required as failure occurs at the location of the applied load.



Test series 3. This series resembles test series 1. However, instead of exterior blocking beneath the concentrated loads, a 150 mm length of profiled sheeting was placed between the specimen and the transverse spreader beam. This profiled sheet was the same shape and thickness as the specimens tested.

2.3 Test results

Series 1. The ultimate load of the test specimens were compared to the ultimate load calculated using the ECCS Recommendations. This comparison is shown in Table 1. A very good correlation between test results and calculated values was observed; the maximum difference between theoretical and test values of ultimate moment was 5 %.

Series 2. An interaction diagram of moment and support reaction at ultimate load, calculated using the ECCS Recommendations, is shown in Figure 3. Test results are also presented on this figure. Again, good correlation between experimental and analytical results was observed. The maximum difference between theoretical and test values of ultimate moment was 9 %, the standard deviation 4.5 %.

Series 3. Ultimate loads from these test specimens and theoretical values calculated using the ECCS procedure are presented in Table 2. The theoretical values of ultimate load do not correspond to experimental results. The maximum difference between theoretical and experimental values was 37 % and the minimum difference was 21 %. The test values of ultimate load were always larger than those predicted by the ECCS procedure. The difference between the experimental ultimate load and the ultimate load predicted by ECCS represents the reserve capacity due to moment redistribution near the interior support. The redistribution factor, α , is defined as the reserve capacity of the specimen divided by the ultimate load predicted by ECCS.

Table 1 : Test results of series 1 in kNm/specimen.

PROFILE TYPE	TEST NUMBER	STATIC SYSTEM			
		$M_u^+ = 0,92 P_u$		$M_u^- = 0,92 P_u$	
		$M_{u,series1}^+$	$M_{u,ECCS}^+$	$M_{u,series1}^-$	$M_{u,ECCS}^-$
MONTANA 57/0,80 $f_y = 294 \text{ N/mm}^2$	MO22	3,243	3,321		
	MO21			3,114	3,124
	MO23			3,197	3,085
HI-BOND 55/0,88 $f_y = 306 \text{ N/mm}^2$	HI22	3,340	3,485		
	HI21			3,257	3,227
	HI23			3,243	3,163
HOLORIB 51/0,75 $f_y = 291 \text{ N/mm}^2$	HO23	3,229	3,257		
	HO21			2,995	3,106
	HO22			2,967	2,969

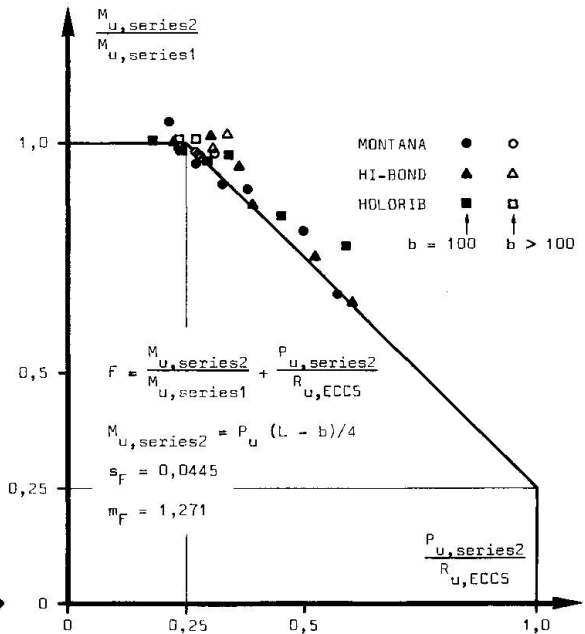


Fig. 3 : M-R interaction diagram.

PROFILE TYPE	f_y [N/mm ²]	$M_{u,series2}^-$ [kNm/specimen]	$P_{u,series2}$ [kN/specimen]	$P_{u,series3}$ [kN/specimen]	$\alpha = \frac{P_{u,series3}}{P_{u,series2}} - 1$
MONTANA 57/0,80	294	2,871	3,370	4,264	0,265
HI-BOND 55/0,88	306	3,094	3,631	4,409	0,214
HOLORIB 51/0,75	291	2,868	3,366	4,623	0,373

Table 2 : Test results of series 3 and redistribution factor.

- 1) The ultimate moment is given by the interaction moment-reaction diagram in series 2 test.
- 2) $P_{u,series2} = M_{u,series2}^- / 0,355 L$ (elastic linear solution).
- 3) Average values of tests.

3. ANALYSIS

The following analysis is used to determine the redistribution factor, α , for multiple-span cold-formed profiles using a semi-analytical procedure. Based on an elastic analysis, the compatibility equation at ultimate load for a beam with two equal spans, L , uniformly loaded, is given by :

$$\frac{M_0 L}{3 EI_0} = \frac{p_0 L^3}{24 EI_0} \quad (1)$$

M_0 : moment at the interior support of a two span continuous beam assuming linear behaviour; this is calculated using the simple beam formula and the yield stress of the material,

I_0 : moment of inertia of the entire cross section,

L : single span length, both span lengths equal,

E : modulus of elasticity,

p_0 : uniform applied load at M_0 .

In equation (1), the left hand term represents the end rotation in a simply supported span due to a single end moment, M_0 . The right hand term represents the end rotation in a simply supported span uniformly loaded. By equating these two components, an expression for the moment at the interior support of a two span beam is obtained. To account for the additional capacity observed during testing, equation (1) may be rewritten to include the non-linear components of rotation at the interior support. Overall plasticity does not occur in most sheeting and thus, this new expression is written as follows :

$$\frac{M_0 L}{3 EI_0} + \Delta\theta_{el} + \Delta\theta_p = \frac{p_u L^3}{24 EI_0} \quad (2)$$

$\Delta\theta_{el}$: rotation at the interior support due to local buckling of individual flat plate elements,

$\Delta\theta_p$: rotation at the interior support due to the presence of a concentrated support reaction; this rotation is permanent,

p_u : uniform applied test load at failure or predicted ultimate load.

In expression (2) the left hand terms represent three separate components of rotation. The sum of these three components equals the rotation which occurs at the interior support in a cold-formed profile. To define these three components of rotation, illustrated in Figure 4, the following assumptions are made :

- the negative moment region near the interior support of a two span uniformly loaded specimen can be modelled by a simple span beam with a concentrated load at midspan,
- the effect of concentrated load is so localised that the magnitude of $\Delta\theta_p$ is independent of span length.

A typical series 2 load-midspan deflection curve which is shown in Figure 5. Theoretically, a compact cross section with no initial imperfections will attain overall plasticity without instability taking place and therefore, complete moment redistribution. This behaviour is identified by curve OAB. In reality, both initial imperfections and local buckling cause failure at a lower applied load than that predicted by OAB. Curve OKN represents this behaviour. When a concentrated load is present at the same location as the maximum moment, a further reduction in capacity is observed due to web crippling. This is shown by curve OEF. As loading is increased, four different types of behaviour are predicted by curve OEF. In the first region, OC, linear behaviour prior to local buckling is observed. In region CD nonlinearity, primarily caused by local buckling in the different flat plate elements of the specimen, is observed. In region DE, the effects of the concentrated load dominate behaviour. At point E, failure of the entire section occurs. Curve GJF is typical of the post-elastic failure behaviour of cold-formed sheet-

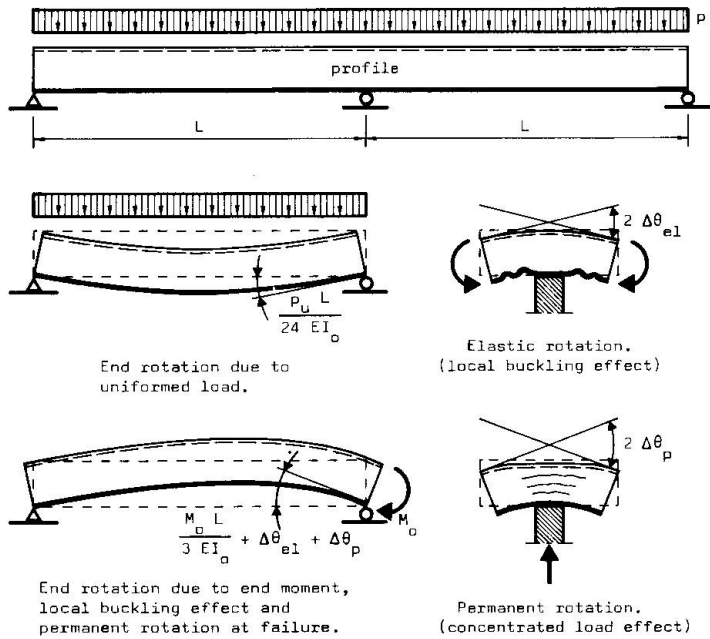


Fig. 4 : Components of compatibility equation (2).

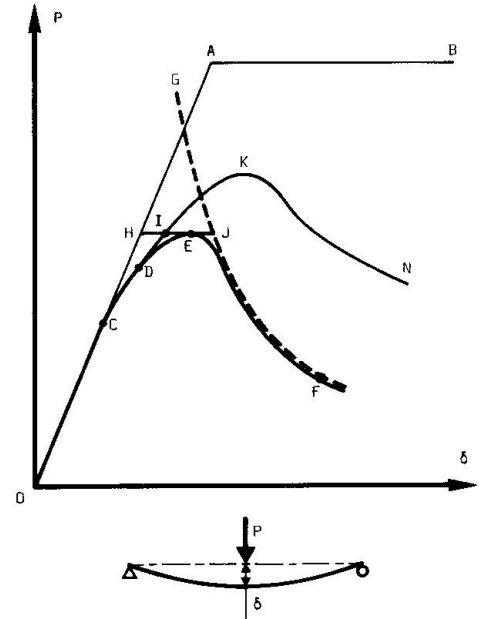


Fig. 5 : Typical load-midspan deflection curve.

ing. The nature of this curve has been investigated by several researchers [5] [6] [7]. Schardt [7], for example, has used a straight line. Unfortunately, this curve is difficult to obtain by theoretical means for cold-formed sheeting.

To obtain $\Delta\theta_{e1}$ and $\Delta\theta_p$ the following procedure is proposed : rotation due to buckling of individual plate elements is dependent upon moment gradient, span length, and the moment-curvature relationship. Using the moment-curvature relationship from test series 1 and a finite difference model, $\Delta\theta_{e1}$ can be plotted as a function of span length, for each sheeting. The magnitude of this component of rotation on the midspan deflection of test series 2 is shown in Figure 5 as HI. Rotation due to support reaction is localised and independent of span length. Thus, $\Delta\theta_p$ is determined by the nonlinear rotations taken from testing; provided that the span length is sufficiently short to insure elastic local buckling of the flanges does not occur. For the sections tested, this length is less than ten times the depth of the section. Component HI approaches zero and the remaining nonlinear component of midspan deflection, for test series 2, is represented by IJ in Figure 5.

Using this procedure two different tests obtain the two components of rotation, $\Delta\theta_{e1}$ and $\Delta\theta_p$. These rotations are used to compute the ultimate load capacity of multispan profiled sheeting. The first test, series 1, establishes the moment curvature characteristics of the section subject to bending moment alone. The second test, a small span with a single concentrated load, determines the effects of concentrated reaction. The non-linear components of rotation at the interior support can thus be expressed as :

$$\Delta\theta_{e1} + \Delta\theta_p = \alpha \frac{p_0 L^3}{24 EI_0} \tag{3}$$

Using equations (1) and (2) the ultimate load capacity, p_u , is expressed as :

$$p_u = (1 + \alpha) p_0 \tag{4}$$

Values of α have been calculated using this procedure for the sections tested. These values are compared to the experimentally determined redistribution factors

and are listed in Table 3. Good agreement between observed and predicted redistribution was obtained, the average difference being 14 %.

PROFILE TYPE	$I_o \cdot 10^6$ [mm ⁴ /specimen]	$\Delta\theta_{el} \cdot 10^{-3}$ [rad]	$\Delta\theta_p \cdot 10^{-3}$ 1) [rad]	α_{cal} a)	α_{test}
MONTANA 57/0,80	0,386	3,31	3,75	0,228	0,265
HI-BOND 55/0,88	0,389	2,62	3,90	0,205	0,214
HOLORIB 51/0,75	0,420	3,72	3,93	0,284	0,373

Table 3 : Comparison of the tested and calculated redistribution factor.

1) $\Delta\theta_p$ is obtained from a 560 mm span series 2 test.

a) Calculated from equation (3).

4. DISCUSSION

The differences in reserve capacity, shown in Table 3, between predicted and test values of α , are due to several factors. However, it is presently believed that there are two components which account for the majority of these differences. Firstly, the deformation of the sheeting at the interior supports of a multispan specimen is larger than that observed under the concentrated load of test series 2. Secondly, even though the same sheeting was used for test series 1, 2 and 3, dimensional differences between specimens exist. M_o , however, was calculated using the measured section properties of the sheeting used in test series 1. This difference in section properties will always be present due to the flexible nature of these specimens.

To improve this procedure, theoretical work is now being conducted in two areas. These areas are the definition of the post elastic behaviour of profiled sheeting (curve GJF) and an improved model of web crippling. In addition, future testing is planned to better define the accuracy of this method.

5. CONCLUSIONS

The following conclusions are based upon an analysis of the test results presented in this paper :

- 1.- Variations between measured and nominal dimensions for profiled sheeting can be substantial. Actual section dimensions should be used when analyzing test data.
- 2.- The present ECCS Recommendations predict successfully the ultimate load capacity of single span cold formed sheeting.
- 3.- The ECCS procedure under-estimated the ultimate load capacity of continuous profiled sheeting by 21 to 37 %.
- 4.- The semi-empirical procedure outlined in this paper may be used to conservatively predict ultimate loads on multi-span profiled sheeting.

REFERENCES

- [1] ECCS. European Recommendations for the design of profiled sheeting. Croydon (GB), Constrado, 1983 (Publication ECCS No. 40).
- [2] ECCS. European Recommendations for the testing of profiled metal sheets. Croydon (GB), Constrado, 1977 (Publication ECCS No. 20).
- [3] Norme Internationale ISO 86-1974 (F) : Acier - Essai de traction des tôles et feuillards d'épaisseur inférieure à 3 mm et au moins égale à 0,5 mm. Genève, Organisation Internationale de Normalisation, 1974.
- [4] TSAI, Y.-M., CRISINEL, M. Essai de flexion sur tôles d'acier profilées à froid. Ecole polytechnique fédérale de Lausanne, (Publication ICOM 145) 1985.



- [5] UNGER, B. Ein Beitrag zur Ermittlung der Traglast von querbelasteten Durchlaufträgern mit dünnwandigen Querschnitt, insbesondere von durchlaufenden Trapezblechen für Dach und Geschossdecken. Der Stahlbau, Berlin, vol. 42, no 1, 1973.
- [6] LEACH, P. Tests on profiled sheeting for composite floors. University of Salford, Report 84/199, 1984.
- [7] SCHARDT, R. Simulated internal support test. Notes T7/1/41 at ECCS working group TWG 7.1 meeting, Linz, Austria, February 1984 (unpublished).

Inelastic Behavior and Earthquake-Resistance Design Method for Thin-Walled Metal Structures

Comportement inélastique et méthode de calcul des structures métalliques en profilés minces résistant aux séismes

Unelastisches Verhalten und erdbebensichere Entwurfsmethode für dünnwandige Metallkonstruktionen

Tetsuro ONO

Dr. Professor
Nagoya Inst. of Technology
Nagoya, Japan



T. Ono, born 1944, graduated from Nagoya Inst. of Tech. in 1968. He received his Dr. degree at Tokyo Inst. of Tech. in 1976. He is Professor at Nagoya Inst. of Tech., Dep. of Architecture since 1979. His special research interests are stability problems, aseismic design and system reliability.

Toshiro SUZUKI

Professor
Tokyo Inst. of Technology
Tokyo, Japan



T. Suzuki, born 1936, received his doctor's degree from the University of Tokyo in 1963. He was awarded the Prize of the Architectural Institute of Japan for his studies on steel structures in 1981.

SUMMARY

This paper discusses the behaviour of cold-formed light-gauge steel, in particular the yield strength and the deformation capacity of frames by means of a horizontal loading test on the frame, and presents the methods for evaluating these properties and the ideas on which earthquake-resistant design is based.

RÉSUMÉ

Cette contribution, relative aux structures en profilés minces en acier formé à froid, concerne l'étude de la résistance plastique et de la capacité de déformation des cadres au moyen d'essais sous charges horizontales. Des méthodes d'évaluation de ces propriétés sont présentées ainsi qu'un concept de dimensionnement de telles structures résistant aux séismes.

ZUSAMMENFASSUNG

Die vorliegende Arbeit behandelt kaltgewalzte Stahlleichtkonstruktionen und diskutiert Fließlasten und Verformungsvermögen eines Rahmens unter Horizontalbelastungen. Methoden zur Bewertung der Eigenschaften insbesondere im Hinblick auf erdbebensichere Bemessung werden vorgelegt.



1. INTRODUCTION

In Japan, four years have passed since the new design codes for earthquake resistance were put into effect. The design methods stipulated in the new design codes aim at securing safety for structures against the strong ground motion during earthquakes on the basis of energy absorption capacity of the frame. Therefore, it is absolutely necessary in application to accurately grasp and evaluate the ultimate strength and the deformation capacity of the frame and its component members. The various prescriptions in the new design code for earthquake resistance currently being applied were provided so as to comply with large amounts of experimental data on heavy steel structures built up of hot-rolled members. For light-gauge steel structures, which are mainly composed of members of large width-thickness ratios, represented by light-gauge steel and lightweight wide-flange members, not much data is available on their ultimate strength and deformation capacity and the evaluation methods for these properties have not been established. In fact, there is a tendency that enough considerations are not given to those properties in designing steel structures. One notable result of this problem is the damage of warehouses and houses caused at the 1978 Miyagi-ken-oki earthquake.

With this reality in mind, this research was conducted to obtain fundamental data for the evaluation of the earthquake resistance of light-gauge steel structures which are used in buildings of three stories or less and, on the basis of research data, to improve earthquake-resistance design. Taking up cold-formed light-gauge steel, this paper discusses the yield strength and the deformation capacity of and presents the evaluation methods of these properties and the ideas of earthquake-resistance design.

2. PLAN OF EXPERIMENT

This test was conducted for light-gauge steel structures for low-rise buildings and with the aim of finding inelastic deformation characteristics in horizontal loading of the frames composed of light-gauge steel members with sectional dimensions of rank III or IV under the new design codes for earthquake resistance. To prevent the frame being subjected to torsional deflection, the test specimen was formed in a 1-story, 1-span portal space frame with 4 columns,

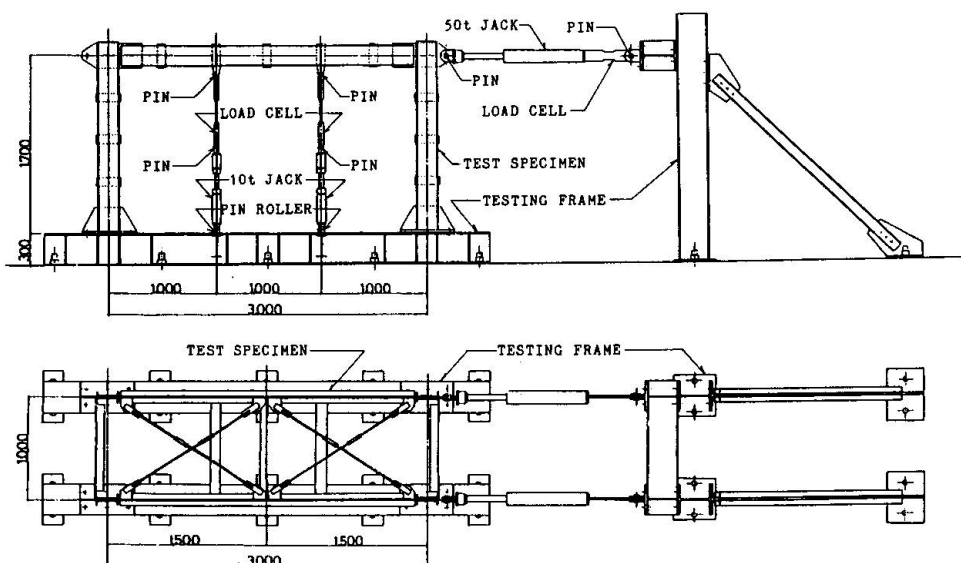


Fig.1 Set-Up of Frame Test

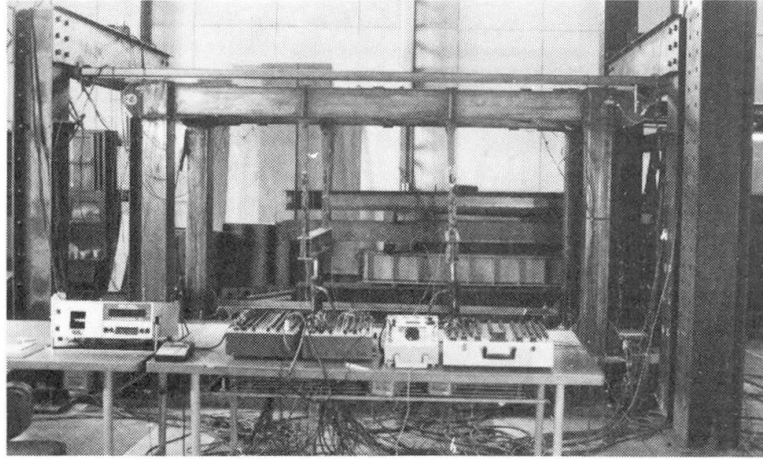


Photo.1 Test Set-up

consisting of two portal frames of the same type, arranged in parallel. The test parameters taken up were the shape of column cross section, rigidity of the connections and the degree of column base fixation. Fig. 1 shows the general view of the testing equipment. As shown in Fig. 1, a horizontal force was applied gradually in horizontal loading to the column capital of the test specimen. In addition, as gravity load for design, gravity loads were applied in two-point concentrated loading on the trisecting points of a beam so that it was $0.2M_y$ at the ends of the beam ($M_y =$ yield moment of a beam member). The test specimens are outlined in Table 1.

3. INELASTIC DEFORMATION CHARACTERISTICS OF FRAMES

3.1 Elasto-Plastic Behavior of Frames

Figs. 2 to 8 show the test results of the frames. Fig. 2 indicates the hinge points and the order of the test pieces. Photo.2 shows the local buckling deformation of LG-1. Figs. 3 to 8 show the load-deflection curves of the frames obtained by the test. The vertical scale indicates the horizontal load Q (ton) of the column capital and the horizontal scale represents its horizontal displacement δ (cm). Fig. 3 presents the result of repeated loading to LG-1. The broken lines show the load-deflection curve in unidirectional loading converted from the curve in repeated loading. This indicates that the idea regarding the accumulated plastic deformation of heavy steel frames is applicable to this type

Table 1 Dimensions of Frame Test Specimen

SPECIMEN		SECTION (mm)	FLANGE b/t_f	WEB b/t_w	σ_y (t/cm^2)
LG-1	BEAM	2C-200×50×3.2	19.4	58.5	3.65
	COLUMN	2C-200×75×20×3.2	13.6	58.5	3.65
LG-2	BEAM	2C-200×50×3.2	19.4	58.5	3.65
	COLUMN	2C-200×50×3.2	19.4	58.5	3.65
LG-3	BEAM	2C-200×50×4.5	9.1	40.4	3.70
	COLUMN	□-175×175×6.0	25.2		3.65
LG-4	BEAM	2C-200×75×20×3.2	13.6	58.5	3.65
	COLUMN	2C-200×75×20×3.2	13.6	58.5	3.65
	BRACE	18φ			3.50
LG-5	BEAM	2C-200×50×3.2	19.4	58.5	2.70
	COLUMN	2C-200×75×20×3.2	13.6	58.5	3.70
LG-6	BEAM	2C-200×50×4.5	9.1	58.5	3.65
	COLUMN	□-175×175×6.0	25.2		4.00
LG-7	BEAM	2C-200×50×3.2	19.4	58.5	2.70
	COLUMN	2C-200×50×3.2	19.4	58.5	2.70
LG-8	BEAM	2C-200×50×3.2	19.4	58.5	2.70
	COLUMN	2C-200×50×3.2	19.4	58.5	2.70
SEPARATOR	E 6	$\sigma_y=2.64t/cm^2$	E 9	$\sigma_y=2.62t/cm^2$	
	E 13	$\sigma_y=2.54t/cm^2$	E 16	$\sigma_y=2.60t/cm^2$	

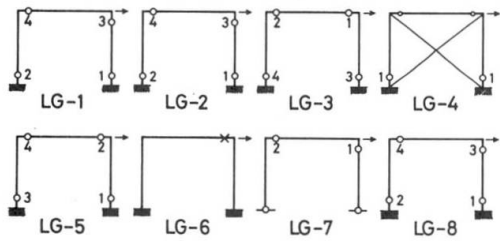


Fig.2 Location of Plastic Hinge

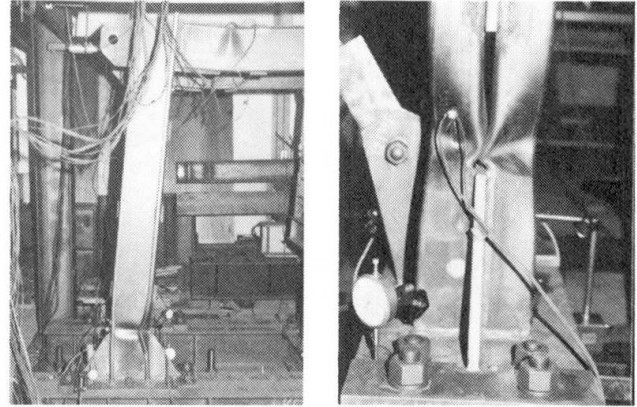


Photo.2 Local Buckling of LG-1

of frame. Fig. 4 shows the test result of LG-5, the connections of which were designed on the basis of ultimate strength, though the cross section of its member is the same as in LG-1. Fig. 5 shows a combined test result of LG-2, LG-7 and LG-8 with the boundary condition of the column bases varied. Comparing the load-deflection curves of LG-2 made of 32mm-thick plate and LG-8 made of 13mm-thick plate, we find hardly any difference despite the difference in yield stress of the members. LG-7 with hinged column bases decreased in the redundant strength by the reduction of the degree of redundancy. Hence, it was confirmed that the first hinge was formed at the column capital in the neighborhood of 3.2 tons. Thereafter, the load hardly rose. Fig. 6 shows the test result of LG-3 which used box-sections for the column members. Here the load-deflection curve shows stable features, including the lowering gradient. Shown in Fig. 7 is the test result of LG-6 which is of the same section as LG-3 and its connections are designed on the basis of maximum stress. When the load is 22.0 tons, the rigidity decreases to approximately 1/30 of the elastic rigidity and a relatively distinct bi-linear load deflection behavior is witnessed. At this time, clearly recognizable hinges were not found in the column and beam members. Later, while the rigidity was about 1/30 of the elastic rigidity, the load was gradually increased. After reaching the maximum strength of 23.8 tons, the strength started to decrease rapidly and when it dropped to about 23.0 tons, a failure was confirmed visually in the splice plates at the beam-column connection on the load-applied side. From the observation of the hinge formation and also from the comparison with the test result of LG-3, the decrease in rigidity and strength are considered to have resulted from the failure of the splice plate. The failure of the splice plate, which was in the final collapse mode, is considered attributable to the fact that the yield stress became about 1.54 times the basic

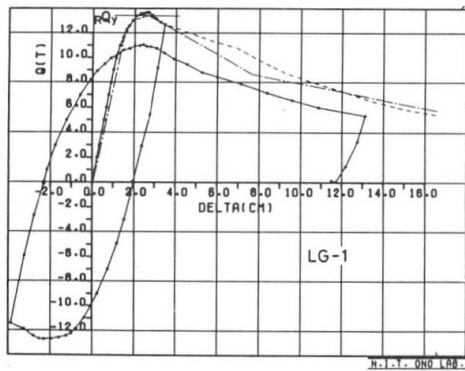


Fig.3 Load-Deflection Curve of LG-1

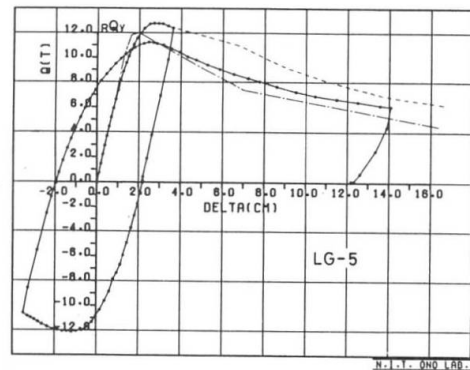


Fig.4 Load-Deflection Curve of LG-5

value of F used in design due to the effect of cold working. The connections of LG-6 are designed on the basis of the maximum stress of the members to be jointed and the shape of the splice plate was determined by the following formula.

$$f M_u = 1.2 M_p = 1.2 \cdot F \cdot Z_p \quad (1)$$

where $f M_u$ = maximum bending moment of the splice plate
 F = basic value of steel
 M_p = full plastic moment of the beam

In LG-6, the full plastic moment of the beam M_p is $1.54 \cdot F \cdot Z_p$ because of the raised yield stress. This exceeds $1.2 M_p$ (actually, $1.31 M_p$ if the rise in the yield stress of the separators is taken into consideration) on the right-hand side of formula (1) even if the rigid zone is not taken into account. If, from the test result of the members, the strength of the members is considered not larger than the yield moment M_y , the right-hand side of formula (1) should be $1.54 \cdot (M_p / 1.3) = 1.18 M_p$, since the shape factor of the beam members is 1.3. Yet if the rise in the moment at the connections due to the extension of the rigid zone by the separators is taken into account, the moment will be $1.5 M_p$ at the ends of the beam, which exceeds the $1.31 M_p$ calculated by taking account of the rise in the yield stress. From the foregoing, when the frame is designed on the basis of ultimate strength and is made up of cold-formed light-gauge members, the rise in the yield stress by the effect of cold working is so large that it is considered problematical to design beams according to the nominal yield stress without discrimination. Fig. 8 shows the test result of LG-4, a braced frame.

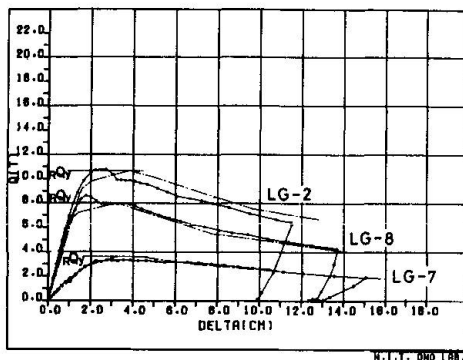


Fig. 5 Load-Deflection Curves of LG-2, LG-7 and LG-8

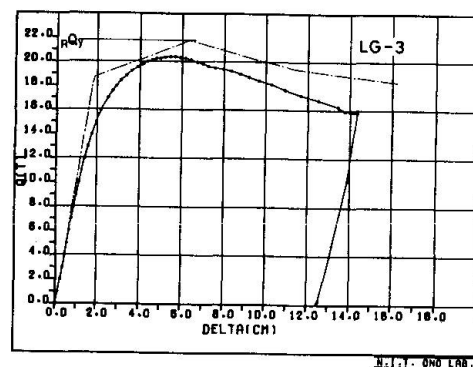


Fig. 6 Load-Deflection Curve of LG-3

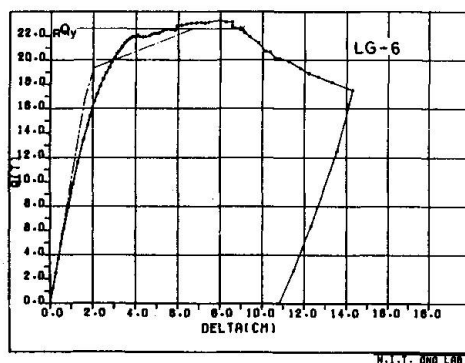


Fig. 7 Load-Deflection Curve of LG-6

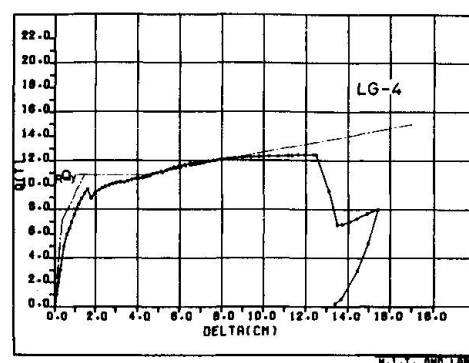


Fig. 8 Load-Deflection Curve of LG-4



3.2 Ultimate Horizontal Strength and Load-Deflection Curves of Frames

This section, on the basis of the test results, presents the evaluation of the ultimate horizontal strength of light-gauge steel structures and the induction of the load-deflection curves of the frame. The ultimate horizontal strength is RQ_D when the limit moment of members is expressed by the full plastic moment M_P and the ultimate horizontal strength is RQ_Y when the limit moment of members is expressed by the yield moment M_Y . Incidentally, for LG-3 and 6, since their column members are of closed section and the width-thickness ratios are small (rank I), in the calculation of RQ_Y of the column members the limit moment is expressed by the full plastic moment. As for LG-6, the limit moment of the end of the beam is determined by the maximum bending strength of the splice plate in accordance with the test results. The ultimate horizontal strength Q thus obtained are compared with the test results in table 2. Except for LG-6, the beam-end limit moment of which is determined by the maximum bending moment of the splice plates, none of the test specimens have the maximum strength which measures up to the ultimate strength by the evaluation of the full plastic moment. On the average, maximum strength is no more than 80 percent of the ultimate horizontal strength RQ_Y . On the other hand, the ultimate strength RQ_Y by the evaluation of the yield strength shows good agreement with the maximum strength measured in the test. In the table, RQ_E is the horizontal load when some part of the frame reaches the yield strength. From the above results, it is considered adequate to evaluate the ultimate strength of frames using the maximum strength RQ_Y by the evaluation of the yield strength. The dotted broken lines show the analysis results by using the plastic hinge method based on the evaluation of yield moment.

3.3 Evaluation of Inelastic Deformation Capacity of Frames

When discussing the safety of structures against the strong ground motion during an earthquake, it is essential to grasp their deformation capacity. This section presents the evaluation of the inelastic deformation capacity of frames by the method indicated in Fig. 9. The η corresponds to the equivalent multiplying factor of accumulate plastic deformation¹. As shown in the figure, the η is calculated using the yield strength EQ_Y which is determined by the intersection of the tangent when the quadratic gradient is averaged as 0.05 ($k = \text{elastic gradient}$) with the elastic line. The R is calculated with reference to the deformed amount δ_E , used as the basic value, which corresponds to the horizontal load RQ_E when some part of the frame yields. The point of plastic deformation when the strength drops again to RQ_E , after reaching the maximum strength, is

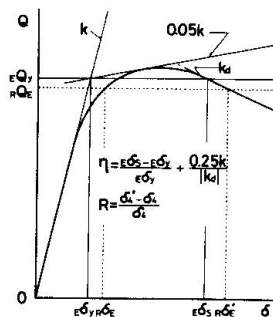


Table 2 Experimental Results and Evaluated Value of Frame Test

SPECIMEN	Q_{max}/RQ_D	Q_{max}/RQ_Y	Q_{max}/RQ_E	η	R	RANK OF STRUCTURE
LG-1	0.83	1.02	1.14	2.88	2.03	III
LG-2	0.80	1.00	1.23	4.36	3.58	II
LG-3	0.86	0.94	1.14	7.27	2.62	I
LG-4	0.92	1.16	1.80	15.90	15.75	I
LG-5	0.87	1.07	1.24	4.07	3.69	II
LG-6	1.03	1.03	1.39	5.35	6.38	II
LG-7	0.73	0.92	1.15	5.77	3.89	II
LG-8	0.86	1.07	1.37	5.59	5.19	II

Fig.9 Evaluating Method of Deformation Capacity

considered as the limit of plastic deformation. The R and η are compared in Table 2. In LG-3 in which the rigidity decreased considerably early and in LG-7 of which the lowering gradient is small, the value of η became fairly larger than the value of R , but the value is almost the same as with other test specimens. The structural ranking in the table is set by the value of η based on the new design code for earthquake resistance in Japan. Also in LG-1 which is the minimum in the amount of plastic deformation, the inelastic deformation capacity of rank III could be secured, while for the other test pieces the plastic deformation capacity of rank I or II could be confirmed. As for LG-6, though it belongs to rank I in terms of sectional dimensions, the plastic deformation capacity of rank I could not be confirmed, the reason for this is ascribed to the failure the splice plate. As described above, it was found that the plastic deformation capacity of rank I to III can be secured even for the frames which fall under rank III or IV in terms of sectional dimensions (width-thickness ratio of plate element). This suggests the possibility of applying the earthquake resistance design method, which takes into account the plastic deformation capacity of the frame to light-gauge steel structures.

3.4 Evaluation of Earthquake Resistance of Light-Gauge Steel Frames

The Japanese design code for earthquake resistance provide a formula for the judgement of the safety against earthquake as follows.

$$Q_{un}' \geq D_s \cdot F_{es} \cdot Q_{ud} \quad (2)$$

where Q_{un}' = required ultimate horizontal strength of each layer of frame
 D_s = reduction factor depending on the deformation capacity of frame
 F_{es} = shape factor
 Q_{ud} = maximum horizontal force that each layer of frame would be subjected to if it responds elastically to a strong earthquake

When formula (2) is applied to rigid-frame light-gauge steel structures, the problem is what reduction factor (D_s) should be set and what maximum strength Q_{un}' should be given. In the light-gauge steel structures composed of members of relatively large width-thickness ratios such as are dealt with as the object of this paper, it is difficult to form stable hinges at the full plastic moment described up to the preceding section. Therefore, it is difficult to apply to them the above formula intended for heavy steel structures. Because the ultimate strength RQ_y of the frame by the evaluation of the yield moment M_y better exceeds the maximum strength obtained by the test by replacing Q_{un}' with RQ_y in Eq. (2), we have:

$$RQ_y \geq D_s \cdot F_{es} \cdot Q_{ud} \quad (3)$$

However, in view of the simplicity when relatively small-scale steel structures are designed, it is more practical to consider the allowable strength for temporary loading RQ_E to be basic value for frame design. Assuming that $RQ_y = \alpha RQ_E$, formula (3) will be as follows.

$$RQ_E \geq \frac{1}{\alpha} \cdot D_s \cdot F_{es} \cdot Q_{ud} \quad (4)$$

The ratio of RQ_y to RQ_p is about 0.8 to 1.0 as obtained by the test, but 0.8 for ensuring safety. Assuming that the ratio of RQ_p to RQ_E is 1.5, the value of α is given by

$$\alpha = (RQ_y / RQ_p) \cdot (RQ_p / RQ_E) = 0.8 \cdot 1.5 = 1.2 \quad (5)$$

On the other hand, the plastic deformation capacity of the frames, if evaluated by η , falls into rank I, II or III even if the component members are of rank IV. Therefore, the design of frames with sufficient aseismic properties is con-



sidered possible by using the allowable strength for temporary loading R^{QE} as the basic value if a value corresponding to rank III for higher safety is set for the reduction factor D_s and formula (4) is applied using the value of given by formula (5).

Since the diagonal bracing is $B^{QP} \cong B^{QE}$ in the case of a frame, the left-hand member of formula (4) is $1/\alpha \cdot B^{QE}$.

4. CONCLUSION

To summarize the results obtained by this research,

- 1) The maximum strength of frames composed of members of relatively large width-thickness ratios such as light-gauge steel can be nearly determined by the ultimate horizontal strength in the evaluation of the yield moment.
- 2) When cold-formed steel products such as light-gauge steel are used and connected on the basis of the ultimate strength, a considerable rise occurs in the yield stress by the effect of cold working and it is problematic to design structures based on the basic strength F indiscriminately.
- 3) To secure, aseismic properties at the same level as is provided by the new earthquake-resistance design method in Japan, following two design methods are presented. One is limit load design method by estimating the plastic hinge by the evaluation of the yield moment M_y . Otherwise, frames should be designed without calculating the ultimate horizontal strength and by applying formula (6) taking as the basic value a short-term allowable strength based on the allowable stress design method.

REFERENCES

1. Akiyama H., "Aseismic Limit Design of Building Structure", Tokyo Univ. Publisher, 1980.
2. Architectural Institute of Japan, "Recommendations for the Design and Fabrication of Light Weight Steel Structures" 1985
3. Kato B., Akiyama H. and Kitazawa S., "Deformation Characteristic of Box-Shaped Steel Members Influenced by Local Buckling", Trans. of AIJ, NO. 268, 1978.
4. Ono T., "Deformation Capacity and Ultimate Strength of Cold Formed Steel Members and Frames", Proc. of 7th ECEE, 1982.
5. Suzuki T. and Ono T., "Experimental Study of Inelastic Steel Beams" (1),(2), Trans. of AIJ, NO. 168, NO. 171, 1970.
6. Suzuki T., Ono T. and Kanabako Y., "Local Buckling and Inelastic Deformation Capacity of steel Beams under Shear Bending", Trans. of AIJ, NO. 260, 1977.

Distortion of Thin-Walled Open Cross Section Members

Distorsion des profils à section ouverte et parois minces

Deformation von dünnwandigen Bauteilen mit offenem Querschnitt

Kunihiro TAKAHASHI

Associate Professor
Keio University
Kanagawa, Japan



Kunihiro Takahashi, born 1945, received his Ph.D. in engineering from Keio University. He has been concerned with the analysis of thin-walled structures.

Masao MIZUNO

Professor
Keio University
Kanagawa, Japan



Masao Mizuno, born 1922, received his Ph.D. in engineering from Tokyo University. He is a past president of the Society of Spring Research of Japan.

SUMMARY

In the analysis of thin-walled open-cross-section members, the effect of distorting contours of the cross sections has, up till now, not been taken into account. In this study a «theory of bars with distortion» is developed. This theory includes the conventional theory of warping torsion. An index showing rigidity of distortion is proposed. In particular, many experiments have been carried out.

RÉSUMÉ

Jusqu'à présent, l'analyse des profils à section ouverte et parois minces ne prend pas en compte l'effet de la distorsion du contour de la section droite. Cette étude présente une théorie qui rend compte de cette distorsion en plus du gauchissement admis en torsion non-uniforme. On propose en particulier un indice de rigidité à la distorsion. Des résultats d'essais permettent de vérifier cette théorie.

ZUSAMMENFASSUNG

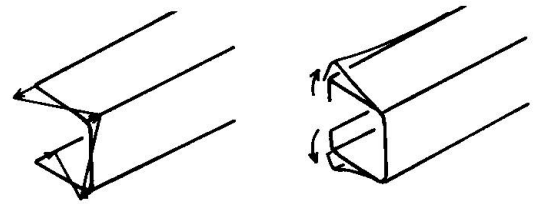
Mit den bisherigen Berechnungsmethoden konnte bei dünnwandigen Stäben mit offenem Profil der Verformungseffekt für die Konturlinien nicht berechnet werden. In dieser Abhandlung wird eine «Theorie für Stäbe mit deformierbaren Querschnitten» entwickelt, wobei die bekannte Theorie für Wölb torsion berücksichtigt worden ist. Im besonderen schlägt man die Einführung eines Steifigkeitsindex für die Deformation vor. Weiterhin wurde eine grosse Anzahl von Experimenten durchgeführt.



1. PREFACE

Recently, the use of cold-formed thin-walled members for building construction has especially increased. From the viewpoint of the strength and rigidity of thin-walled structural members, closed cross section members are more advantageous than open cross section members, but cases requiring the use of open cross section members often occur. The theoretical analysis of open cross section members has been established in the theory of warping torsion which has been used by structural designers long since. However, this theory of warping torsion is made up on the basis of the assumption that the in-plane distortion of cross sections does not occur. The distortion mentioned here is the deformation of a contour in the plane of a cross section, and is a different deformation from warping which is the deformation in the direction normal to it, that is, in axial direction(Fig.1).

In this paper, a new concept of the theory of bars with distortion is to be discussed, in which the effect of distortion besides warping is taken into account for thin-walled open cross section members(Fig.2).



(a) Warping (b) Distortion

Fig.1 Deformation of cross section

2. DISTORTION OF CROSS SECTION

The loading condition which causes the deformation of cross sections is typically shown as Figs.3 and 4. The loading condition as shown in Fig.3(a) is often seen in actual structures, but it can be decomposed into two loading conditions as shown in Figs.3(b) and (c). (b) can be regarded nearly as the loading condition of bending, but (c) is a loading condition of a different type, which is neither bending nor torsion, but it is the force causing distortion. Similarly, the load in Fig.4(c) does not cause bending nor torsional deformation. Only distortion arises.

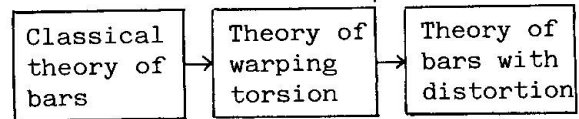


Fig.2 Theory of bars

In the loading conditions of Figs.3(c) and 4(c), since the flanges (I) of the upper and lower edges are subjected to in-plane bending, the effect of distortion is transmitted to a long distance. However, if the flanges (I) do not exist, and the members are channels with simple C-form cross section, they will be subjected to the loading by the out-of-plane bending of the flanges (II). In this case, because force is transmitted by out-of-plane bending, the effect of distortion remains in local effect. In this way, it can be decided to distinguish by calling the distortion as subjected to in-plane bending distortion of first kind, and the case as subjected to only out-of-plane bending distortion of second kind(Fig.5). In the first kind,

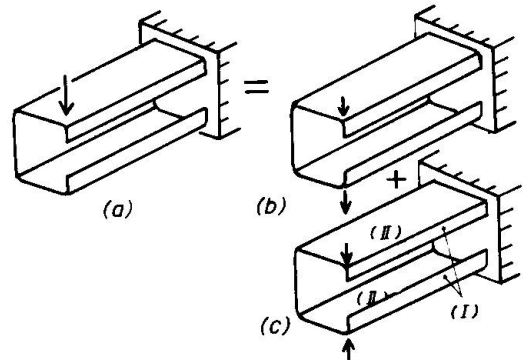


Fig.3 Force which causes distortion

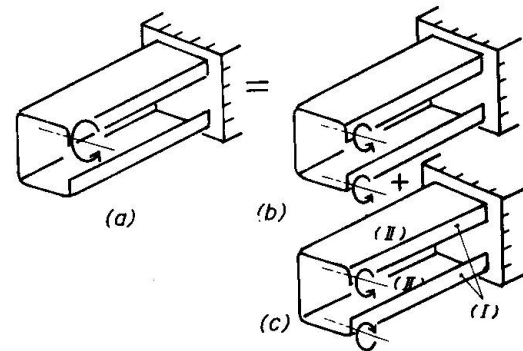


Fig.4 Moment which causes distortion

the effect is exerted on a whole member, while the second kind remains in local effect. Of course, as shown by the broken line in Fig.5(a), the first kind deformation includes the accompanying deformation of second kind. The cross sectional deformation of second kind can be restrained by local reinforcement, therefore hereinafter, the cross sectional deformation of first kind is discussed in detail.

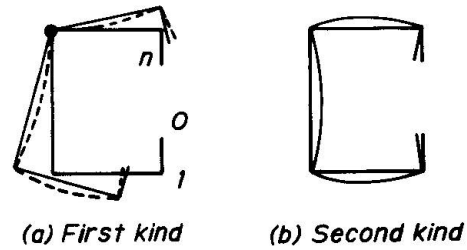


Fig.5 Distortion of first and second kind

The cross sectional deformation of first kind can be further classified according to the number of the deformation mode. The number of mode that is, the degree of freedom was enumerated by regarding the case that a cross section deforms making a hinge at only one folded point (mark ●) as one as shown in Fig.5(a). If the end point (point 0 or n) is considered to be a hinge, it becomes ordinary torsion. The degree of freedom m is expressed by $m=n-3$ (n : number of composing plates, $n \geq 3$, $m \leq 0 \rightarrow m=0$), assuming $m=0$ as torsion. As mentioned above, analysis can be made generally, including torsion in distortion. The example of classifying cross sections according to this degree of freedom m is shown in Fig.6. As m is larger, the probability that the distortion of first kind occurs under general loading is higher, accordingly, it means that the possibility of causing the effect of distortion to far points is strong.

m	Cross section			
0				
1				
2				
⋮				

Fig.6 Classification of cross sections

3. THEORY

As to the distortion of thin-walled open cross section members, research has been carried out already by the author [1], and here, only its outline is shown. The coordinate system is shown in Fig.7. The displacements u, v, w in directions s, N, z of any point of a cross section can be expressed as follows.

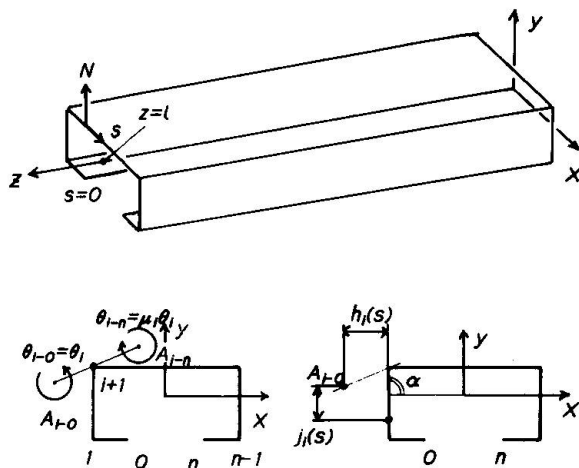


Fig.7 Coordinate system

$$u(s, N, z) = \xi \cos \alpha + \eta \sin \alpha + \sum_{i=0}^m \theta_i \mu_i (h_i \pm N) + \sum_{i=0}^m u_{bi}(s, N, z) \dots \dots \dots (1)$$

$$v(s, N, z) = -\xi \sin \alpha + \eta \cos \alpha + \sum_{i=0}^m \theta_i \mu_i j_i + \sum_{i=0}^m v_{bi}(s, N, z) \dots \dots \dots (2)$$

$$w(s, N, z) = \zeta(z) - \xi'x - \eta'y + \sum_{i=0}^m \theta_i \phi_i + \sum_{i=0}^m w_{bi}(s, N, z) \dots \dots \dots (3)$$

Here, ξ, η and ζ are rigid body translations in x, y and z directions. x, y and z are the principal axes of a cross section, and θ_i is the angle of turning around a hinge point corresponding to the i -th degree of freedom. The added displacement (the broken line in Fig.5(a)) due to accompanying out-of-plane bending is expressed by (u_{bi}, v_{bi}, w_{bi}) . $\mu_i(s)$ is a proper rotation ratio. This value of μ_i is determined by orthogonalizing axial stress. Besides, at the stage of orthogonalizing, the necessity to separate two centers of rotation on



the left and right sides of a hinge which were considered to be the centers of rotation arises. These two points (A_{i-0} , and A_{i-n} in Fig.7) obtained by orthogonalizing can be named distortional shear centers. This concept is that extending the ordinary concept of shear center. Besides, $\phi_i(s)$ is a function having generalized a warping function, and forms the system of orthogonal functions regarding $i=0, \dots, m$. Differentiating Eqs.(1)-(3), infinitesimal strains are given, and using the constitutive equations for linear elastic bodies, stresses can be determined. It is assumed that the external forces F_q and F_p in s and z directions per unit length of direction s are applied to both end surfaces ($z=0, l$) of a bar, and the principle of virtual work is used, then the following basis equations are obtained.

$$EI_y \xi'''' = 0 \dots\dots\dots(4)$$

$$EI_x \eta'''' = 0 \dots\dots\dots(5)$$

$$EF\zeta'' = 0 \dots\dots\dots(6)$$

$$EI_{\phi} h \theta_h'''' - \sum_{i=0}^m GJ_{hi} \theta_i'' + \sum_{i=0}^m M_{hi} \theta_i = 0 \dots\dots\dots(7), \text{ where } M_{hi} = \int_s \frac{M_h M_i}{EI} ds. (h=1, \dots, m)$$

M_i is the bending moment distributing in a frame having the form of a cross sectional contour, cut into unit breadth in z direction, and I is $t^3/12$. E and G are moduli of elasticity. When the case of $m=0$ in Eq.(7) is considered, that is, only torsion occurs, it is reduced to the conventional equation for warping torsion. In the above equations, respective constants of cross sections and generalized forces were given in Table 1. J_{hi} is the generalized St. Venant's torsional constant.

Table 1

4. PROPERTIES OF CROSS SECTIONS

In the left column in Table 1, the quantities from the top down to the fourth are those well known so far. That is, F : area of cross section, I_y : moment of inertia around y axis, I_x : moment of inertia around x axis, and I_{ϕ_0} : constant of warping torsion. All these are expressed as the integral of square of respective generalized coordinates, $1, x, y$ and ϕ_0 over a whole cross section. Accordingly, the constants regarding squares of $\phi_1, \phi_2, \dots, \phi_m$ may be grasped similarly as the concept having extended moment of inertia. Now, I_x and I_y express the rigidity resisting bending moments. Similarly, also $I_{\phi_1}, I_{\phi_2}, \dots, I_{\phi_m}$ can be considered as the rigidity regarding the distortion of the corresponding degree of freedom. Then, these I_{ϕ_i} ($i=1, \dots, m$) can be used as the indices of rigidity peculiar to respective cross sections. It is desirable to take these values large at the time of design.

Constant of cross section	Generalized force	Generalized coordinate
$F = \iint ds dN$	$F_z = \int F_p ds$	1
$I_y = \iint x^2 ds dN$	$M_y = - \int F_p x ds$	x
$I_x = \iint y^2 ds dN$	$M_x = \int F_p y ds$	y
$I_{\phi_0} = \iint \phi_0^2 ds dN$	$F_{p0} = \int F_p \phi_0 ds$	ϕ_0
$I_{\phi_1} = \iint \phi_1^2 ds dN$	$F_{p1} = \int F_p \phi_1 ds$	ϕ_1
\vdots	\vdots	\vdots
$I_{\phi_m} = \iint \phi_m^2 ds dN$	$F_{pm} = \int F_p \phi_m ds$	ϕ_m

Next, in the middle column in Table 1, four upper quantities are well known external forces. That is, F_z : axial force, M_y and M_x : bending moments, and F_{p0} : bimoment of torsion. These are all the quantities having integrated F_p multiplied by the orthogonalized coordinates, $1, x, y$ and ϕ_0 , over a whole cross section. Similarly, it may be said that the external forces obtained by integrating F_p multiplied by $\phi_1, \phi_2, \dots, \phi_m$ are the generalized forces causing corresponding distortion. These are grasped as the concept having extended bimoment in warping torsion, accordingly, these are to be called distortional bimoment. These are to exist as many as the number of the degree of freedom.

The right column in Table 1 shows the orthogonalized generalized coordinates. Furthermore, the longitudinal stress σ_z is to be as follows.

$$\sigma_z = \frac{Fz}{F} - \frac{M_y}{I_y}x + \frac{M_x}{I_x}y + \frac{Fp_0}{I_{\phi_0}}\phi_0 + \frac{Fp_1}{I_{\phi_1}}\phi_1 + \dots + \frac{Fp_m}{I_{\phi_m}}\phi_m \quad (8)$$

By taking an example of the cross section having the degree of freedom of one, Fig.8 shows the generalized coordinates which are the distribution of σ_z .

On the other hand, when load is applied in the direction orthogonal to the longitudinal axis of a member, the position of shear centers is related. The practical examples of shear centers are shown in Fig.9. A_0 is the shear center of torsion. A_{1-0} and A_{1-n} are the centers of turning of the left and right parts of a cross section regarding the distortion of the first degree of freedom, which can be called shear centers of distortion. A_{2-0} and A_{2-n} are the shear centers regarding the second degree of freedom. When load P in the figure is applied through these points, distortion of its degree of freedom is not to occur. This fact may serve as a reference concerning the position to fix a bracket for transmitting load.

5. EXPERIMENTAL RESULTS

In order to verify the above theory, the following experiments were carried out. The specimens for the experiment were made by bending structural aluminum sheets. Figure 10 shows the case of applying the self-equilibrated force to the cross section having the degree of freedom of one. One end of the specimen was fixed, and load was applied to the other end. (a) and (b) in Fig.10 are the strains measured along the cross section. Where, ϵ_z is the longitudinal strain, and ϵ_s is the strain in direction s . Fig.10(c),(d) show the longitudinal distribution of strain ϵ_z and of quantity $\theta_1(z)$. $\theta_1(z)$ is defined in Chapter 3, and it indicates the magnitude of distortion.

Figure 11 shows the similar measured results for the cross section having the degree of freedom of two.

Figure 12 shows the measured results when four bulkheads were used.

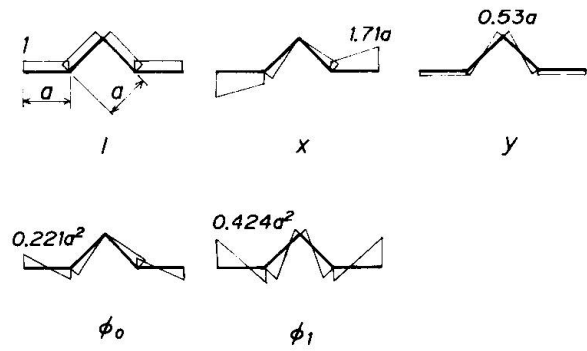


Fig.8 Generalized coordinates: distribution of σ_z

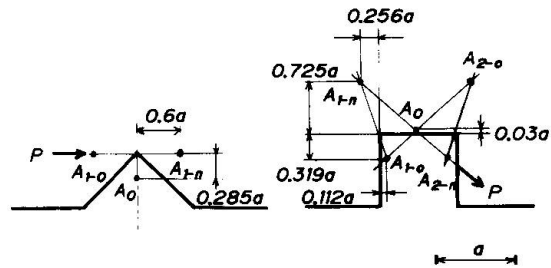


Fig.9 Shear centers of distortion

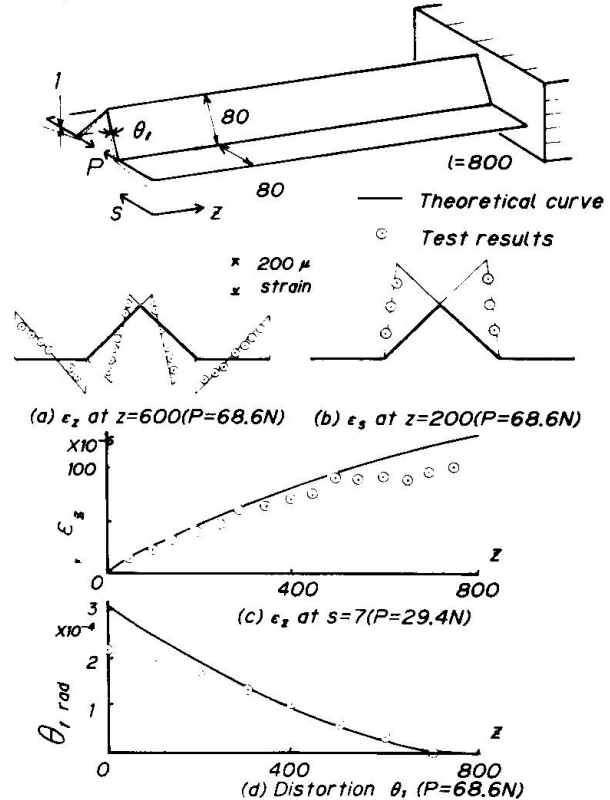


Fig.10 Test results (cross section of one degree of freedom)

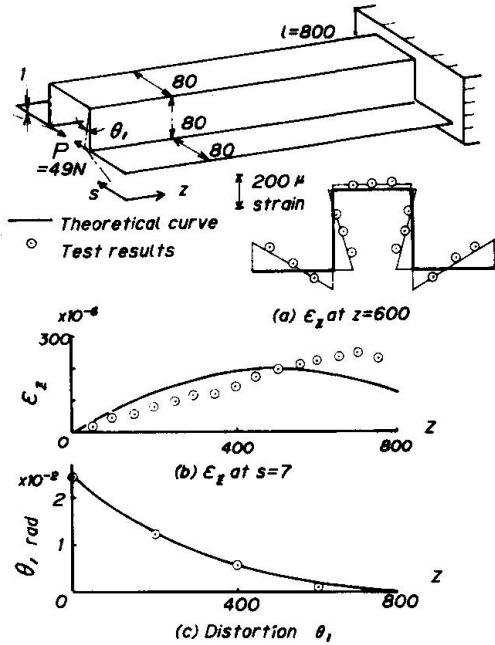


Fig.11 Test results (cross section of two degree of freedom)

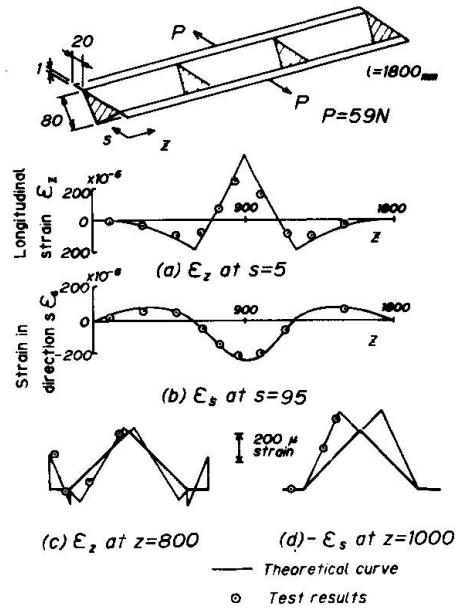


Fig.12 Distortion of a bar with bulkheads

The calculated values at this time can be obtained by solving a statically indeterminate problem based on the equations in Chapter 3.

Finally, the author would like to discuss a buckling problem which was not mentioned in Chapter 3. Flexural buckling and torsional-flexural buckling have been well known, but in addition, the new buckling mode by distortion as shown in Fig.13 exists. The distortional buckling load for the cross section as Fig.13 is expressed by the following equation. The details of this equation is discussed in the paper which is to be published.

$$P_{cr} = (EI_{\phi 1} (\frac{n\pi}{l})^2 + M_{11} (\frac{l}{n\pi})^2) / r_d^2 \dots \dots (9)$$

Here, r_d is the value peculiar to the cross section. In this example, the calculated value of $P_{cr} = 5.98$ KN was obtained, and it is lower than conventional elastic or plastic buckling loads. As the result of the experiment using a structural aluminum column having the dimensions shown in Fig.13, the column buckled in distortional mode and critical load was about 7 KN.

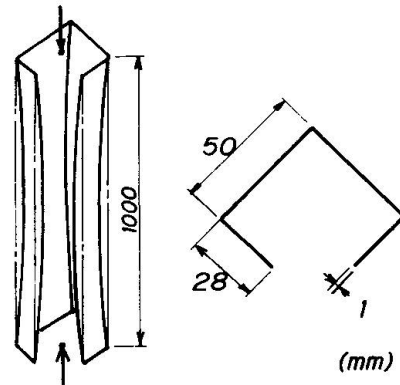


Fig.13 Distortional buckling

6. CONCLUSION

In the conventional theory of warping torsion, the strain and deformation of Figs. 10,11,12 due to distortion have become zero. Then, it is important to estimate the effects of the distortion in the design stage of the thin-walled metal structures in buildings.

REFERENCE

1. TAKAHASHI K., M. MIZUNO, Distortion of Thin-Walled Open-Cross-Section Members. Bull.JSME, 23-182, 1980, 1290-1296.

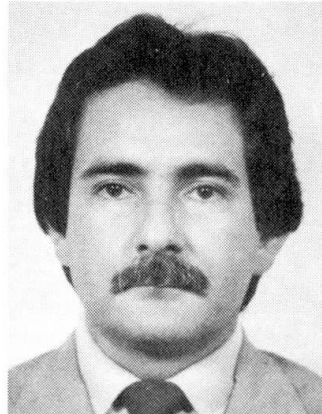
Relevant Dynamic Effects in the Design of Thin-Walled Structures

Effets dynamiques à considérer lors du dimensionnement
des structures à parois minces

Massgebende dynamische Effekte bei der Bemessung von
dünnwandigen Bauteilen

Marco Antonio SOUZA

Dr. Engineer
PUC/RJ – Dep. Eng. Civil
Rio de Janeiro, Brasil



Marco Antonio Souza, born 1951, received his Ph.D. degree at University College London, England, in 1982. Since then he has been involved with different aspects relevant to the vibration analysis of structural elements liable to buckling.

SUMMARY

The present paper discusses relevant aspects to be considered in the design of thin-walled structural elements liable to buckling. The effects presented are of even greater importance if time dependent loads are to be considered.

RÉSUMÉ

Cette contribution met en évidence certains phénomènes qui doivent être pris en considération lors du dimensionnement d'éléments de structures à parois minces sensibles au flambement et au voilement. Ces effets sont d'autant plus importants si les charges à prendre en compte sont variables au cours du temps.

ZUSAMMENFASSUNG

In diesem Beitrag werden einige für die Bemessung von beulgefährdeten dünnwandigen Bauteilen massgebende Grundgedanken vorgestellt. Die Schlussfolgerungen erweisen sich als besonders wichtig, wenn auch zeitabhängige Beanspruchungen zu berücksichtigen sind.



1. INTRODUCTION

Resonance is one of the main concerns in the design of any structure which should respond safely to time dependent loads. The accurate calculation of the natural frequencies of the structure is therefore of major importance.

What the present paper discusses is relevant to the accurate calculation of the natural frequency of perfect and initially imperfect structural elements liable to buckling.

Since the purpose of this paper is to focus attention to aspects not often mentioned, the discussion will be based on results obtained by the author. A list of references containing the theoretical analysis will be presented at the end of the paper.

2. STABILITY AND VIBRATION CHARACTERISTICS

2.1 Stability Characteristics

The stability characteristics of perfect and also imperfect columns, plates and cylindrical shells are relatively well known. A summary of such characteristics is presented in figure 1 in terms of the equilibrium paths, diagrams of axial, or in-plane load in the case of plates, versus the transverse displacement.

As it can be seen from the diagrams shown in figure 1, the effects of the

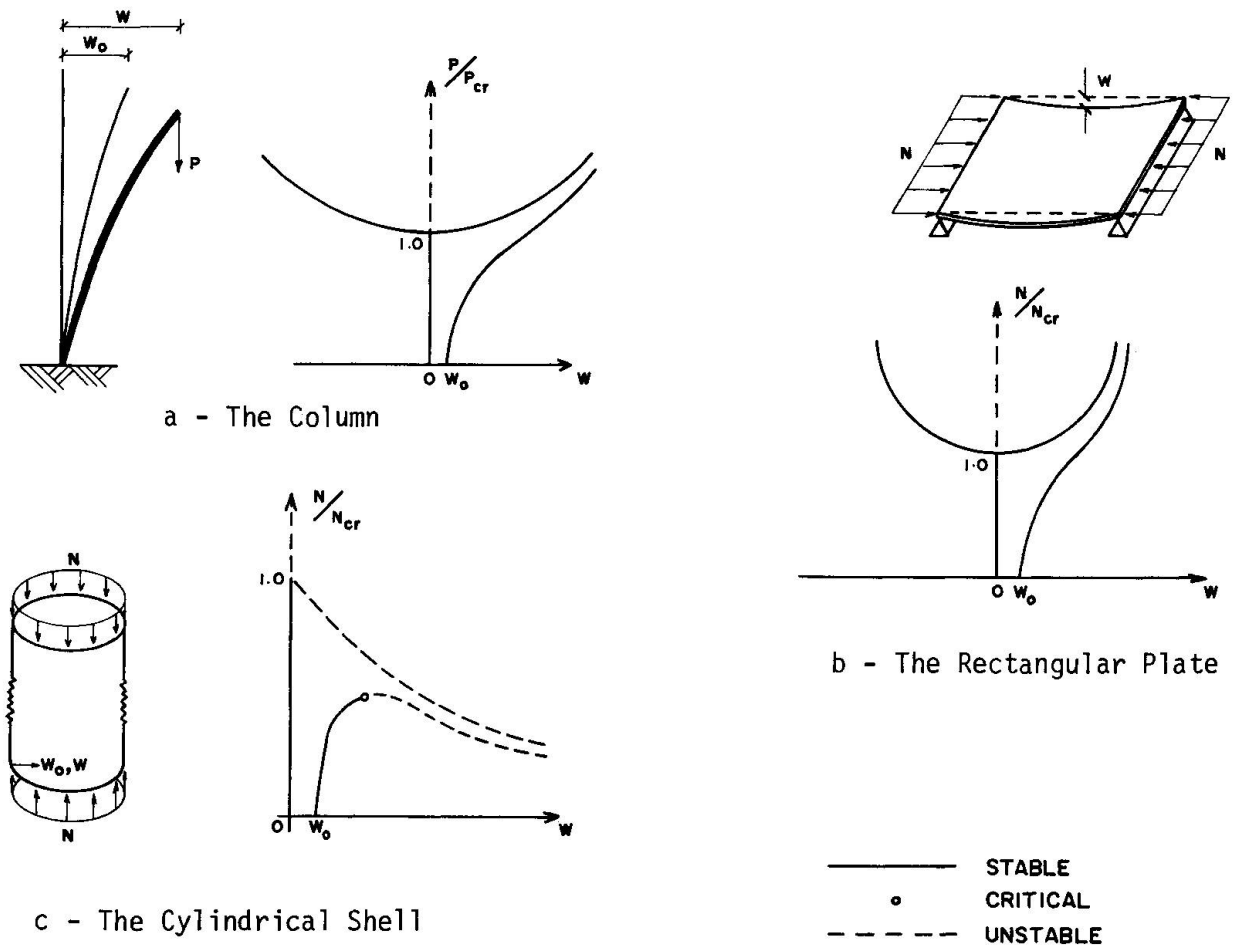


Fig. 1 Typical Equilibrium Paths

initial imperfection, represented by w_0 , on the stability characteristics of columns, rectangular plates and cylindrical shells are evident. In order to investigate the effects of the initial imperfection on the vibration characteristics of columns, plates and cylindrical shells the author used [1] a simplified model which reproduce similar stability characteristics to those of figure 1. The model and the stability characteristics are presented in figures 2 and 3, respectively.

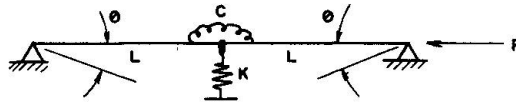


Fig. 2 The Model

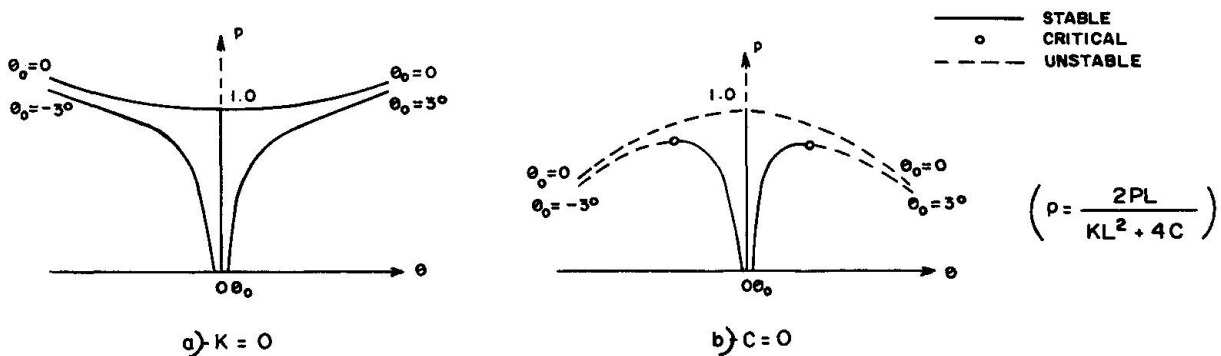


Fig. 3 Equilibrium Paths

The main advantage of the simplified model is the possibility it gives of considering different factors, such as the initial imperfection, without making the analysis too complex. This procedure was used and the vibration characteristics were determined.

2.2 Vibration Characteristics

The vibration characteristics of columns, plates and cylindrical shells can be obtained in terms of the relationship between the applied axial load and the square of the natural frequency. Such a relationship is obtained by investigating the vibration of the model around the equilibrium configurations [1].

Diagram of the square of the frequency versus the applied axial load for the model of figure 2 are presented in figure 4.

Therefore the relationship between the level of the axial load, the equilibrium configuration and the natural frequency is well determined. Figures 4-a,b corresponds to the equilibrium paths of fig. 3-a,b respectively.

Figure 4 illustrates how the initial imperfection affects the natural frequencies of vibration, for a certain load level: it raises the level of the natural frequency for columns and plates and lowers the level of the natural frequency in the case of cylindrical shells. The comparison being between the imperfect and the perfect structural element.

Major contributions to the subject were given by Massonnet [2,3]. His works are of great significance for anybody involved in the investigation of vibration char-

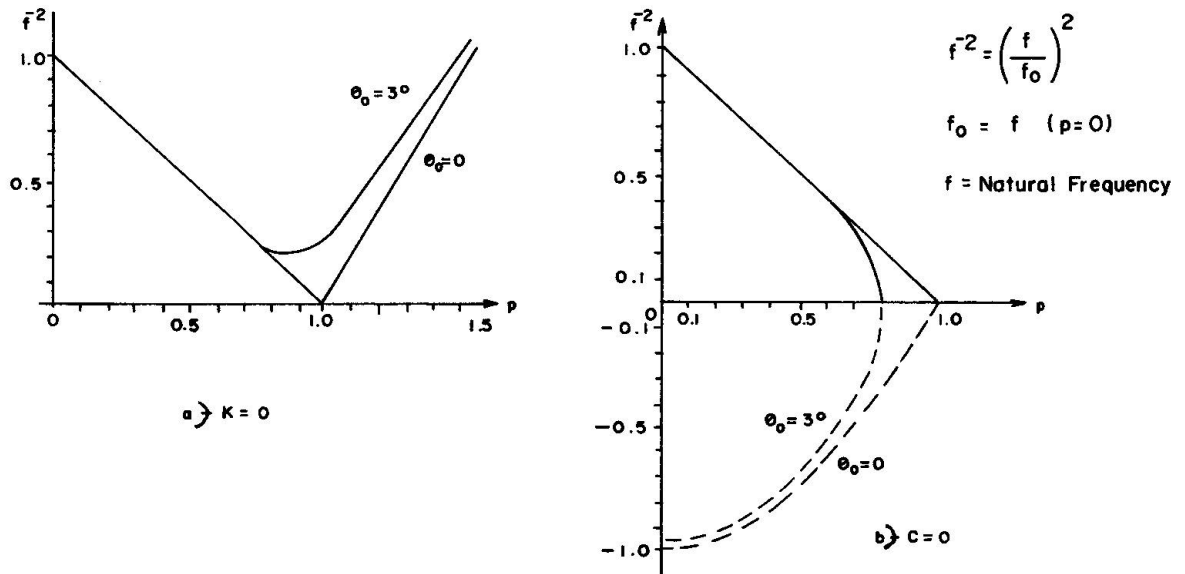


Fig. 4 (Frequency)² vs. Axial Load for the Model of fig. 2

acteristics of structural elements liable to buckling. Curves similar to those of figure 4 can be found in references [2,3].

Experimental results confirm the theoretical predictions obtained with such a simplified model as that of figure 2 [4,5,6].

3. DISCUSSION

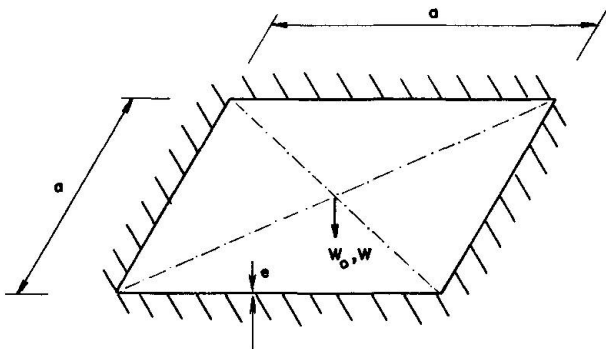
The consequences of the effects showed previously on the design of structural elements liable to buckling will now be discussed. Two structural elements will be used in order to highlight the main aspects: a rectangular plate and a cylindrical shell model. The difference in the calculations of the level of frequency corresponding to resonance will be carried out stressing the importance of the consideration of the initial imperfections in the analysis.

3.1 The Rectangular Plate

The stability and the vibration characteristics of a square plate clamped along the edges were theoretically obtained by the author [7]. The results of the analysis are presented in figure 5 in terms of the in-plane loads versus the transverse deflection of the centre section and the curves of the square of the frequency versus the in-plane loading. The initial imperfection is taken into account in the analysis.

In order to illustrate how the level of the natural frequency is affected if the initial imperfection is considered or not let us consider the following values for the load ratio P/P_{cr} : 0.50; 0.70 and 2.00. The results of the calculations are presented in Table 1, where ϵ represents the difference between the value corresponding to the imperfect and the perfect cases.

As it can be seen from Table 1 the difference between the actual level of the natural frequency (if initial imperfection is present) and that corresponding to the perfect plate can be quite significant, even for levels of in-plane load much lower than the critical.



e = thickness

a = length of the sides

w_0 = deflection of the centre section

w = total deflection of the centre section

P = in plane loading

P_{cr} = critical load

f = natural frequency

f_0 = natural frequency corresponding to $P = 0$

$p = P/P_{cr}$

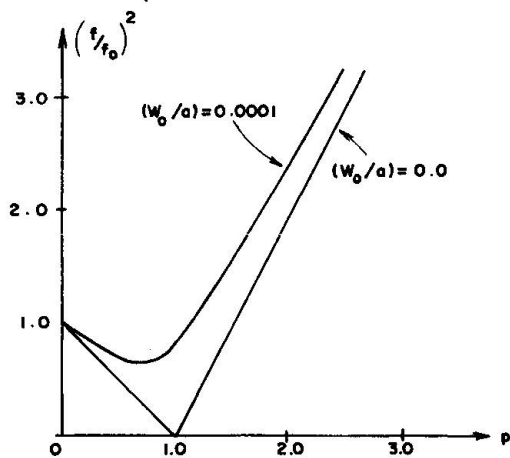
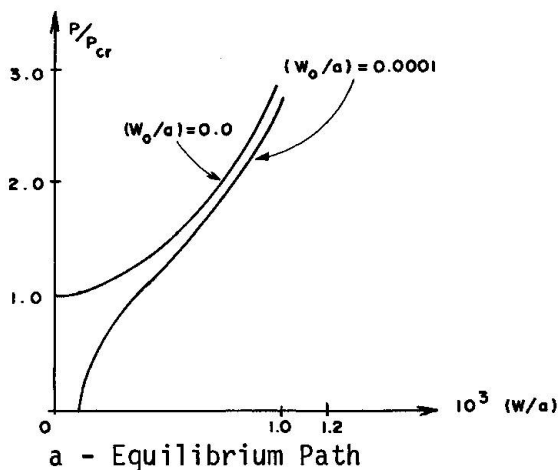


Fig. 5 The Rectangular Plate [7], ($e/a=0.0025$)

The implications on design are evident: suppose the plate was considered to be perfectly flat in the analysis and the actual plate exhibited an initial imperfection even before the in-plane loading started. As a consequence, for instance, for $P = 0.70 P_{cr}$ the square of the frequency will be 113% higher than the calculated value since the plate was assumed to be perfect. Resonance therefore will not occur in the expected level of the natural frequency. This example illustrates the importance of the consideration in the analysis of realistic initial imperfection profiles.



P	$(f/f_0)^2$		$\epsilon\%$
	$w_0/a=0.0$	$w_0/a=10^{-4}$	
0.50	0.50	0.68	36.0
0.70	0.30	0.64	113.0
1.00	2.00	2.43	21.5

Table 1 Effects of the Initial Imperfection - Rectangular Plate

3.2 The Cylindrical Shell

In order to illustrate how the initial imperfection affects the vibration characteristics of cylindrical shells a simplified model was introduced by the author [8]. The model and its stability and vibration characteristics are reproduced in figure 6.

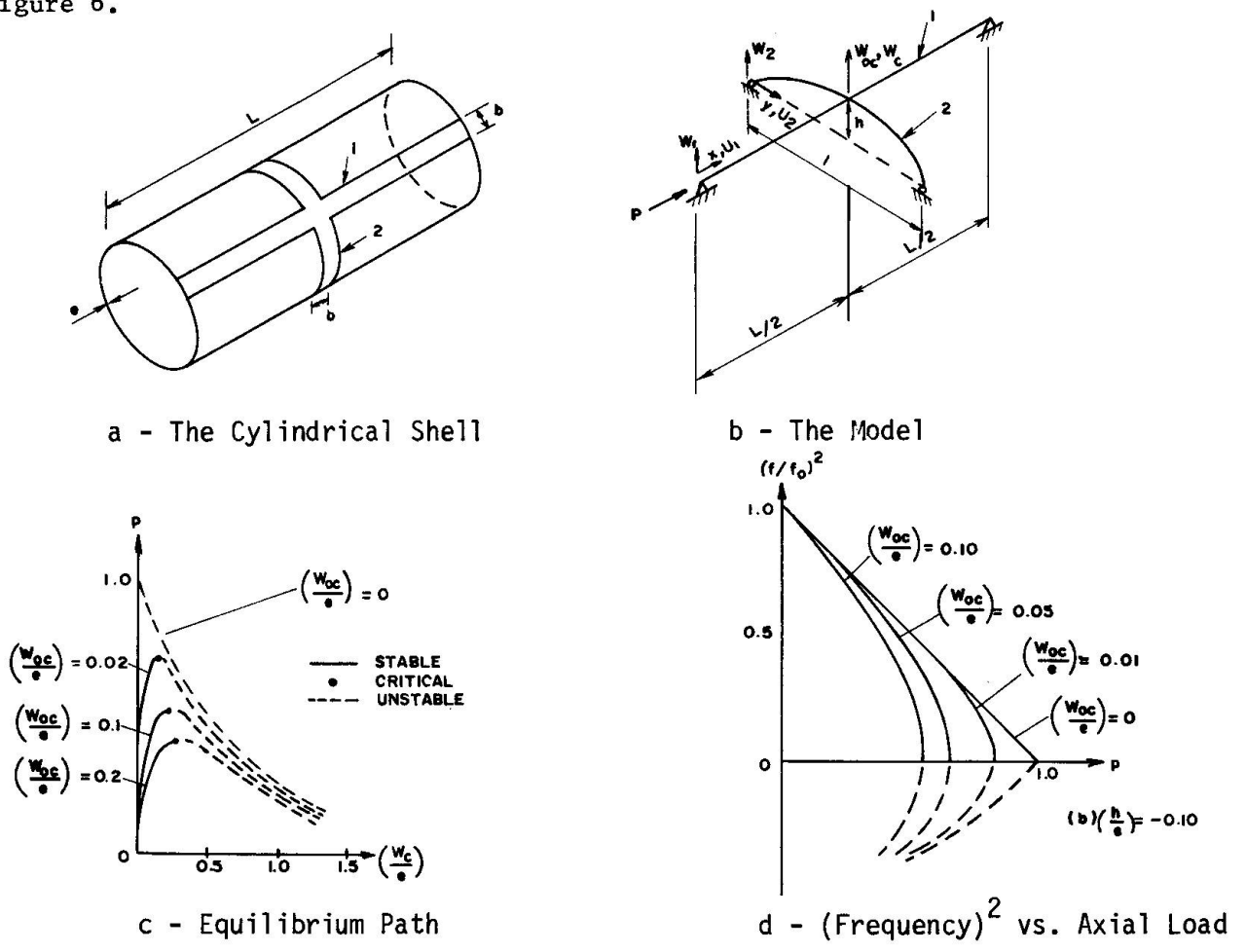


Fig. 6 The Cylindrical Shell Model

As it can be seen from figure 6 the equilibrium paths are similar to those corresponding to the actual shells. In the case of cylindrical shells the consequences are even more dramatic since the initial imperfection lowers the load carrying capacity of the shell. In the frequency range resonance can occur for a much lower level of axial load than expected if the initial imperfection is not included in the calculations.

As an example let us consider $P = 0.60 P_{cr}$ in figure 6-c. Table 2 contains the

values of interest for the discussion. ϵ represents the difference between the imperfect and the perfect values.

p	$(f/f_o)^2$			
	$w_o/e = 0.0$	$w_o/e = 0.01$	$w_o/e = 0.05$	$w_o/e = 0.10$
0.60	0.40	0.38	0.22	-
$\epsilon\%$	0.0	-5.0	-45.0	-

Table 2 Effects of the initial imperfection - Cylindrical Shell

Therefore resonance can occur for levels of frequency much lower than expected: 45.0% (for $w_o/e = 0.05$) of difference in the square of the frequency corresponding to 67.08% in the frequency level. The shell can be destroyed much earlier than feared.

This is another example used in order to stress the necessity of accurately calculating the natural frequency.

4. CONCLUSIONS

Relevant aspects to be taken into account in the design of thin-walled structures liable to buckling were presented. The need of incorporating realistic initial imperfection profiles in the calculation of the natural frequency was stressed. Examples were presented highlighting the fact that resonance can occur for different levels of the natural frequency if the structural element to be designed is assumed to be perfect.

Other effects such as residual stresses, temperature, changes of support conditions during the loading process, material non-linearity on the stability and vibration characteristics of structural elements liable to buckling must also be accounted for. Such effects have also been investigated by the author and hopefully the results will give extra information to be considered in the design of thin-walled structural elements liable to buckling subjected to time dependent loading.

REFERENCES

1. SOUZA M.A., Post-Buckling Vibration Characteristics of Structural Elements. 1984. SSRC Annual Technical Session, pp. 183-190.
2. MASSONNET C., Les Relations entre les Modes Normaux de Vibration et la Stabilité des Systèmes Elastiques. Bulletin des Cours et des Laboratoires d'Essais des Constructions du Génie Civil et d'Hydraulique Fluviale, Tome I, Nos. 1 and 2, 1940, Brussels, Belgium.
3. MASSONNET C., Le Voilement des Plaques Planes Sollicitées dans Leur Plan. Final Report of the International Association for Bridge and Structural Engineering, Liège, Belgium, 13-18 September, 1948, pp. 291-300.
4. JUBB J.E.M.; PHILLIPS I.G. and BECKER H., Interrelation of Structural Stability, Stiffness, Residual Stresses and Natural Frequency. Journal of Sound and Vibration, 1975, Vol. 39(1), pp. 121-134.
5. LURIE H., Lateral Vibrations as Related to Structural Stability. Journal of Applied Mechanics, June 1952, pp. 195-204.
6. SINGER J., Buckling Experiments on Shells - A Review of Recent Developments.



Euromech Colloquium No. 128: Stability, Buckling and Postbuckling Behavior; Foundations and Analysis, Delft, Holland, March 31 - April 2, 1980.

7. SOUZA M.A., Vibration Characteristics of Buckled Structures. Ph.D. Thesis, University of London, 1982.
8. SOUZA M.A. and WALKER A.C., Vibration Characteristics of Buckled Cylinders. International Symposium on Offshore Engineering - Brasil Offshore'81, Rio de Janeiro, Brasil, 14-19 September, 1981, Pentech Press, 1982, pp. 382-394.

Spacing of Connections in Thin-Walled Compression Elements

Ecartement des points d'assemblage dans les éléments
à parois minces comprimés

Abstände von Verbindungsmitteln bei dünnwandigen Druckelementen

Muzaffer YENER

Assist. Professor
Purdue University
West Lafayette, IN, USA



Muzaffer Yener, born 1947, received his B.S. degree in civil engineering and M.S. degree in structural engineering from New York University in New York, NY. He worked a total of five years as a design engineer and a supervisor. He received his Ph.D. degree from Cornell University, Ithaca, NY.

SUMMARY

A great variety of cold-formed steel shapes are often used in combination with cover plates to form closed cellular panels. In this paper, the spacing requirements of connectors that are used to fasten the cover plate to the fluted sheet are investigated. First, an experimental investigation for the design of cellular cold-formed steel panels with intermittent connections is described. Based on elastic plate buckling theory and experimental observations, an analytical development of criteria for maximum connection spacing is presented.

RÉSUMÉ

Une grande variété de profils ouverts formés à froid est utilisée en combinaison avec une tôle plane de façon à constituer une plaque à cellules fermées. Cette contribution concerne l'étude de l'écartement nécessaire des points d'assemblage fixant la tôle plane à la tôle profilée. En premier lieu, on décrit une recherche expérimentale sur le dimensionnement des plaques cellulaires en acier formé à froid à points d'assemblages discontinus. Puis on présente le développement analytique des critères d'espacement maximal des assemblages basé sur la théorie du voilement élastique des plaques et sur les observations effectuées lors des essais.

ZUSAMMENFASSUNG

Eine grosse Vielfalt von kaltgeformten Profilen wird oft in Verbindung mit Deckplatten verwendet, um geschlossene kastenförmige Elemente zu bilden. Dieser Artikel beschreibt die Anforderungen an die Abstandswahl von Verbindungsmitteln, welche zur Befestigung der Deckplatte an das Wellblech verwendet werden. Zuerst wird eine Untersuchung über die Bemessung dieser Elemente mit nicht kontinuierlichen Verbindungen beschrieben. Basierend auf der elastischen Beultheorie für Platten und auf experimentellen Untersuchungen wird eine analytische Herleitung des Kriteriums für die beste Abstandswahl der Verbindungen vorgestellt.



1. INTRODUCTION

A great variety of cold-formed steel shapes is often used in combination with cover plates, as shown in Fig. 1, to form closed cellular panels. In this paper, experimental and analytical investigations of the spacing requirements of connectors that are used to fasten the cover plate to the fluted sheet to resist gravity loads are summarized. Comparisons with test results are also made.

It is of economical importance to design such composite sections so that the cover plate can be considered as an integrated, load-carrying component of the assembly. In composite thin-walled members, the maximum allowable spacing of connections in compression elements is governed either by the allowable strength of the connection, or by separation of the component compression plates along the lines of connections.

An experimental investigation was conducted on single-span, two-span, and multi-span panels with the geometry shown in Fig. 2. Panel strength and stiffness under gravity loading were measured on cellular panels made from a fluted sheet and a cover plate connected with four lines of rivets. Some of the test panels had either the cover plate or the flats of the fluted sheet perforated, with or without a wire mesh placed between them, in order to improve acoustic properties. The test program and results are described in Ref. 4. The behaviors of identically designed riveted and welded panels are compared. Shear strength and the slip load value of the rivets were determined with single-shear strap tests for several combinations of sheet thickness. Based on the information obtained from 190 strap tests, 25 full-scale flexural tests (17 single-span, 4 two-span, and 4 three-span) were conducted to determine panel strength and deflection behavior.

Based on experimental observations, the elastic plate buckling theory is used to develop criteria for maximum connection spacing in cold-formed steel cellular panels. The spacing criterion developed here for preventing the separation of the cover plate from the fluted sheet of the panel ensures the continuous stiffening effect along each line of connections. The requirement regarding unstiffened flanges is determined by assuming a slight amount of rotational restraint along their supported edges.

2. EXPERIMENTAL OBJECTIVES

The primary function of fasteners in cold-formed steel roof decks and floor panels is to resist shear stresses produced by flexural loading. Allowable shear force for spot welded connections, and allowable shear and bearing stresses for bolted connections are given in the AISI Specification [1]. For riveted connections, it is suggested that shear strength of rivets be experimentally determined on representative specimens. Thus, one of the main objectives of this investigation was to determine the strength of the rivet connectors in 24-in. wide panels, using single lap joint shear tests.

In the present AISI Specification the maximum intermittent connection spacing is based on the assumption of preventing the cylindrical buckling of the compressed element between adjacent connectors, as shown in Fig. 1. In addition to preventing cylindrical buckling, consideration is also given to the local buckling of the unstiffened edge compression flanges of the fluted sheet. On the basis of the speculation that the AISI provisions may be overly conservative for cellular

panels, the following question was raised: How would the strength of the assembly be affected if the spacing were made so large as to allow slight separation of the connected compression elements? That is, would local plate buckling really terminate the useful life of the cover plates? This concern was the primary impetus in undertaking this investigation.

Separation of the compressed elements, if allowed, would tend to cause reduction in panel flexural stiffness, in addition to that produced by connection slip. At present, there is no available method for predicting deflections in a connected light-gage assembly, taking into account the slippage and separation. Therefore additional questions of importance to be considered in the investigation were: (1) How would rivet slippage and slight separation of cover plates affect the stiffness of the assembly? (2) Taking the effects of both separation and slippage into account, could the deflection be predicted with sufficient accuracy?

Two additional issues related to strength were also studied: (1) What is the maximum value of connection spacing which can be tolerated in cases where deflection is of secondary importance? and (2) How would the behavior of identical panels with riveted and welded connections differ?

3. PRELIMINARY DESIGN CONSIDERATIONS AND TEST RESULTS

After the characteristics and strength of the connections were determined from strap tests [3,4], attention was focused on the design of simple and multiple span beams. For the flexural strength determinations, a panel was considered to consist of three identical box beams situated side by side [3].

The testing of uniformly loaded single span panels with cover plates down was proposed to verify panel strength and stiffness with connected elements in tension where only connector strengths should be of concern. In order to observe the effects the plate separation along the lines of rivets had on the strength and stiffness of the assembly, single-span beams with cover plates up (connected plates in compression) were also proposed for testing. Furthermore, to simulate actual field application more precisely, the testing of full-scale continuous beams was thought to be essential. Uniform load is plotted against the average of the maximum span deflections in Fig. 3 for the two-span continuous panel specimens. The detailed test results are given in Ref. 3.

4. PROPOSED THEORETICAL SPACING CRITERIA

On the basis of experimental observations, spacing intermittent connections in cellular panels in accordance with the AISI Specifications appears to be overly conservative. The proposed alternative provision for the prevention of the separation of a compressed cover plate from the fluted sheet is based on the buckling configuration shown in Fig. 4, as observed in experiments. If the connection spacing is such that the cover plate can be suppressed into this configuration, a continuous stiffening effect along the lines of connections is achieved until the maximum edge stress σ_c reaches the yield stress σ_y . There are three possible ways in which the development of the assembled member strength predicted on the basis of monolithic action may be hindered. The maximum allowable connection spacing s is the smallest value obtained by simultaneously considering the three criteria described in the following.



4.1 Allowable Strength of Connection

This is a rather straightforward stipulation which simply states that the spacing s is not to exceed that which is required to transmit the force induced by applied loads at connections, on the basis of allowable connection strength.

4.2 Separation of Compressed Cover Plate

In Ref. 2, the buckling configuration in Fig. 4 is used to develop a spacing requirement to prevent the separation of the cover plate. Considering each cell separately, a general expression for one half-wave length $\lambda = a/m$ (Fig. 4), in terms of the compressive stress σ_c is found:

$$\sigma_c = \frac{0.904E}{(w_c/t)^2} \left(\frac{1}{c} + c\right)^2 \quad (1)$$

where $c = a/mw_c$. Solving this quadratic equation for c , and assuming that, if the buckling configuration shown in Fig. 4 is to occur, at least one extra fastener should be placed within one half-wave length (i.e., $\lambda = 2s$) results in,

$$s = 0.5t \sqrt{\frac{E}{\sigma_c}} \left[1 + \left(\frac{0.95}{w_c/t} \sqrt{\frac{E}{\sigma_c}} \right)^2 \right] \quad (2)$$

Eq. 2 is further simplified by considering the effective section properties of real plates to give $s = 0.6w_c = 0.6w/n$, in which $n =$ number of typical cells in the panel of width w , and $w_c = w/n$.

4.3 Separation of Unstiffened Compression Plate Elements

When the cover plate is in compression, both of the outstanding flanges of the fluted sheet would also be in compression. Such unstiffened compression elements tend to buckle at smaller stresses and into longer half-waves than corresponding stiffened plates. The buckling configuration of a compressed unstiffened plate is shown in Fig. 5.

Assuming that a small amount of rotational restraint is provided by the web element, the half buckling wave length is found in Ref. 2 to be $\lambda = 17w_u$. Again, placing one extra connection within the length λ gives $s = 8w_u$. The lower bounds for s are also provided in Ref. 2.

5. CONCLUSIONS AND COMPARISON WITH TESTS

This paper contains a summary of the experimental behavior of composite cold-formed steel panels with riveted and welded connections. The validity of predicting panel strength, regardless of whether the cover plate is in compression or in tension, by assuming a fully composite action has been substantiated by the testing program. Tests have also indicated that panels were somewhat more flexible than predicted on the basis of fully composite action.

In addition, based on elastic plate buckling theory, design criteria for intermittent connection spacing in thin-walled steel cellular panels under flexural loading are developed. The proposed requirements are simple and suitable for direct use in practical design. The proposed requirements as well as the AISI provisions

are compared with the available test data in Ref. 2. Comparison of the spacing values for specimens in which the cover plate was in compression indicates that for these cellular test panels, the proposed criteria require only one fastener for every three required by the AISI provisions, corresponding to a savings of approximately 67%. The comparison has also revealed that, even though the proposed requirements result in larger values for maximum connection spacing, they appear to be considerably conservative when compared with the test results.

REFERENCES

1. Specifications for the Design of Cold-Formed Steel Structural Members, American Iron and Steel Institute, Washington, D.C., 1980.
2. YENER, M., "Criteria for Connection Spacing in Cold-Formed Steel," J. of Struct. Engrg., ASCE, Vol. 110, Sept., 1984, pp. 2178-2195.
3. YENER, M., and WHITE, R.N., "Cold-Formed Steel Panels with Riveted Connections," J. of Struct. Engrg., ASCE, Vol. 110, May, 1984, pp. 1035-1050.
4. YENER, M., and WHITE, R.N., "Progress Reports on Walcon Corporation 24-in. NDU Panels, R1 through R8," Dept. of Struct. Engrg., Hollister Hall, Cornell University, Ithaca, N.Y., 1978-1980.

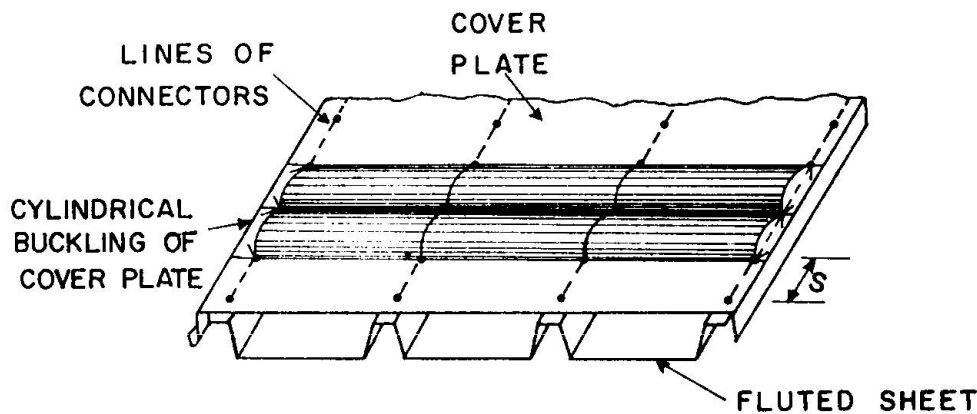


Fig. 1 - Cellular Panel with Flat Cover Plate

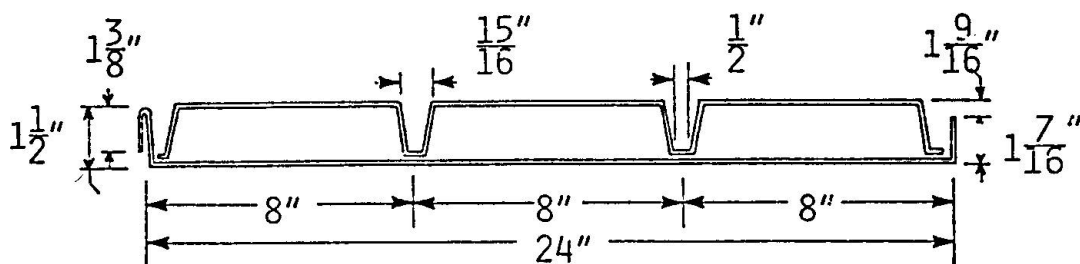


Fig. 2 - 24" Wide Panel Without Stiffeners

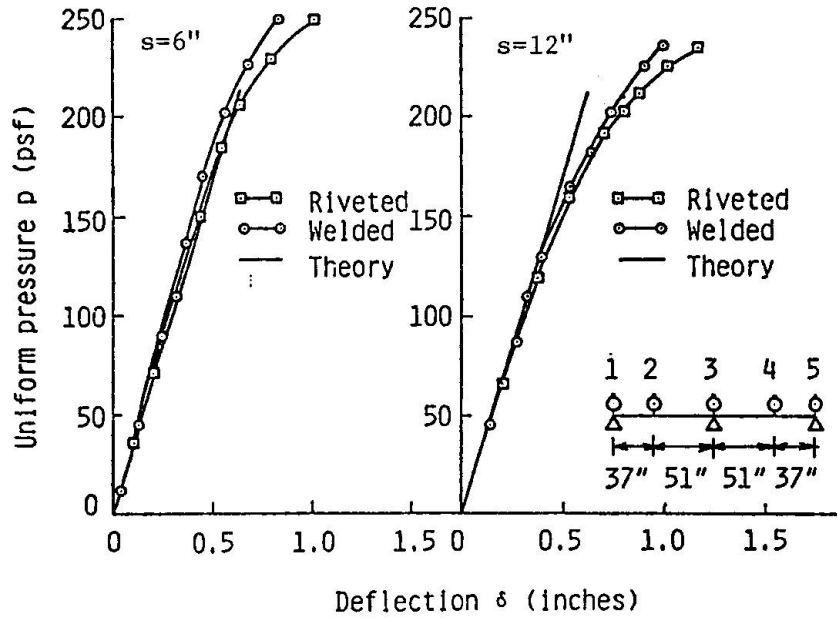


Fig. 3 - P-δ Curves for Two-Span Continuous Panels

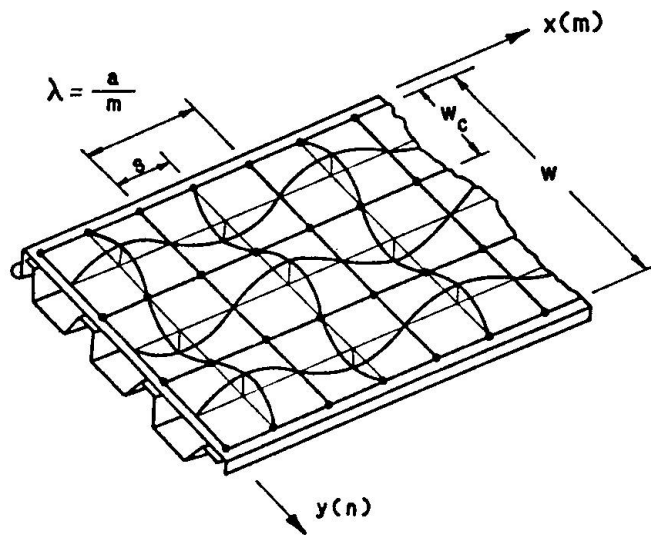


Fig. 4 . - Buckling Configuration of Cover Plate With Adequate Connection Spacing

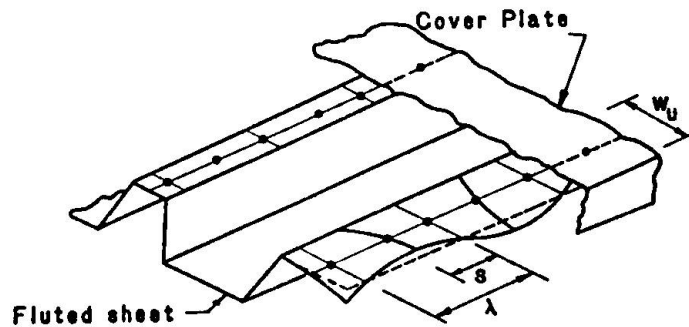


Fig. 5. - Buckling of Outstanding Unstiffened Flanges

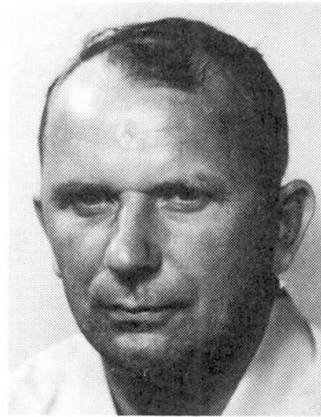
Design of Slender Webs in Steel Structures

Dimensionnement des âmes élancées dans les structures en acier

Bemessung schlanker Stege von Stahlkonstruktionen

Jozef DJUBEK

Assoc. Prof.
Slovak Academy of Sciences
Bratislava, Czechoslovakia



J. Djubek born 1926, received his civil engineering degree from the Slovak Technical University in Bratislava, the Ph.D. degree at the Leningrad Technical University (LISI) and the D.Sc. degree in Bratislava. As Associate Professor he spent one year at the University College Cardiff. He is Head of Department.

SUMMARY

The paper deals with the effects of initial geometrical imperfections, residual stresses and in-plane boundary conditions of slender webs. The limit state of the web is defined by the elastic and plastic portions of the pre- and postbuckling range. The coefficient of local sheet buckling of a web, subjected to compression for boundary flange sheet panel and for inner sheet panel is discussed.

RÉSUMÉ

Cet article étudie l'effet des imperfections géométriques initiales, des contraintes résiduelles et des conditions limites pour les âmes élancées de poutres d'acier. L'état limite de l'âme est défini par les portions élastique et plastique dans le domaine pré-et post-voilement. L'auteur étudie le coefficient de voilement local de l'âme soumise à la compression dans le cas d'un panneau de bord et d'un panneau intérieur.

ZUSAMMENFASSUNG

Der Artikel befasst sich mit der Wirkung anfänglicher geometrischer Imperfektionen, mit der Wirkung der Eigenspannungen und der Randbedingungen schlanker Stege. Der Grenzzustand eines Steges wird mit dem elastischen und plastischen Anteil des elastischen und überkritischen Beanspruchungsbereiches definiert. Weiter wird der Koeffizient lokaler Ausbeulung des Stegbleches besprochen, welcher entweder in einem Randfeld oder in einem inneren Stegfeld druckbeansprucht wird.



1. INTRODUCTION

In book [1] we have dealt with geometrically and physically non-linear analysis of slender webs with initial imperfections among which the effect of residual stresses was also accounted for. The limit state of the web has been defined by the load-carrying capacity if both the elastic and plastic portions of the post-buckled range were taken into account.

In the following analysis the effects of residual stresses, of boundary conditions and that of initial geometrical imperfections are treated separately. Consequently, the objective of the analysis is to find out, for certain boundary conditions, the stress state in a compressed web with a/ initial geometrical imperfections and b/ residual stresses.

2. A RECTANGULAR WEB SUBJECT TO COMPRESSION

In the edition of Czechoslovak Standard ČSN 73 6205 "Design of Steel Bridge Structures" 1984, pp. 23-24, the ultimate load of the web /or flange/ subject to compression is written as follows:

$$\sigma_{ult} = \varphi_n R_d \quad /1/$$

where φ_n is the coefficient of local web sheet buckling /isotropic web/ and R_d the s. c. design strength of the web material /which in the Czechoslovak Limit State Design approach replaces the yield stress R_y ; $R_d = 0,87 R_y$ if $R_y \leq 300$ MPa and $R_d = 0,80 R_y$ if $R_y > 300$ MPa/.

The local reduction factor φ_n is worked out as follows:

Type I - for boundary flange sheet panels

$$\varphi_n = \frac{40}{b/t + 10} \sqrt{\frac{210}{R_d}} \quad /1a/$$

Type II - for inner sheet panel

$$\varphi_n = \frac{40 \sqrt{210/R_d}}{b/t + 10} \left(1.3 - \frac{12 \sqrt{210/R_d}}{b/t + 10} \right) \quad /1b/$$

/but no more than one/,

where t is the thickness of the web /flange/ sheet and b_{st} the spacing of the longitudinal ribs /or web panel width/.

The above strength, R_d , of the material being inserted in MPa. The above formula /1a/, was derived by Z. Sadovský and the 1b by the Author /Table 1/.

The aforesaid isotropic reduction factor φ_n is a part of orthotropic plate approach, discussed in the final report of 12th Congress of IABSE in Vancouver.

Table 1

$\frac{b}{t} \sqrt{\frac{R_d}{210}}$	30	40	50	60	70	80	90	100	120	140	160	200
$\varphi_{n I.}$	1	0,80	0,67	0,57	0,50	0,44	0,40	0,36	0,31	0,27	0,23	0,19
$\varphi_{n II.}$	1	0,85	0,73	0,64	0,57	0,52	0,47	0,43	0,37	0,32	0,29	0,24

In the paper we deal with an isotropic web loaded in compression. The following results demand some deviation from the solution of the formulae /1a/ and /1b/.

3. BASIC SYSTEM OF DIFFERENTIAL EQUATIONS

The problem under consideration is described by the system of von Kármán-Marguerre's differential equations, generalized for elastoplastic webs. The problem is solved by Papkovich's method, that means the compatibility equation is solved exactly and the equilibrium one approximately. The equilibrium equation is solved by Bubnov-Galerkin method. The obtained equations are algebraic cubic equations [1].

The support of the web on its boundaries is assumed to be hinged which in the case of larger depth to thickness ratios is fully compatible with the behaviour of the web. The functions of the initial and additional deflections are considered in the form of series

$$w(x,y) = \sum_{m,n} w_{mn} \sin \frac{m\pi x}{a} \sin \frac{n\pi y}{b} \quad /2/$$

all term of which satisfy boundary conditions. As far as the deflection function $w(x,y)$ is concerned, one coefficient, w_{11} , was sufficient for small width-to-thickness ratios of the web, while for larger width-to thickness ratios three coefficients /i.e. w_{11} , w_{13} , w_{33} / were considered.

3.1 Unrestrained and restrained non-loaded edges

It is necessary to distinguish between the low and high width-to-thickness ratio of the web.

In the case of lower width-to-thickness ratio the deflections of the web are distributed relatively uniformly /the influence of membrane stresses is negligible/. For lower width-to-thickness ratios there is no difference between flexible and inflexible non loaded edges in the web plate plane /e.g. type I and type II of the boundary conditions, table 3/.

If the web slenderness grows the disagreement of the local reduction factor ρ_n for two boundary conditions rises. In Fig. 2 that difference for real initial imperfections $w_0 = b/100$ and $w_0 = b/200$ is remarkable.

Comment: The results of equal reduction factor ρ_n for the treated boundary conditions /unrestrained and restrained non-loaded edges/, becomes obvious in the theory of slender webs. In the stability theory of ideal web plates /e.g. linear problems in the solution of critical stresses, there exist no boundary conditions in the web plate plane. There are no flexible edges in the web plane either.

3.2 The influence of geometrical imperfections

It has been known that unavoidable initial imperfections can exhibit a significant effect on the behaviour of steel thin-walled plated structures. For this reason an international Task Group "Tolerances in Steel Plated Structures" chaired by Professor Ch. Massonnet, some time ago was formed within the framework of IABSE.

To obtain reliable information regarding the magnitude of imperfections occurring on ordinary steel bridges or other similar steel constructions we can start with the initial imperfections on four Czechoslovak steel box-girder bridges. The initial curvature /the stiffeners and sheet panels of both webs and flanges were measured/ was conducted on erected bridges, i.e. inclusive the effect of dead weight of the structure. The contribution is confined to the initial



imperfections of the lower flange, since it is in the compressed portion of these flanges where the effect of the unavoidable "distorting" is expected to be most significant. The measured maximum geometrical imperfections are as follows: a/ the motor-way bridge over the river Oslava at Velké Meziříčí - $w_0 = b/109$, b/ the railway bridge at Ivančice - $w_0 = b/320$, c/ the fly-over crossing the railway station Prague-Centre - $w_0 = b/227$ and d/ the new structure of the Barricade Fighters Bridge over the river Vltava in Prague.

By the large deflection theory analysis was determined the coefficient of local web buckling ϕ_n /for initial imperfections $w_0 = b/200$ and $w_0 = b/100$ / on the relative slenderness $b_{st}/t \cdot \sqrt{R_d/210}$.

The buckling coefficient ϕ_n is depending not only from the width-to-thickness ratio of the web, but depends also from the side ratio of the web panel $\alpha = a/b$. The smallest value of the buckling coefficient ϕ_n of the web subject to compression /for the same value of the width-to-thickness ratio/ is approximately for $a/b = 0.8$, that have been used in calculation.

The influences of geometrical imperfections for high width-to-thickness ratio is negligible. On the other hand for the low width-to-thickness ratio this influence is greater /for the relative slenderness $b/t \cdot \sqrt{R_d/210} = 40$ the difference ϕ_n is about 20-25%/.

3.3 Residual stresses

Residual stresses develop as results of the welding process. Welds as well as their immediate vicinity are subjected to tension equal to the yield stress, and the remainder of the cross-section is subject to residual compression. The residual tension and compression stresses satisfy equilibrium condition.

The depth of tension field, practically independent of the total depth of the web, can be found out with due regard to the welding speed, heat sources, preheating, web thickness and the like. In bridge structures or in civil engineering structures the tension zone is assumed to extend to the distance $c = 2t$ to $c = 4t$, where t is the web thickness /Fig. 1/.

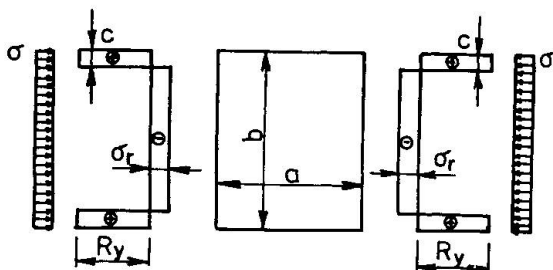


Fig. 1

When the web has been cooled, the longitudinal stresses near the weld remain close to the yield stress and are balanced by compressive stresses. It is advantageous /for the sake of calculations/ to work with idealized residual stresses, which very satisfactorily describe the actual stress distribution. A simple rectangular tension distribution of the residual stresses would be suitable for using in the analysis /Fig. 1/.

The residual stress on loaded boundaries of the web is of the form

$$n_r = R_y \frac{2c}{b - 2c},$$

where n_r is the compressive residual stress.

The compressive residual stress n_r reduces as the width-to-thick-

ness ratio b/t increases. The value of n_r/R_y are taken as follows

b/t	30	45	60	90	120
n_r/R_y	0.25	0.15	0.11	0.07	0.05

In all cases the value $c = 3t$ is introduced the yield stress of web material $R_y = 230$ MPa being considered.

The increment of the deflection w_{11}/t was taken by 0.0025 for the elasto-plastic region which did not affect the results.

The residual stresses were calculated as percentage of relative ultimate stress $\sigma_n = \sigma/R_y$ for geometrical imperfections $w_0 = b/100$ and $w_0 = b/200$. The flexible unloaded edges in the web plane were considered. The resulting maximum residual stresses σ_r for width-to-thickness ratios of the web b/t are as follows

b/t	30	45	60	90
$\sigma_r \%$	20.60	8.13	6.86	3.02

The stress σ_r for higher geometrical imperfections $w_0 = b/100$ is presented. For lower w_0 the residual stress would be smaller. So, for example, if $w_0 = b/200$ and $b = 30$, the residual compressed stress $\sigma_r = 9.83 \%$, for $b/t = 60$, $\sigma_r = 3.44 \%$.

The stress distribution in the slender web /for the points $x, y, z = \pm t/2$ / can be followed in Table 2. The results refer for 1/4 of the compressed web. By $c_1 = 1$ are denoted the points, where the relative effective stress σ_e/R_y /where $\sigma_e =$

$$(\sigma_x^2 + \sigma_y^2 - \sigma_x \sigma_y + \tau^2)^{1/2}$$

is lower or equal to one.

Table 2

The relative effective stress σ_e/R_y in the web loaded in compression

1	1	1	1	1	1
1	1	1	1	1	1
1.15	1.25	1.31	1.33	1.33	1.32
1	1.04	1.14	1.24	1.31	1.33
1	1	1.03	1.16	1.27	1.32
1	1	1	1.13	1.25	1.31

Let us mention that the welding residual stress depends not only of the web slenderness but also from the geometrical imperfection.

4. COMPARISON OF RESULTS

According to the obtained results /the effect of residual stresses and that of the geometrical imperfections and boundary conditions is treated/ the conclusions can be written. The magnitude of initial imperfections was taken as $w_0 = b/200$, that it is also the conclusion of the work of International Task Group "Tolerances in Steel Plated Structures" formed a few years ago within the framework of IABSE. Welding residual stresses /that depend also on geometrical imperfection/ are taken also by the value $w_0 = b/200$.

There follows from the obtained results, that it is advantageous to design slender webs, with minimal effect of residual stresses, which refer to higher width-to thickness ratio /Fig. 2/.

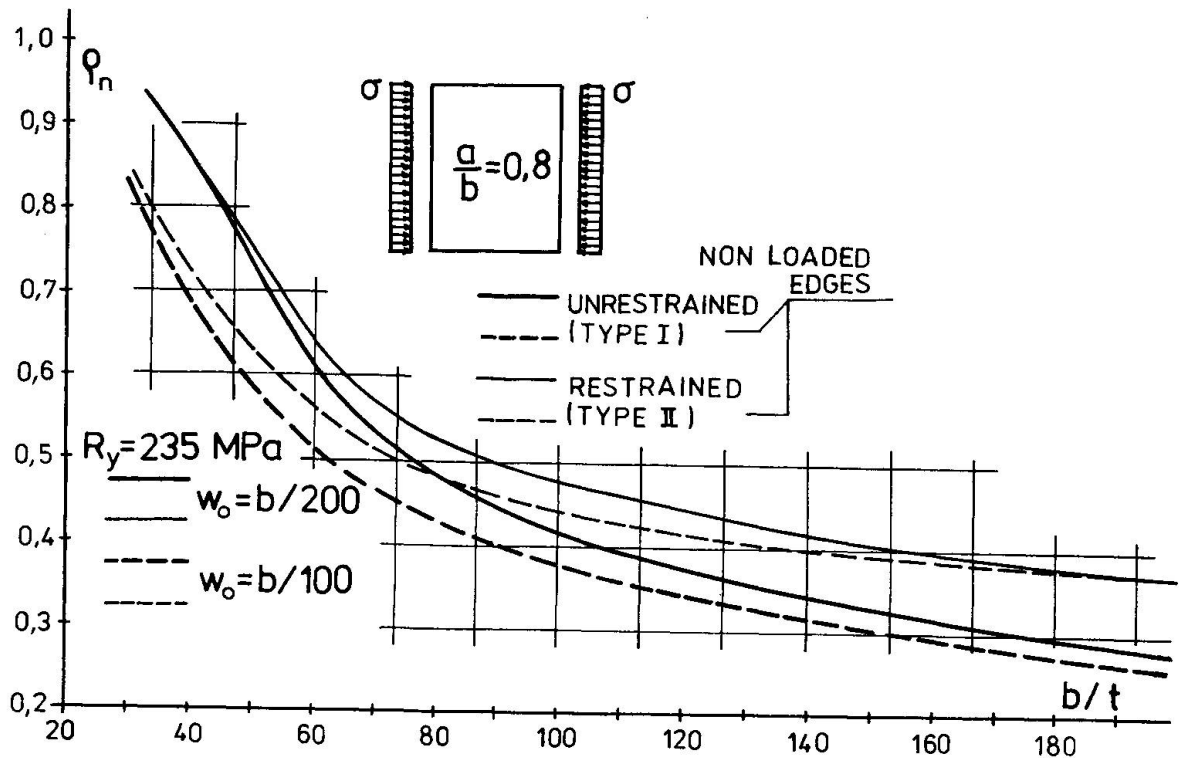


Fig. 2

If the initial imperfections /less or equal to $w_0 = b/200$ / are considered, the coefficients of local web buckling ϕ_n /type I for boundary sheet panels, type II for inner sheet panels/ according to Table 3 should be used.

Table 3

Coefficient ϕ_n of sheet buckling of rectangular simply supported web subject to compression

$\frac{b}{t} \sqrt{\frac{R_d}{210}}$	30	40	50	60	70	80	90	100	120	140	160	200
I.	1	0.80	0.67	0.58	0.53	0.48	0.45	0.42	0.38	0.35	0.32	0.28
II.	1	0.82	0.73	0.64	0.57	0.52	0.50	0.48	0.44	0.42	0.39	0.36

5. OTHER TYPES OF WEB LOADING

We have dealt in detail with the slender web subjected to compression. The obtained results /the effect of initial imperfections and residual stresses/ are of the same character for other types of web loadings such as bending, shear and combined bending and shear.

References

1. DJUBEK, J. - KODNÁR, R. - ŠKALOUD, M.: Limit State of the Plate Elements of Steel Structures. Birkhäuser Verlag, Basel-Boston-Stuttgart, 1983.